Micro–Climate Modelling and Engineering Design for a Horticultural Grow–Cell Prototype

Ioannis Tsitsimpelis

MSc Mechatronics Engineering

A thesis submitted in partial fulfilment

for the degree of Doctor of Philosophy

Lancaster University

Engineering Department

UK

November 2017

Abstract

This thesis is concerned with controlled environment horticulture, with a particular focus on two practical examples, namely a laboratory scale forced ventilation chamber and a full-sized prototype grow-cell developed in collaboration with an industry partner. The grow-cell belongs to a relatively new category of plant factory in the horticultural industry, for which the motivation is the maximization of production and the minimization of energy consumption. Significantly, the plants are grown under artificial lights and there is recycling of water.

The thesis is organized into two main parts. Part A of the thesis takes a systems design approach to identify the engineering requirements of the new grow-cell facility, with the prototype based on a 12 m $\times$ 2.4 m $\times$ 2.5 m shipping container. Research contributions are made in respect to: (i) the design of a novel conveyor-irrigation system for mechanical movement of plants; (ii) tuning of the artificial light intensity; and (iii) investigations into the environmental conditions inside the grow-cell. In particular, the conveyor-irrigation and lighting systems are optimized by the present author to make the proposed grow–cell more effective and sustainable. In future research, the prototype unit thus developed can be used to investigate production rates, plant quality and whole system operating costs. Nonetheless, preliminary growth trials reported within the thesis, demonstrate that *Begonias semperflorens* and *Impatiens divine* can be harvested to the satisfaction of a commercial grower.

The prototype has a standard commercial air-conditioning unit to maintain the required temperature and humidity set points. However, data collected by the author from a distributed sensor array demonstrates heterogeneous conditions arising during the growth trials. Hence, the research associated with Part B of the thesis concerns the development of a novel data–based approach for the modelling and control of micro-climate in a building or room, with a particular focus on thermal

stratification. In particular, use of statistical clustering techniques are investigated for the partitioning of indoor environment into a number of zones that have a relatively uniform thermal behaviour. The quantitative data-driven approach proposed here, first characterizes the system dynamics using measured data and, secondly, exploits Agglomerative Hierarchical Clustering (AHC) and k-means clustering to determine the thermal zones. The practical utility of the new approach is evaluated using the laboratory example i.e. a 2 m × 1 m × 2 m chamber with two axial fans, a heating element, and an array of thermocouples. In this case, the modelling approach yields Hammerstein type models which are subsequently used for both single and multi–zone control system design. The laboratory facility was used for this research since it was readily available for these closed-loop control experiments.

The thesis concludes with recommendations for future developments in the micro-climate control unit for the grow–cell, and for further research into the grow–cell concept more generally.

Declaration

I declare that this Thesis is my own work, and has not been submitted in substantially the same form for the award of a higher degree elsewhere.

Ioannis Tsitsimpelis

Date:........................

Signature:................

Acknowledgements

Dedication

To my mother Sappho, grandmother Ioanna, brother George, and cousin Costas.

In loving memory of my father, Apostolos.

Contents

List of Figures

List of Tables

Chapter 1

Introduction

This thesis is concerned with controlled environment horticulture, with a particular focus on the monitoring, modelling and control of environmental variables, such as temperature and humidity. The research behind the thesis consists of two separate although complementary activities, both lead by the author within the framework of a Centre for Global Eco-innovation graduate research project[1]. Part A of the thesis reports on the development, optimisation and testing of a closed–environment prototype grow–cell. As illustrated in Fig. 1.1, this belongs to a relatively new category of plant factory in the horticultural industry, for which the motivation is the maximization of production and the minimization of energy consumption.

Part B of the thesis develops a novel approach for the modelling and control of the environment inside buildings more generally, particularly in relation to the statistical identification of spatial zones with similar thermal characteristics. Although motivated by measurements from the grow-cell, the new approach is developed and evaluated using a more readily available, laboratory forced ventilation test chamber. The present Chapter 1 briefly introduces the overall aims and motivation for the work, and the structure of the thesis. However, more detailed research objectives and literature reviews are provided in the opening chapter to each part of the thesis i.e. Chapter 2 (Part A) and Chapter 6 (Part B).

---

[1]The project is supported by the Centre for Global Eco-innovation (Lancaster University) and part financed by the North West UK operational programme for European Regional Development Funds. The industrial partner, NP Structures Limited, specialises in the design and manufacture of structures for applications in the horticultural, retail, agricultural and construction industries.
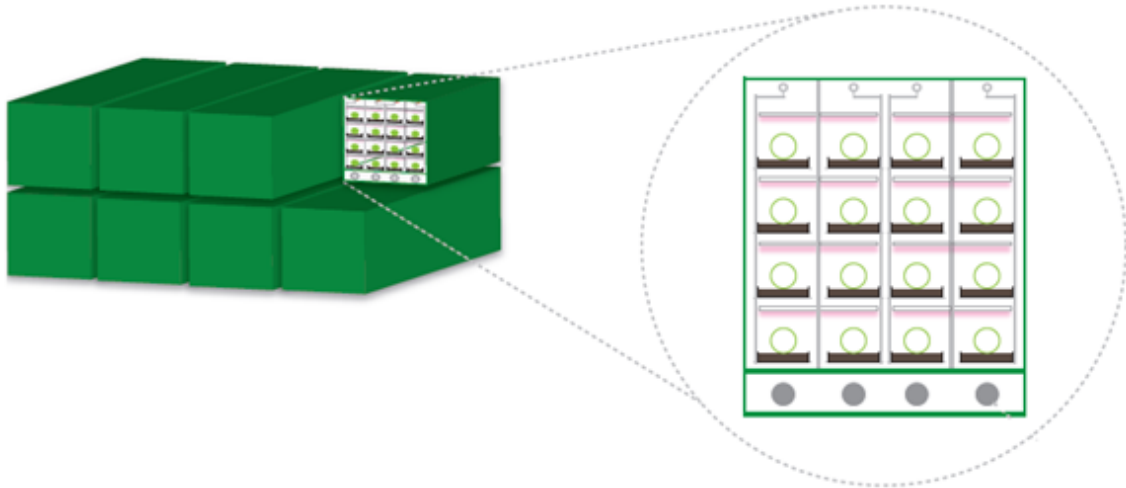
Figure 1.1: General grow-cell concept: a closed-environment mobile system, fully occupied with plants, which are grown under artificial light in a multi-tier configuration. The figure shows how multiple units can be stacked. However, the research in this thesis is based on one unit, namely a modified shipping container.

1.1 Motivation and aims

Controlled environment horticulture is a subject nested within the wider agenda of optimising the food system, in order to deal with forthcoming changes in population and climate [FAO, 2002, 2015]. Today's established protected crop growth medium is the glasshouse (and related plastic covered systems), globally occupying an estimated 8000 km^2, in which intensive use of pesticides and excess water supply generally takes place [Wainwright et al., 2014]. Hence, there is a considerable effort by stakeholders in the agricultural industry to optimize a range of sub-processes, with the aim to decrease harmful residues and energy inputs.

Such research includes investigations into the physical structure in which plants are grown, and the exploitation of modern technological know-how in order to deploy a higher level of system automation. For instance, significant work has been carried out by the industry to realize what are typically known as plant factories. These are multi-layer growing systems installed in thermally insulated, fixed or mobile buildings, and equipped with artificial light [GreenTech, 2016, FreightFarms, 2016, Markham, 2014, Hughes, 2015, Payne, 2014, Oguntoyinbo et al., 2015, Ohara et al., 2015, Park and Nakamura, 2015, Sugano, 2015]. Some immediately perceived benefits of this

approach are: the flexibility to grow crops at any geographical location regardless of the external climatic conditions, reduced pesticide use and the decrease of food miles, all of which induce savings in terms of transportation costs, greenhouse gas (GHG) emissions and crop nutritional and economic value. Furthermore, by incorporating a multi-tier (vertical farming) arrangement, as in Fig. 1.1, there is the potential to significantly reduce the land area currently occupied by greenhouses. Finally, there is scope for investigation of various biological and horticultural issues, for example crop delivery date and flavour, by on–line regulation of the lights, micro-climatic and feed systems.

Plant production by means of artificial climate and artificial or hybrid light dates back to the first quarter of the 20th century. Initially, the primary motivation was to facilitate research into plant responses for different environmental conditions, with illustrative early citations including Harvey [1922], Popp [1926], Davis and R. [1928]. However, thanks to recent technological advances relating to the performance and operating costs of light emitting diode (LED) lights, it is now possible to realize such facilities for industrial use, with the long term expectation being to outpace the use of greenhouses in terms of production and energy efficiency.

A number of systems have been brought into the industrial domain over the past few years, particularly in Japan and the USA (see e.g. GreenTech [2016], FreightFarms [2016], Markham [2014]), and interest is expected to further increase as big corporations are investing in the erection of indoor farms [Hughes, 2015, Payne, 2014]. Nevertheless, there are numerous on-going research challenges relating to their design and operation. For example, their energy requirements, air movement, dehumidification, internal racking design, different ways to deploy artificial LED lighting, and the monitoring of crop reaction to these.

In principle, a holistic approach to the optimisation of all these will allow for the minimization of total GHG emissions and water consumption, and the concurrent maximization of year round production. Hence, for the research behind the present thesis, a systems design approach is used to identify the engineering requirements of a new grow-cell facility, with novel contributions made in three interconnected areas. These relate to the systems for mechanical movement and irrigation of the plants, the control of artificial light and an analysis of the environmental conditions inside

the grow-cell, including temperature and humidity.

1.2   Micro-climate modelling

Ventilation rate and heat are significant inputs in the control of micro-climate surrounding plants within agricultural buildings, and the lack of effective regulation of these is a major cause of production losses. Heating and ventilation systems employed in many buildings presently deal with environmental variables in an averaging manner, utilising measurements from single locations and assuming these represent the micro-climate of the whole area. Hence, multi-zone models often approximate the problem by considering an entire room or floor as one thermal zone [Liao and Dexter, 2004, De Persis et al., 2008, Mossolly et al., 2009, Goyal and Barooah, 2012]. This is particularly true for agricultural buildings such as glasshouses (e.g. Taylor et al. [2004b]). Dealing with such micro-climatic gradients in agricultural buildings generally leads to higher costs and energy losses e.g. as staff have to physically move plants around [Kittas et al., 2003, Teitel et al., 2010]. However, the importance of manipulating environmental variables in an energy efficient manner, whilst taking account of the gradients that arise, is also clear for many other types of indoor environment (e.g. Van Brecht et al. [2003], Brande [2006], Chen [2009]).

Multi-zone models are commonly based on physically defined locations in the facility, for which relatively homogeneous environmental conditions are assumed, say the inlet, outlet and different rooms of a building. Bleil De Souza and Alsaadani [2012] discuss some common strategies for thermal zoning, focusing on the human-built environment. However, in some practical situations, different thermal zones with similar characteristics emerge in an open space (one room) that will not necessarily be obvious from the physical layout. This is evident for the horticultural grow-cell and laboratory ventilation chamber considered in the present thesis.

To address these limitations, the thesis proposes a novel data-driven approach to the formulation of suitable thermal zones, for subsequent single-zone and multi-zone modelling and control. Apart from the raw data being directly utilised for thermal zone partitioning, model structures are also initially identified from the latter, thus

avoiding undue reliance on prior hypotheses and ensuring that the resulting models are identifiable from the available environmental data. However, the identified model is only considered fully acceptable if it is also capable of interpretation in a physically meaningful manner. This represents a novel example of the *data-based mechanistic* (DBM) concept (see e.g. Price et al. [1999], Young [2011, 2013]).

1.3 Research objectives

Although more details are provided in chapters 2 and 6, the overall objectives of the research can be briefly summarised as follows:

- To identify the engineering requirements of a new grow-cell facility, and to support the industry partner in the conversion of the shipping container procured for this purpose.

- To optimise the conveyor-irrigation system in advance of the plant growth trials. The conveyor allows for operator access to the plants and potentially provides for the automatic insertion, inspection and harvest of crops. It also ensures a more equal treatment of plants in terms of environmental variables, and adds to the circulating effect provided by the fans.

- To adapt the commercial LED units so that they are capable of varying the output light intensity; to investigate their spectral characteristics; and to use these results to optimise the balance between light intensity and energy consumption.

- To utilise statistical tools for data-driven identification of thermal zones in a building, and to use these to develop both single-zone and multi-zone control systems for temperature. Because of limitations in the existing grow-cell air conditioning unit, these new algorithmic developments are evaluated using a laboratory forced ventilation chamber.

- To collaborate with a commercial operator in plant growth trials, and to monitor and visualise the environmental conditions inside the grow-cell. Finally, to use all the above practical and methodological results in order to make

recommendations for future developments in the grow-cell air conditioning unit, and for further research into the grow-cell concept more generally.

1.4 Articles arising

The following peer reviewed articles have arisen as a result of the research in this thesis:

- Tsitsimpelis, I. and Taylor, C. J., *Micro-Climate Control in a Grow-Cell: System Development and Overview*, 19th IFAC Triennal World Congress, Cape Town, South Africa, 2014. (Conference article with preliminary design considerations from Chapters 2-3 of the thesis).

- Tsitsimpelis, I., Wolfenden, I. and Taylor, C. J., *Development of a grow-cell test facility for research into sustainable controlled-environment agriculture*, Biosystems Engineering, vol. 150, pp. 40–53, 2016. (Journal article based on Chapters 2-5 of the thesis).

- Tsitsimpelis, I. and Taylor, C. J., *Partitioning of indoor airspace for multi-zone thermal modelling using hierarchical cluster analysis*, European Control Conference, Linz, Austria, 2015. (Conference article with preliminary results relating to the clustering analysis in Chapter 7).

- Tsitsimpelis, I. and Taylor, C. J., *A 2-Dimensional Hammerstein model for Heating and Ventilation Control of Conceptual Thermal Zones*, 10th UKACC Control Conference, Loughborough, UK, 2014. (Conference article with preliminary results relating to the Hammerstein thermal models in Chapter 8).

The following article is in preparation for submission to a suitable journal:

- Tsitsimpelis, I. and Taylor, C. J., *Data-based identification of multi-zone thermal models for control* (based on Chapters 6-9).

1.5   Thesis organisation

The following Chapter 2 introduces Part A of the thesis i.e. concerning the development of the grow-cell prototype. Chapter 3 discusses each grow-cell subsystem in turn, followed by their preliminary testing and optimisation. This includes: the design and implementation of the conveyor-irrigation system; the tests, selection, and modification of the lighting system; and an investigation into the micro-climate that dominates the growing area. Chapter 4 presents the results of the two growth trials, held in February 2015 and June 2015. Chapter 5 concludes the first part of the thesis with a discussion of the lessons learnt, the energy use and costs derived from the growth trials, and suggestions for future development.

Chapter 6 introduces Part B of the thesis i.e. modelling and control of thermal zones. The previously developed laboratory ventilation chamber is also described. Chapter 7 develops the new approach to the identification of thermal zones, whilst Chapter 8 presents the estimation of non-linear models for temperature in the ventilation chamber, and includes the use of results from the previous chapter. Chapter 9 considers control examples that relate to temperature distribution and presents the conclusions to Part B. Finally, the overall conclusions of the thesis and recommendations for further research are summarised in Chapter 10.

Part A
Development of Grow-Cell Prototype

Chapter 2

Introduction to Part A

The present Chapter 2 introduces Part A of the thesis, which is concerned with the development of a grow-cell prototype. There is significant research effort globally towards maximising the production capacity of closed growing systems, to minimise energy inputs and to minimise the use of pesticides. Many studies have shifted their research focus towards the development of plant factories and a number of tangible examples have been developed by industry. These demonstrate current technology and show that industry has the capacity to put together such structures [Markham, 2014, Payne, 2014, FreightFarms, 2016, GreenTech, 2016, Hughes, 2015]. However, research being conducted around the world also highlights that a wide optimisation margin, beyond the minimum necessary to just grow plants, has yet to be reached i.e. there is considerable scope for improvements in regard to production costs, energy consumption and so on [Hendrawan et al., 2014, Despommier, 2009, Kozai et al., 2015, Oguntoyinbo et al., 2015, Ohara et al., 2015, Park and Nakamura, 2015, Sugano, 2015].

In fact, conventional greenhouse technology inherently outpaces the performance of plant factories, since the latter has only recently become commercially practical thanks to developments in LED technology [Sager and McFarlane, 1997]. At the same time, it is mainly the artificial lighting requirement that puts plant factories at a relative disadvantage over greenhouses. Furthermore, technological advances in terms of renewable resources and wireless monitoring/control may be applied to both growing mediums for the purposes of optimization. However, there are three key points that make plant factories different and potentially more interesting for a

large range of medium and small edible crops: a) they are not affected by external climatic conditions; instead a dedicated micro-climate is applied, which makes a crop growth task simpler and more predictable to control; b) they require negligible use of pesticides because their isolated environment inevitably reduces the number of potential infecting agents; and c) in an optimised setting, water usage can be minimised by recycling irrigated water, and by environmental controllers recycling water vapour and regulating this to minimize the frequency of the required irrigation cycles. However, in order to make such facilities viable, significant multidisciplinary research is still required.

Section 2.1 reviews the protected environment crop growth literature from its early days. Sections 2.2 through to 2.5 consider more specialist work in relation to two key topics of interest, namely (i) the options for artificial light and (ii) issues arising in relation to the mechanical movement of plants. This information is used to identify the system requirements of the prototype, representing an early research contribution of this thesis. As a result of these requirements, section 2.6 summarises the research objectives for the following chapters 3–5 of the thesis.

2.1 Protected environment crop growth

Future food supply and optimization of agriculture was already a concern by the early 20th century. Ball [1921], for example, observed that smart land manipulation by merging know–how from various scientific fields would compensate for the rapid increase of population and the lack of remaining lands suitable for cultivation. At the research end, the driver for erecting closed growing apparatuses was the inconsistent results between similar growth studies [Davis and R., 1928, Arthur et al., 1930]. At the time, this type of structure was not regarded to be commercial, but a research tool which would allow studies in plant physiology to be standardized. These are now known as growth chambers, which are in essence small scale versions of plant factories, except they are used for research purposes.

At this time, various growth chamber designs were presented and studies undertaken in both laboratory and greenhouse settings. One early study assessed the utility of artificial light at different intensities for areas that did not receive

sufficient sunlight during winter months. Light was provided by 200 and 1000 W nitrogen-filled tungsten lamps, while the apparatus accounted for spatial variability by incorporating phonograph motors to rotate the plant pots [Harvey, 1922]. The sequel of that study, which was published two years later [Hendricks and Harvey, 1924], addressed the rate of growth under continuous lighting, where more than forty plant species were grown and classified in terms of light intensity and temperature needs.

Tottingham [1926] assessed temperature effects in protein content, dry matter, and sugar content of wheat, in culture chambers facilitated within a greenhouse. Wheat was grown in water, sand and soil, and means of illumination was provided both artificially and by the use of daylight. Mazda lights were used, starting from 500 W and reaching up to 2500 W for different growth trials. Two years later, Davis and R. [1928] presented an environment chamber in which wheat was grown hydroponically. Their results demonstrated the possibility to obtain better growth than that emerging in nature, as well as the feasibility of reproducing similar growth results. The greenhouse presented by Arthur et al. [1930] featured supplementary artificial light from incandescent sources mounted on retractable rails, and the use of mixing fans for air circulation. It was further equipped with isolated rooms, which comprised gas-filled tungsten lamps put before water-glass in order to filter out infra-red radiation. Brown [1939] presented three growth chambers installed inside a greenhouse. Each one had separate soil and air temperature control systems. The chamber boundaries were made of glass in order to receive sunlight, while the air would be heated or cooled when leaving the chamber, depending on the control set-point; and diverted in turn back to the chamber through another duct. In his review paper, Parker [1946] reports on several other similar studies that were held during those years.

Instrumentation on the aforementioned studies included galvanometers connected with electrical resistance thermometers, "two-pen Brown" thermometers, and "Cambridge and Paul" electric thermographs, while the control of temperature was achieved by means of bimetal thermostats and three-point mercury switches in an on-off manner. Similarly, humidistats were employed to control relative humidity. Mixing fans were used to circulate the air around the plants and to force humidity and

temperature generated in separate small chambers through air ducts. Air velocity was usually measured by "Tycos" anemometers. Carbon dioxide was also monitored and supplied by steel cylinders. Moreover, ways of measuring light intensity included iron-nickel thermocouples in the circuit with galvanometers, Macbeth illuminometers, Sharp-Miller photometers and pyrheliometers; while wavelength was commonly measured using quartz spectrographs.

In the following years, growth chambers and greenhouse experimental facilities become more versatile, comprising for example air-conditioned greenhouses and darkrooms, diverted ventilation, automatic irrigation, and rotating tables. One novel example is seen by Went [1943], who presented the hardware of a state-of-the-art at the time facility for plant growth research. Here, it is observed that effort was given to entirely automate the process of controlling the growing environment. The facility consisted of two greenhouses and two dark rooms. Two air-conditioning (A/C) systems were employed to control the air temperature and humidity of a greenhouse and a closed darkroom. The incoming air would go through the basement of the facility where it would be filtered before entering the growing areas. For the first A/C system the air would be optionally pre-heated, humidified and then reheated to a set-point defined by a thermostat. The second A/C system also incorporated a pre-cooling element before the pre-heater to allow a lower temperature-humidity environment to be created. The air would then enter the growing areas through ducts and on to diffusing louvres for distribution at configurable angles. Five dampers were installed in the facility and depending on their positions, air would be either recirculated or enter and exit the growing area. Their positions were electrically controlled by means of potentiometers. Additional fans were used in the dark rooms in order to remove the excess heat generated by the artificial light sources. A time-clock operated relay was used to change set-points for day and night air temperature. Irrigation was also time operated. Temperature was recorded at eighteen different locations by a galvanometer. The majority of plants were grown in movable tables (one revolution every five minutes), in order to expose them to different conditions when moved from one room to another, or to receive equal light energy when grown in the greenhouses. Finally, 560 W light panels were used in the darkrooms (Mazda and fluorescent tubes). Based on this facility, eight studies were published within four

years, covering aspects of tomato growth [Went, 1944a,b, 1945, Went and Cosper, 1945], chilli pepper [Dorland and Went, 1947] and ornamental plant growth [Lewis and Went, 1945].

In 1949, the Earhart Plant Research Laboratory opened. This hybrid facility was designed to simulate any type of weather conditions in order to assess plant growth and ecological problems [Went, 1952], and it was equipped with twenty air-conditioning systems and artificial lights. The Earhart Laboratory is regarded as a major stepping stone in the development of field sciences and is known to be the first facility to which the term *Phytotron* was given [Downs, 1980, Kingsland, 2009, Munns, 2014].

In 1969, the American Society for Horticultural Sciences (ASHS) was established in the U.S.A. The group consisted of researchers in controlled environment plant growth, who shared very similar considerations about the process of monitoring and controlling the growing environment. Their concerns generated a set of goals, including the specification of guidelines and growth curves. In terms of specifying growth curves, the involved institutions agreed on conducting growth trials using the same monitoring and control equipment and applying exactly the same growing procedures. Their results showed that there were growth differences even when the studies were undertaken at the same laboratory. Variations in terms of the amount of the light energy provided in each study was later accounted for those differences, with the amount of infra-red radiation varying between light modules. Furthermore, the lack of climatic uniformity in the growing airspaces was also reported as a source for arriving at inconsistent growth results. In the guidelines produced by Tibbits and Kozlowski [1979], it became apparent that precision of environmental control should be revised with respect to spatial variability [Van Bavel, 1979]. Eighteen years later, the revised guidelines also included suggestions for design, maintenance, and requirements specification [Sager and McFarlane, 1997]. Currently, there is a large number of academic institutions and research groups that focus on controlled environment agriculture. For instance, the North Central Extension and Research Activity-101 (NCERA-101), which is based in the U.S.A, and another very active group is the UK Controlled Environments Users Group (CEUG). This group gathers individuals from academia, research institutes and companies, and holds annual

conferences centred around controlled environment plant growth.

In recent years, solid state lighting has been a key factor for the evolution of controlled environment plant growth. One of the first growth tests under artificial light in fact dates back to 1861 [Pfeiffer, 1926, Wheeler, 2008], while artificial light and manipulation of sunlight has been employed since the early 20th century. For example, Popp [1926] separated a greenhouse in five segments, with the glass of each one filtering out different wavelengths. To grow plants however using solely artificial light was too costly for industrialization at this time, mainly because of the short lifetime of the lights. Furthermore, even until the late 80s, the concept of having lights right above the plant canopy was impractical since High Intensity Discharge (HID) lights yield a great amount of heat. LED lights for plant growth made their appearance in the literature in the early 90s, where they started to be considered as candidates for plant growth in both space and on Earth due to their small mass volume [Barta et al., 1992]. With LED lights emerging, the concept of growing plants in a multi-tier configuration under artificial light also became possible. LED lights have all the necessary prerequisite characteristics for commercialisation in this context, such as small size, long life cycle, tailored wavelength output, and much lower heat output than HID lights; but their output efficiency was the main limitation at first [Bula et al., 1991, Barta et al., 1992, Tennessen et al., 1994, Brown et al., 1995, Goins et al., 1997, Sager and McFarlane, 1997, Tibbitts and Krizek, 1997]. However, that technical obstacle has been steadily decaying during the last fifteen years, as their efficiency has been improving significantly. Furthermore, research addresses novel aspects of their shape [Li et al., 2016] and chemical composition [Yang et al., 2015, Kang et al., 2015, Kim et al., 2016], as well as deploying these advances on plant growth investigations [Song, 2016, Chen et al., 2016].

2.2 Engineering requirements

To address the practically orientated aims of the research behind the first part of this thesis, a prototype grow-cell is developed using a combination of both off-the-shelf and novel components. One essential requirement of the prototype, namely that it can be readily transported to different growers for evaluation purposes, is

straightforwardly satisfied by procuring and adapting a standard freight container as the base unit (Fig. 2.1). To convert this container into a grow-cell facility, the immediate requirements relate to the environmental conditions inside the growing area, including both lighting and micro-climate, and the approach to hosting and feeding the plants. Although the proposed conveyor system proves central to all of these, the background and motivation for the micro-climate and lighting systems are first discussed below.

A plant's healthy development depends on its exposure to the required levels of light, water, temperature, humidity and carbon dioxide. For instance, temperature control is reported to have acute impact on plant growth and morphology, while humidity control is essential for dealing with plant transpiration [Vox et al., 2010]. One can control an indoor plant growing environment within a certain range by handling the ventilation rate around it. Fresh air supply drives in essence the levels of temperature, humidity and carbon dioxide, which in turn influences the physiological development of the plants. Its causal relationship with micro-climatic variables is the reason it is regarded as the fundamental factor for many types of indoor environment [see e.g. Taylor et al., 2004b, Brande, 2006, Chen, 2009, and the references therein].

However, the spatial distribution of environmental variables is not well addressed in many growing systems. In conventional greenhouses, the lack of light uniformity due to equipment around the plants, outside weather volatility, staff working around the growing environment and other disturbances, all contribute to a complex situation. By contrast, the grow-cell is intended to generate a relatively undisturbed environment. The thermal insulation ensures minimal disturbances from external weather conditions whilst photosynthetic photon flux density (PPFD) uniformity and unobstructed delivery above the plants is improved by the use of artificial lights.

2.3 Artificial Lighting

Artificial light has been used in greenhouses for many years, mainly to compensate for low sun duration in certain geographical locations, but also as a substitute for sunlight during night hours. High intensity discharge, incandescent and fluorescent
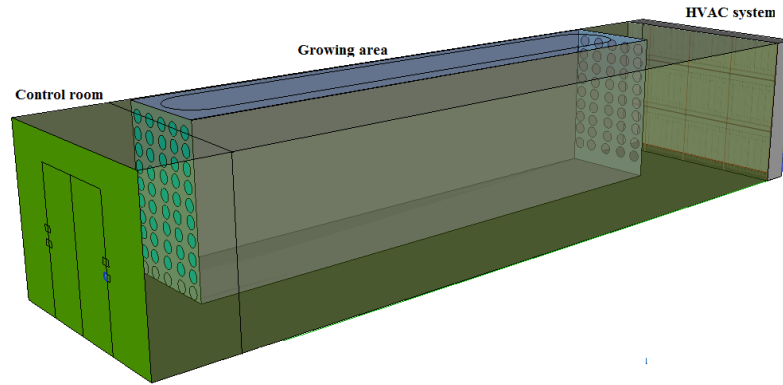
Figure 2.1: Grow-cell prototype drawing showing the basic layout of the modified freight container (12 m × 2.4 m × 2.5 m).

have been the main sources of artificial light [Bourget, 2008]. By contrast, interest in LED technology has only come to the fore relatively recently. LEDs have the ability to emit light at specific wavelengths and can be instantly switched on and off. Furthermore, they produce a relatively low level of thermal radiation as compared to other light sources [Barta et al., 1992, Sager and McFarlane, 1997, Bourget, 2008, Massa et al., 2008, Morrow, 2008], which means they can be placed very close to plants without causing damage, while excess heat may be removed by air extraction and/or utilising heat sinks.

As a result, there are numerous studies on plant growth under LED lights e.g. Hahn et al. [2000], Muthu et al. [2002], Nhut et al. [2003], Kim et al. [2004], Lin et al. [2013]. Much research effort has focused on the effect of different ratios of red, blue and green colours [Kim et al., 2004, Lin et al., 2013], and on the control of the magnitude of light output to minimise energy consumption [Fujiwara and Sawada, 2006, Shimada and Taniguchi, 2011, Harun et al., 2013]. Many studies address the potential energy savings by controlling the on-off frequency cycles of LEDs [Muthu et al., 2002, Shimada and Taniguchi, 2011, Almeida et al., 2014], while others use fewer lights by employing systems that move them at a certain speed around the growing area [Blom and Zheng, 2009, Lee and Kim, 2012]. Recently, Hendrawan et al. [2014] developed an image processing system that scans the plant and controls the operational level of individual LEDs above it. However, in terms of increasing performance and reducing energy consumption, this type of technology is at a

relatively early stage and the initial investment cost might be prohibitive for certain crop species, i.e. those that require high light energy levels.

More generally, resistance to the deployment of artificial light as the sole medium for photosynthesis relates primarily to the initial investment costs and on-going energy consumption. However, the former concern arises because LED technology has not yet reached maturity, whilst its cost is expected to decrease in the coming years. Furthermore, the long operational life of LEDs reduces their replacement and maintenance costs in comparison to other sources of light [Bourget, 2008]. For these reasons, the approach chosen for the present research is based on a straightforward and relatively low cost, white colour LED system.

2.4 Mechanical Movement of Plants

In recent years, conveyor and robotic systems in greenhouses undertake tasks ranging from pre-harvest through to post-harvest management. For example, seeding, watering, transplanting, transportation to different environments, crop spacing and labelling are all typically automated in order to save time and costs. In the commercial version of the grow-cell, plants will occupy the whole container, allowing for maximum growing capacity: this is critical in regard to the efficiency of the system. This leaves no pathway for growers to physically access the plants. Hence, a conveyor system of some type is essential to achieve single point inspection. Furthermore, plant factories, such as the present grow-cell, can potentially generate a higher density of plant foliage at each layer than a conventional greenhouse. As noted above, if these plants are not exposed to sufficiently uniform micro-climatic conditions, significant differences in quality and yield can emerge in different parts of the building.

The concept of physically moving plants around the air space in order to compensate for imperfect mixing in the micro-climate has not been extensively researched, although there are some examples in the literature [Wallihan and Garber, 1971, Hardy and Blumenthal, 2008, Brien et al., 2013]. Went [1943] presents an example from the 1940s of automating growth that encompassed the mechanical movement of plants, while a modern example of a conveyor system employed for this purpose is the rotating vertical farm concept of SkyGreens [2016]. Nonetheless, to date, the

overwhelming majority of greenhouse system controllers do not take into consideration the spatial variability of the micro-climate, which is only partially compensated for by e.g. manually moving trays around on an *ad hoc* basis and by using mixing fans.

2.5   Thermal Stratification

For high density systems such as the grow-cell, spatial variability of environmental variables needs to be addressed by means of feeding information around the airspace into the control system. Such spatial variability is well illustrated by a short investigation into a controlled environment fodder crop facility in the early stages of the present project. This facility (part of a commercially operating farm near Lancaster) utilises a conventional static multi-layer bench system. Its layout is shown in Fig. 2.2. Each of the six growing sections consists of seven layer shelves. Air is supplied by ducts, which are laid out around the ceiling of the facility. The outlet is located at the centre of the east side. Irrigation occurs every two hours by means of spray nozzles, while fresh air is supplied by small orifices around the ceiling. Environmental data (temperature and humidity measurements) were recorded by the present author using 25 data loggers (Fig. 2.2), with a one minute sampling rate, for 11 days. The daily temperature outside the facility was between 14-25 °C (July 2013).

The sensors were evenly distributed in two areas, on the south-east and north-west ends. In each area, 3 sensors were placed at the first layer (top), the fourth (middle), and seventh layer (bottom). Other sensors were placed in an *ad-hoc* manner, e.g. next to the inlet streams, outside the fodder barn, and at the outlet stream.

The fodder barn operators had reported undesirable variation in plant yield and quality. Fig. 2.3 sums up concisely why this is occurring. Subplots (i) and (ii) represent the daily mean temperature of the top (blue trace), middle (red trace), and bottom layers, for the south-east and north-west benches, respectively. The same configuration applies for humidity in subplots (iii) and (iv). The data depicted here are based on one day but are representative of the conditions for all 11 days. Firstly, it is clear that the rather basic industrial on-off temperature controller utilised in
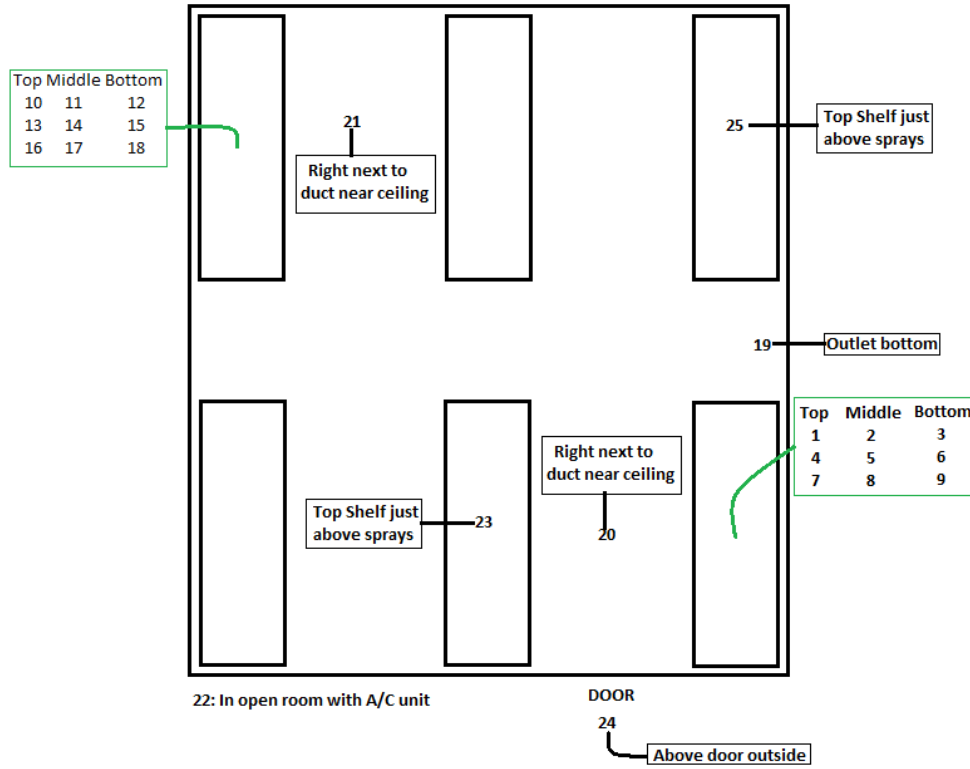
Figure 2.2: Fodder barn layout with numbered sensor locations.

this instance fails to maintain steady conditions around the desired set-points. What is also shown, however, is that the top layers receive fresh air at a much higher rate as compared to the layers below. Hence, even if the controller performed better it would still not have the capacity to compensate for the variations between the layers.

Hence, for the prototype grow-cell, the introduction of a conveyor system aims to manage access to the plants (in the final planned commercial configuration i.e. without room for human intervention inside the growing space) but is also motivated by the above observations of significant variation of key environmental variables.

2.6 Research Objectives

The present chapter has reviewed the literature relating to the grow-cell research problem, from which the main objectives for Part A of the thesis have been derived. These are summarised as follows:

In the first instance, the author and industrial partner procure and adapt a shipping container as the base unit for the grow-cell prototype. The first research
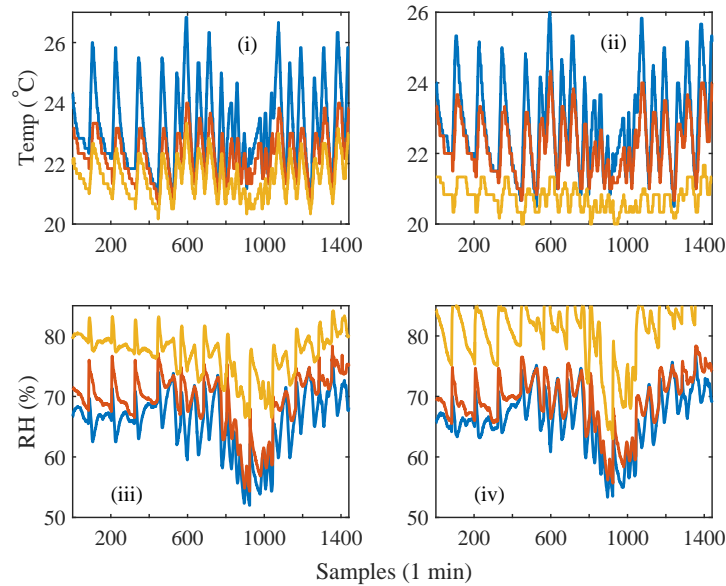
Figure 2.3: Daily temperature and humidity data in the south-east (i, iii) and north-west (ii, iv) areas of the fodder barn. The blue, red and yellow traces correspond to the top, middle and bottom layers of each area.

objective is subsequently to develop and optimise suitable conveyor-irrigation and lighting systems, with the long term aim to make the prototype grow-cell effective and sustainable for growing plants. With regard to the conveyor, the specific objective is to design a mechanical system with low-power consumption that is adaptable for differently sized grow-cells and different types of irrigation (i.e. for future research and possible commercialisation in different contexts); and to evaluate the reliability and practical utility of this design in both a laboratory situation and for an illustrative plant growth trial. For the lighting system, the objective is to adapt readily available commercial units so that they are capable of varying the amount of PPFD, and to investigate their spectral characteristics. The subsequent aim is to use these results to optimise the balance between PPFD magnitude and energy consumption in advance of the growth trial.

The primary objective of the growth trial is to test the entire prototype grow-cell system in an illustrative practical situation and, more specifically, to demonstrate that *Begonia semperflorens* and *Impatiens divine* plantlets can be grown and harvested to the satisfaction of a commercial grower. During these experiments, the aim is to

collect measurements of the micro-climate from sensors placed inside the grow-cell. In this regard, typical practice (e.g. in greenhouses) is to use a relatively small number of individual sensors at locations such as air inlets/outlets, and the middle point of a growing area, to serve as a representation of temperature conditions in the whole facility. By contrast, the present research utilises an array of 33 sensors along the entire length and height of the growing area. The objective is to use these data to gain an improved understanding of the heterogeneous conditions arising, and to identify the limitations of the present air conditioning unit, hence motivating the modelling and environmental control research in Part B of the thesis.

Chapters 3 and 4 consider the prototype hardware design and results of the growth trails respectively. This is followed in Chapter 5 by discussion of the lessons learnt, consideration of energy usage and the conclusions to Part A.

Chapter 3

Development of Grow-cell Prototype

The prototype grow-cell is based on a 12 m × 2.4 m × 2.5 m standard freight container (Fig. 2.1 in Chapter 2), adapted by the present author and industry partner to grow plants under LED lights. This chapter provides technical details about several key subsystems, namely the air-conditioning unit (section 3.1), conveyor system (section 3.2), irrigation system (section 3.3), lighting (section 3.4) and instrumentation framework (section 3.5). The next part of the chapter considers system optimisation issues, using the results from both laboratory-based and preliminary grow-cell experiments. In particular, section 3.6 considers the characterisation and optimisation the LED lighting performance, and discusses the results from an isolated LED growth trial. Sections 3.7 and 3.8 discuss tuning of the conveyor-irrigation system and preliminary interpolated temperature data (obtained during operation of the grow-cell but before the installation of plants), respectively.

3.1   Container and Air-conditioning unit

The freight container base unit is thermally insulated with a foaming system and its maximum heat loss is 40 WK^{-1}. The air-conditioning unit is a Starcool SCI-40, which can create and maintain temperatures as low as -30 $°C$ and as high as 30 $°C$; and can control humidity between 50 and 95 $\%RH$. The cooling and heating capacity of the system is regulated by a Proportional-Integral-Derivative (PID) controller acting
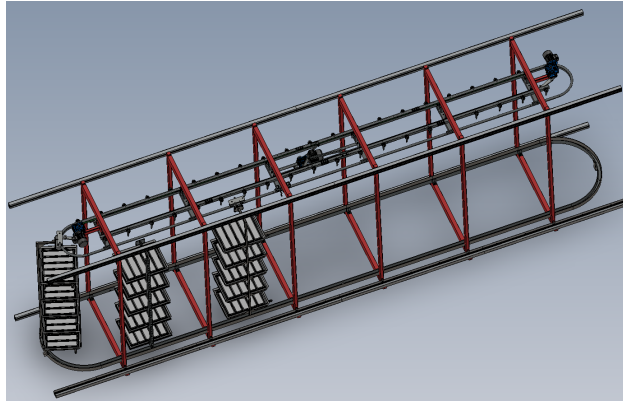
Figure 3.1: Conveyor and racking design schematic diagram.

upon the speed of the compressor. The default air supply configuration comprises a bottom air delivery system, where a t-floor is used to convey the air supplied along the volume of the container. This configuration is modified for the prototype grow-cell, with air delivery entering from the empty space into the growing area, and exiting at its top end. The air is supplied in two speeds, either 4650 m^{3}h^{-1} or 2400 m^{3}h^{-1}, which is determined by the mode of operation (Normal or Economy).

3.2   Conveyor System

The combined conveyor-irrigation system addresses the requirements noted in section 2.4 (Chapter 2). The mechanical form of the conveyor (Fig. 3.1) is an assemblage that can be straightforwardly built and dismantled. It comprises a rounded rectangular circuit, with twenty multi-tray carriers and three motors. The top end of each tray carrier is mounted on the circuit by means of skate wheels, while its bottom end is slotted to a grooved circuit that keeps the body frame vertical to the circuit's trajectory (Fig. 3.2: i–ii). Two motors are employed above the rounded sides of the circuit in order to undertake the sweeping task, while another motor at the centre controls a two sided crank and slotted lever mechanism, which is employed to carry out horizontal movement of the trays (Fig. 3.2: iii–iv).   The levers of the mechanism are steel rods, the bottom sides of which have pegs attached that exert force on the tray carriers. These pegs function as a ratcheting mechanism, allowing each rod to transfer the tray carriers to the respective round side it pushes
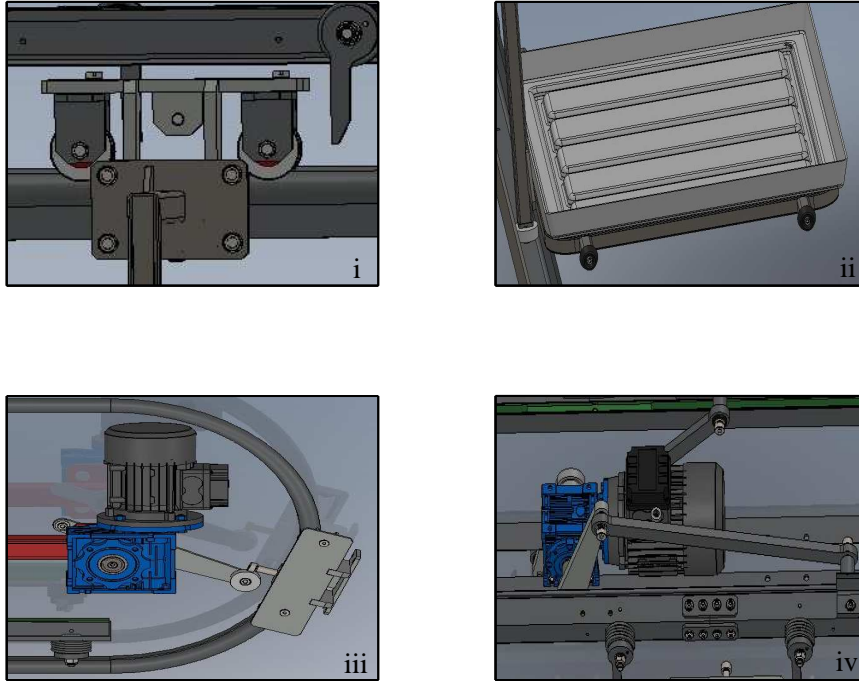
Figure 3.2: Conveyor structure detail showing (i) skate wheels attached to the main circuit, (ii) grooved circuit to keep the body frame vertical, (iii) sweep motion motor and (iv) horizontal motion motor.

towards. All three motors are of an asynchronous type, enclosed and equipped with fan-cooled ventilation. They have cage rotors made of aluminium and are fitted with 100:1 ratio worm gear units in order to simultaneously decrease operating speed and increase output torque. Further manipulation of motor speed can be applied manually through the motor drivers installed at the control panel side.

The circulation of the trays is controlled by a smart relay module (Schneider Electric, model: SR3B261BD). This alternating process (horizontal to sweeping motion) is carried out with respect to the signal output of five sensors. More specifically, two photoelectric sensors monitor the growing trays at the front end, while two proximity sensors and one reflective sensor are used to control the starting position of the sweep and main motors, respectively. The control panel is equipped with a graphical user interface module in order to display the status of sensors and alarms, and also to receive commands from the user.

The two photoelectric sensors that are mounted at each side of the front end of the unit determine the start and stop time for the three motors (Fig. 3.3). The tray carriers are placed in such a configuration that, at both ends, there is eventually a

Figure 3.3: Conveyor structure operation for anti–clockwise rotation (i) system ready for sweeping hangers, (ii) during sweep motion and (iii) system ready for horizontal motion.

carrier waiting to be swept at one side and free space to receive it at the other side. At this state, the first photocell detects a carrier and the second photocell detects the absence of one. This subsequently activates the sweep motors to transfer the trays at both ends (Fig. 3.3: ii). Once the trays are swept across (Fig. 3.3: iii) and the sweep motor arms have returned to their starting position, horizontal motion takes place and the whole process is repeated. The time taken to complete one full circulation can be adjusted. The system was programmed by the present author to operate in three modes, namely Automatic, Manual and Stand-by. The latter is provided in order to stall the system at any time. In Automatic mode, the operation is continuous and each full cycle occurs after a pre-set time delay. The delay timer can be modified from the control panel. In Manual mode, one full cycle occurs at the press of a button.

Several timers are employed in the program in order to monitor the system state and halt it in case of an abnormal signal combination and/or if the time exceeds a threshold for performing a given subtask. The latter time limit for each stage was specified by trial and error experimentation. The nature of the alarm is displayed on

the interface module. Finally, an interlock switch is used to indicate whether the conveyor area is open to allow physical access (curtain open) or not. In this case the system will either not start or will halt immediately to prevent potential damage to people and/or equipment. Detailed information on the design and programming of the control system is laid out in Appendix A.

3.3 Irrigation System

Single point irrigation is provided at the front end of the conveyor structure by five plastic pipes, which are laid out vertically at each layer. Batch control is employed in order to compensate for the water mains pressure variations and ensure consistent delivery of the same volume of water at each layer. During the irrigation phase, the irrigation system is activated each time a new set of trays completes a circulation around the end of the conveyor.

The system used for the growth trial operates as follows: the signal from the photocell that has just received the tray hanger (Fig. 3.3: iii) drives five counters/digital switches. These in turn switch on the solenoid valves and water is injected into the trays. At the water delivery point of each layer a flow-meter monitors the volume of water and yields an impulse output, the frequency of which is linear to the flow. Each of the five outputs is sent to the respective counter, which is pre-set with the desired set-point. Once the set-point is reached the counter switches off the respective solenoid valve. The water drains out of each tray into plastic gutters, which are placed at each layer over the length of the conveyor structure; and collected to a tank for purification and reuse. A main counter and time delay circuit are employed before this system in order to control the irrigation schedule. The frequency of this schedule is adjustable for crop specific water intake requirements (see later section 3.7).

3.4 Lighting

The lighting system comprises 200 thin surface panels, with unit dimensions 0.5 m × 0.3 m × 0.025 m. Twenty adjacent panels are mounted at each side of each layer of the conveyor system in the grow-cell. The distance between the growing trays and the light panels can be changed by adjusting the tray positions (Fig. 3.4). The basic

Figure 3.4: LED lights and empty plant growth trays.

commercial system obtained also has to be adapted so that it is capable of varying its PPFD output. This is necessary in order to ensure suitability for more than one plant species and to reduce energy consumption (see later section 3.6). Hence, the power is provided to the lights via twenty transformers, which are customised for variable DC voltage output that matches the operational range. These are installed in the control room along with the rest of the control and power equipment. Prior to the transformers, configurable time relays are installed in order to control the duration and frequency of the photo-periods for specific growth requirements.

3.5 Instrumentation

Finally, the prototype grow–cell is instrumented in order to obtain a better understanding of the micro-climate, with a particular focus here on temperature and relative humidity as exemplars of spatial variability. Fig. 3.5 shows the approximate location of the combined temperature/humidity USB sensors, which are mounted at the sides and just above the growing trays. An array of 30 equally spaced sensors are distributed within the growing area, each separated by a distance of 1.2 m lengthwise and 0.35 m in height. Three additional sensors are placed in the air supply, growing area inlet (sensor number 32 in Fig. 3.5) and outlet (sensor 33). The sensors have a storage capacity of up to 16382 readings, with a user-selected sampling rate as fast as 1 sample per second. However, the sampling rate for the measurements presented in this article was set at 10 seconds to allow for a longer time series. Finally, their
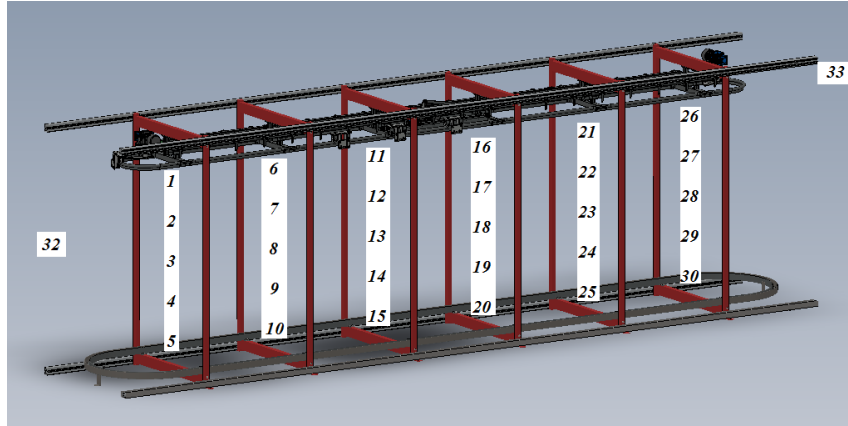
Figure 3.5: Sensor locations in the grow–cell. Note that sensor 31 (not shown) is located at the air intake of the unit.

accuracy is $\pm$ 0.3 °C and $\pm$ 2 %RH. In addition, *ad hoc* airflow measurements were manually taken at various locations using a portable hot–wire air flow meter, which has a resolution of 0.01 ms^{-1}.

3.6 LED Characterisation & Optimisation

To investigate the LED panel characteristics beyond the manufacturers specifications, tests were carried out on selected lights in a laboratory environment. The tests undertaken on other candidate lights are laid out for reference in Appendix B. In the first instance, the spectral characteristics are determined using a light spectrometer (Uprtek AI-MK350D). The spectral output of a typical panel is visualised in Fig. 3.6, where it can be seen that most energy packets arrive from the blue wavelength band, with a peak at 448 nm. However, the phosphor coating that has been applied to the LEDs by the manufacturer, in order to yield a white colour output, results in some additional light arriving from the green and orange–red wavelengths.

Secondly, a broad wavelength photosynthetically active radiation (PAR) meter is utilised to measure the PPFD magnitude (μmols m^{-2} s^{-1}) over the operating range. The latter test was subsequently extended in order to assess the distribution of PPFD in the area directly below and adjacent to the light source, as well as to quantify the accumulation of PPFD when two light sources are placed next to each other. Note that the PAR meter utilised for this research only counts the moles of photons within the 400-700 nm band, hence any relatively little light arriving
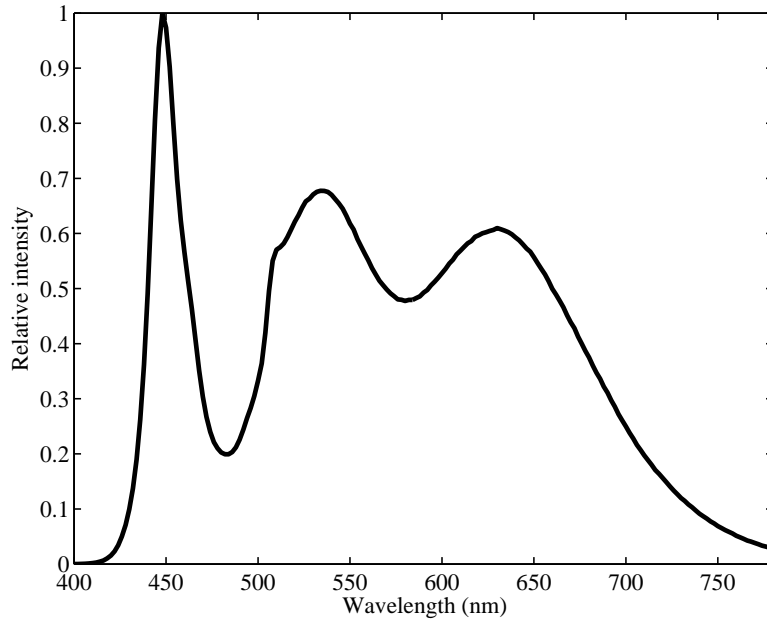
Figure 3.6: Spectral output of lights installed in the grow–cell.

from the near infra-red region is not added to the cumulative PPFD. Fig. 3.7 shows one light panel fixed at 0.2 m above the centre of the measuring board, with the holes representing 104 measuring points below and adjacent to the sides of the light panel. These measurements were taken in a dark room without any other light sources present and with a dark coloured measuring board in order to minimise its reflectivity. Fig. 3.8 shows the spatial distribution of PPFD at a distance of 0.2 m below one panel and under different power supply levels. The area projected in each subplot has the same 0.5 m × 0.3 m dimensions as the light panel. The 40 measuring points pertinent to the panel were interpolated to yield the PPFD distributions. Fig. 3.8 shows that most of the energy is delivered at the centre of the illuminated area, as would be expected. Table 3.1 states the observed PPFD levels at the centre (maximum PPFD) and corner (minimum PPFD) of the board for each power input.

Related to these results, Fig. 3.9 shows that a power supply set to 73% of the standard (maximum) setting, yields a light output only slightly lowered (96%) from the maximum PPFD, indicating considerable scope for energy savings by suitable tuning of the system. In fact, it is clear these light panels operate most efficiently within the 50% to 73% power supply band, which can deliver a PPFD level between 120 to 210 μmols m^{-2} s^{-1}. Here, the 50% limit is based on discussions with growers (this lower bound is considered sufficient for *Begonia semperflorens* and *Impatiens*
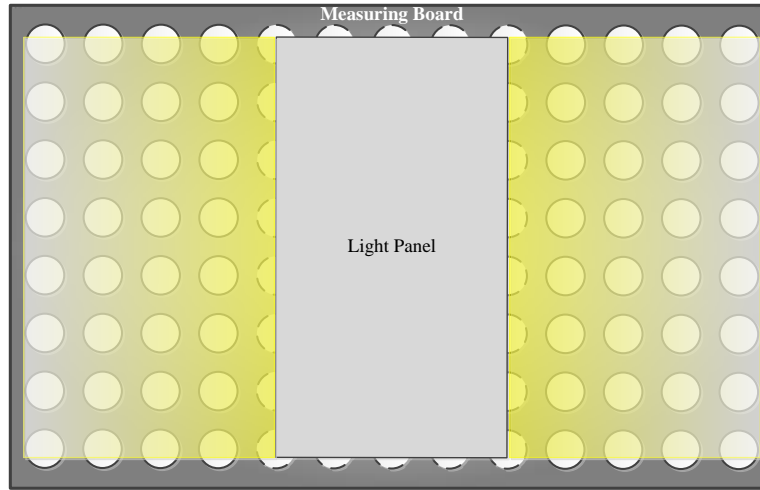
Figure 3.7: Schematic diagram of the 0.9 m× 0.5 m board for measuring PPFD magnitude, with one light panel and 104 measurement points.

Voltage (%)	min (μmols m^{-2} s^{-1})	max (μmols m^{-2} s^{-1})
40.0	33.4	113.0
46.5	38.0	128.0
53.0	42.7	144.4
60.0	48.5	163.8
67.0	56.0	189.0
100.0	64.2	217.0

Table 3.1: Minimum and maximum light intensity for Fig. 3.8.

divine) whilst the 73% is the inflexion point in Fig. 3.9. All twenty transformer units require 15 kW to provide maximum power supply to the lights but at 67% power supply, for example, this drops to 11 kW. For plants that do not require high PPFD levels, it is possible to reduce the power requirements even further.

Although most of the light energy is delivered directly below the panel, some light is naturally dispersed towards adjacent sides. In general, the magnitude of this dispersion depends on the distance of the light from the illuminated area and the angle at which the individual LEDs are manufactured to emit. In this case, the PPFD ramps down to approximately 2 μmols m^{-2} s^{-1} at 0.3 m adjacent to each
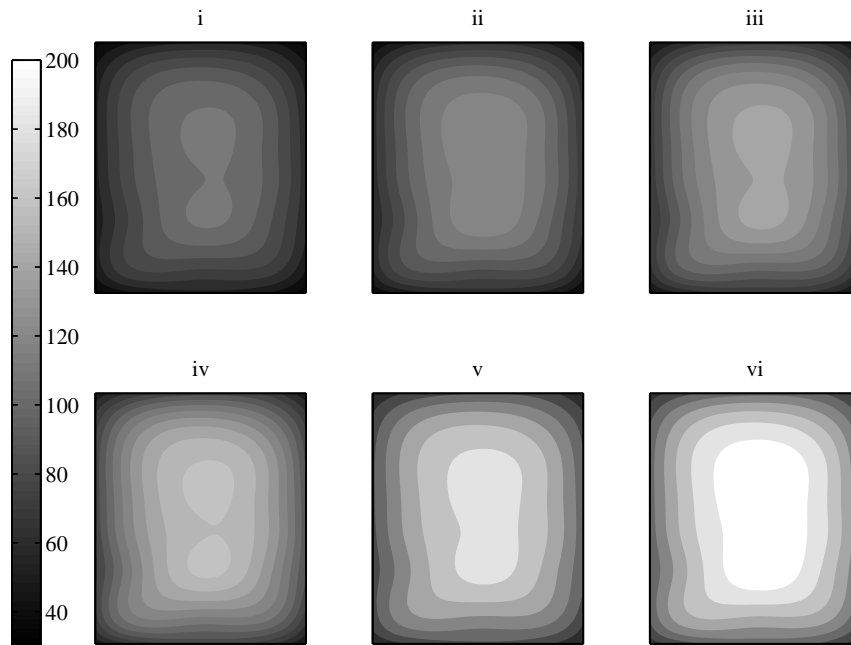
Figure 3.8: Spatial distribution of light intensity (μmols m^{-2} s^{-1}) at a distance of 20 cm. Subplots i through to vi are for voltage levels of 40%, 46.5%, 53%, 60%, 67% and 100% intensity of the variable power supply. Each subplot indicates the light intensity over the 50 cm (vertical axis) by 30 cm (horizontal) light panel.
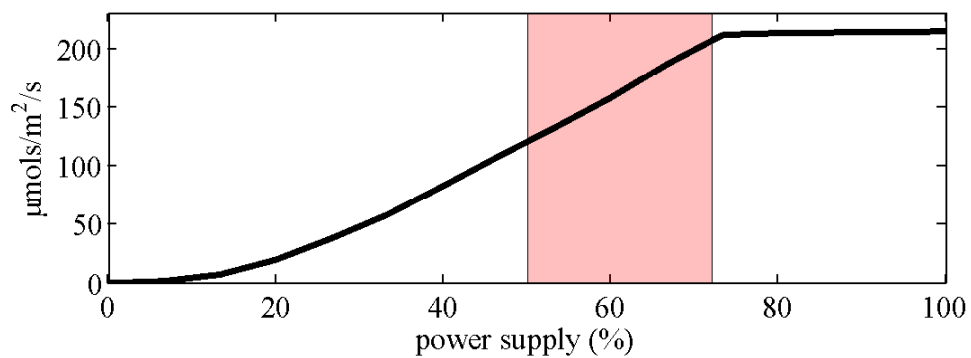
Figure 3.9: Single panel light intensity plotted against supply voltage expressed as a percentage of the maximum, highlighting the most energy efficient intensities (shaded).
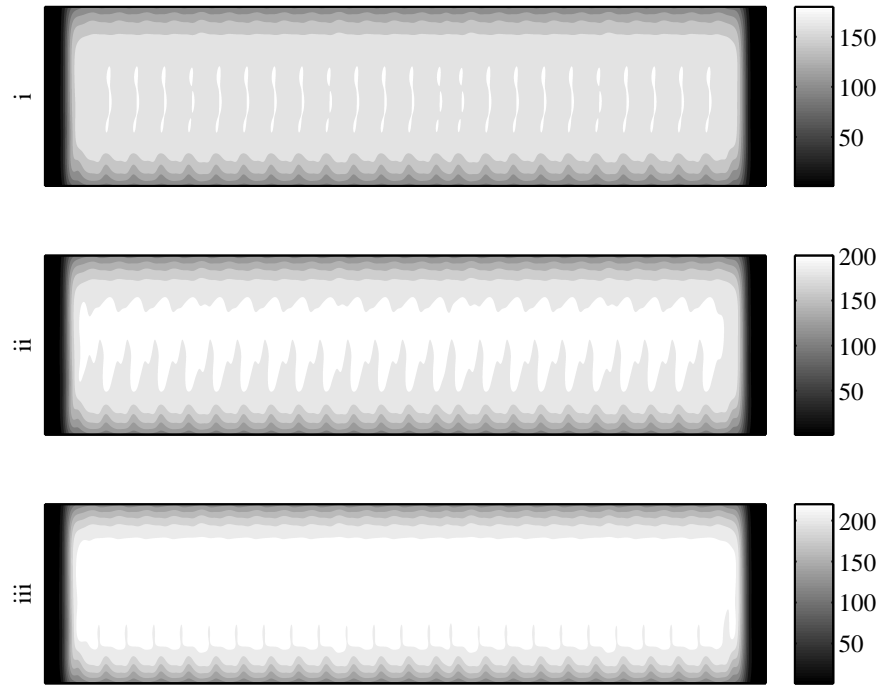
Figure 3.10: Spatial distribution of light intensity (μmols m^{-2} s^{-1}) for 20 light panels in one layer, with i) 60%, ii) 67% and iii) 100% of the maximum power supply. Each subplot indicates the light intensity over 50 cm (vertical axis) by 6 m (horizontal).

side of the panel. Extrapolating from these results, Fig. 3.10 i-iii displays the light intensity distribution along the length of one side layer within the grow–cell (i.e. 20 panels over 6 meters length), for three different power supply levels. On account of the cumulative effect of the dispersed light when light panels are arranged next to each other, it is observed that for all three power supply levels the overall light intensity is increased by 11%.

3.6.1 Preliminary LED Growth Test

A laboratory based test using these lights was conducted for non-stop Tuberous begonias (*Begonia tuberhybrida*), a type of begonia grown for propagation by the third party company that also ran the full scale growth trial. Production takes 13 weeks in their greenhouse environment, whilst it took 50% less time to grow them to the same stage under the LED lights. Fig. 3.11 shows the difference between 4 week begonia plantlets under the LEDs (middle tray) and those grown in the greenhouse. This type of experiment suggests that the energy consumption of LED lights can potentially be compensated for by increased production rates. However, this is an
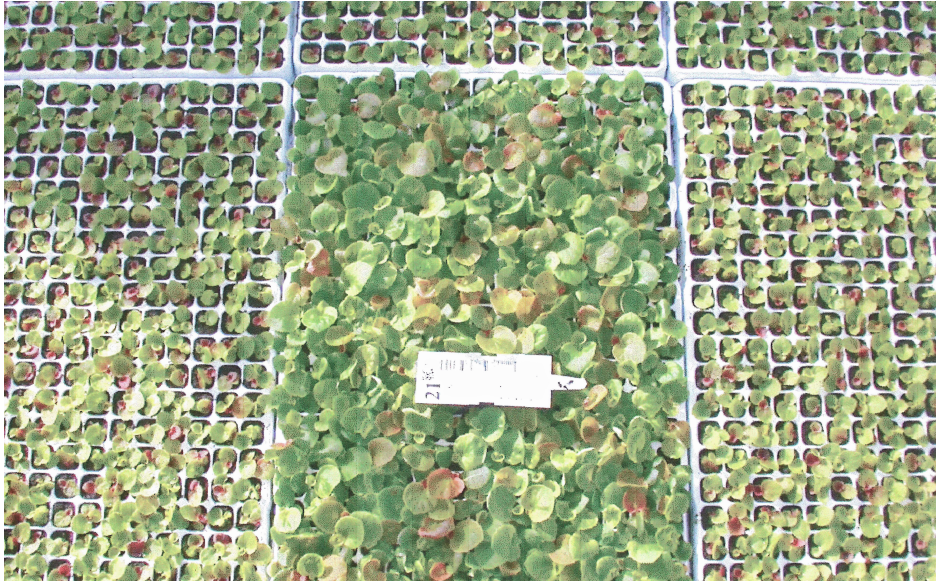
Figure 3.11: Four weeks old *Tuberous begonia* plants grown under white LEDs (middle tray) and in a greenhouse (the other trays).

illustrative result only, used to test the LEDs before proceeding to the growth trials.

3.7 Conveyor-Irrigation System Tuning

To sweep one set of trays around the end of the conveyor racking takes at least 45 s. Experimentation in the laboratory determines this is effectively the fastest speed that can be achieved without risking mechanical problems, i.e. the pegs and sweep motor arms exert just enough force to move the trays. Hence, this setting was selected for practical use and no problems were encountered during the growth trial, when the conveyor system was in continuous operation for nearly 8 weeks. By contrast, the frequency of circulations is intended to be adjusted according to the light and dark periods, irrigation schedule and other pre-programmed tasks, such as inspection and harvesting.

For instance, in regard to inspecting the crops, a delay of 30 s between circulations is found to be sufficient, whereas placing or removing the trays requires at least 60 s. For practical operation, such schedules are decided by trial and error adjustment in consultation with the grower. The batch control approach to irrigation is determined to require 120 s between circulations. This is in order to deliver water within a reasonable time-frame, in such a manner that all the plants get sufficiently wet.

Outside the time frame of an irrigation cycle, a much slower circulation rate is generally employed. During the light period, for example, any adjustments to the frequency are dependent on the distance of the lights from the plants, the PPFD levels used, and the temperature and humidity gradients arising in the grow–cell. Together, these determine the drying rate. For the growth trials, the lights are on 16 hours a day, from 12 am to 4 pm, to take advantage of lower costs during the night, whilst the distance between the trays and LEDs is 0.2 m. For these specific conditions, a frequency of four circulations per hour is found to yield a relatively uniform soil drying rate as required by the grower.

3.8   Interpolated Temperature Data

The following figures are based on measurements taken following completion of the racking and conveyor system but before the installation of plants. In order to visualise temperature distributions in the grow-cell arising from the LEDs, Fig. 3.12 is based on the average steady state temperatures for each sensor, with the data interpolated using MATLAB in order to yield the contour surface shown. These data were logged from 6 pm to 8 am with the lighting period commencing at 6:30 pm for eight hours. The supply air temperature set-point for the air-conditioning unit was 12.5 °C and the RH 65%.

During the photo-period the maximum temperature gradient within the airspace reaches 4.2 °C. The coolest area is closest to the inlet whilst the warmest is above 1 m and between 4 m to 5 m horizontally along the growing area. The effect of the exhaust fan at the outlet is visible in the two lower shelves where heat is extracted quicker than from the upper layers. By contrast, during dark periods, the effect on the temperature distribution due to the circulation of the airflow is insignificant, with the temperature throughout the grow–cell remaining within $\pm$ 0.5 °C of the set-point at all times (Fig. 3.12: lower plot). The truncated-like interpolation depicted in this case is due to the narrow gradient of the raw data. Fig. 3.13 and Fig. 3.14 show a different experiment in which the lights are switched on at 7 pm and remain in that state as the temperature set-point is lowered by 2 °C every three hours, i.e. from 20 to 14 °C. In this case, the steady state temperature distribution shows a similarly
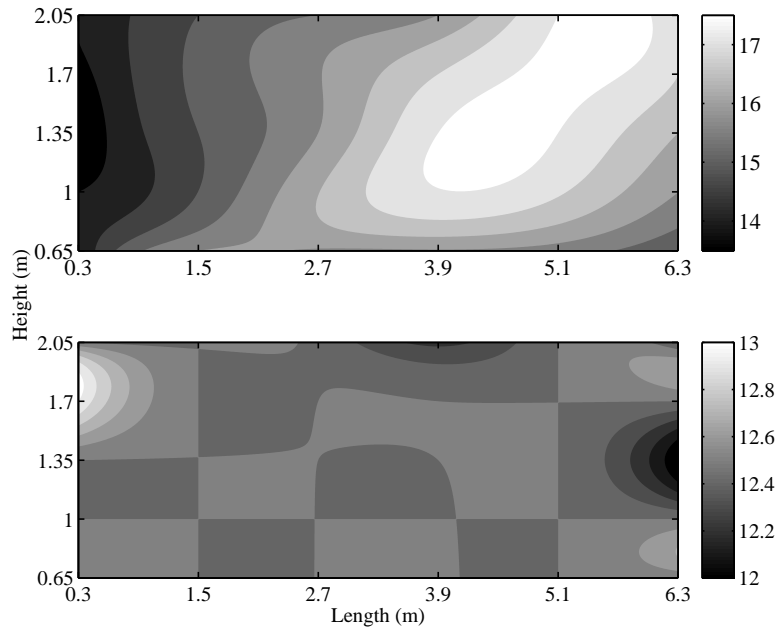
Figure 3.12: Steady state temperature distribution with lights switched on (upper subplot) and off (lower). Spline interpolation from the 30 point measurements using Matlab.

shaped distribution since the incoming ventilation is unchanged. Fig. 3.14 shows that the temperature at the exhaust is constantly warmer by 2.5 °C than the supply temperature.

For a different experiment, Fig. 3.15 shows the transient response of the temperature distribution with a 10 minute interval between plots. From the moment the lights are switched on and for the following 10 minutes, the temperature distribution is relatively uniform (Fig. 3.15 i–ii). However, over the following 1.5 hours the temperature gradient range becomes increasingly obvious. At the 50th minute (Fig. 3.15 vi) it can be seen that the areas around the inlet have reached their steady state level for these heating and ventilation settings. By contrast, it takes the area towards the outlet over one hour and ten minutes after the lights have been switched on to reach steady state (Fig. 3.15 viii).

These results indicate to an extent that the current air-conditioning controller does not have the capacity to fully compensate for the heat generated by the lights and that some regions suffer from a lack of adequate fresh air supply. However, information such as the volumetric inlet air-flow after the grow-cell was partitioned, as well as the number of hourly air exchanges would allow for more confident conclusions.
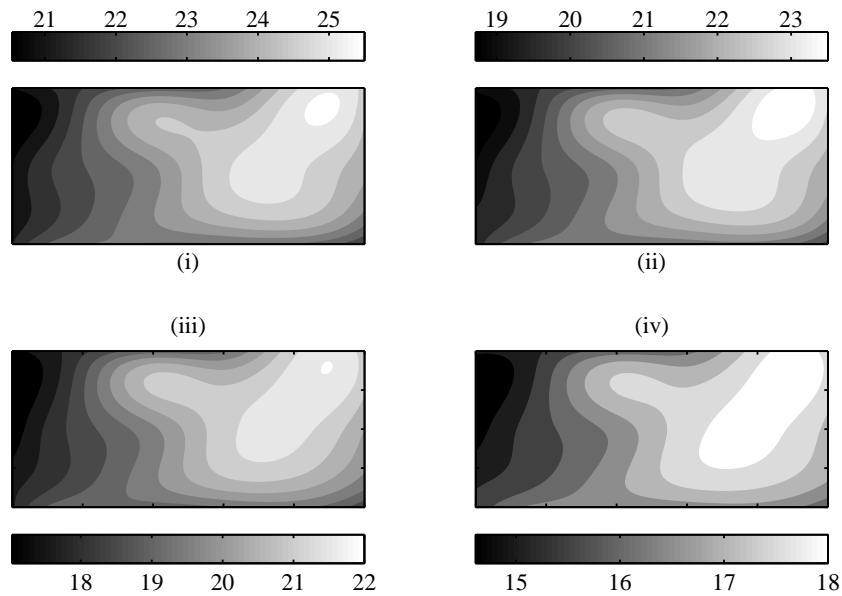
Figure 3.13: Steady state temperature distribution for setpoints 20 °C (i), 18 °C (ii), 16 °C (iii) and 14 °C (iv). The height and length axis (not shown) for each subplot are identical to those in Fig. 3.12.
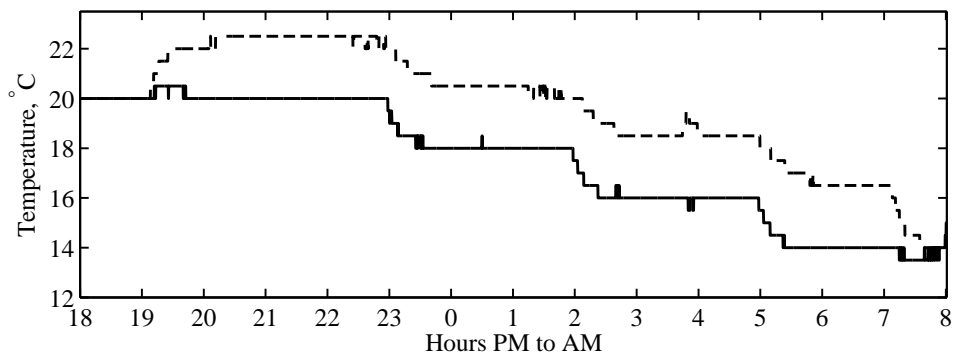
Figure 3.14: Supply and exhaust (dashed trace) temperature associated with Fig. 3.13.
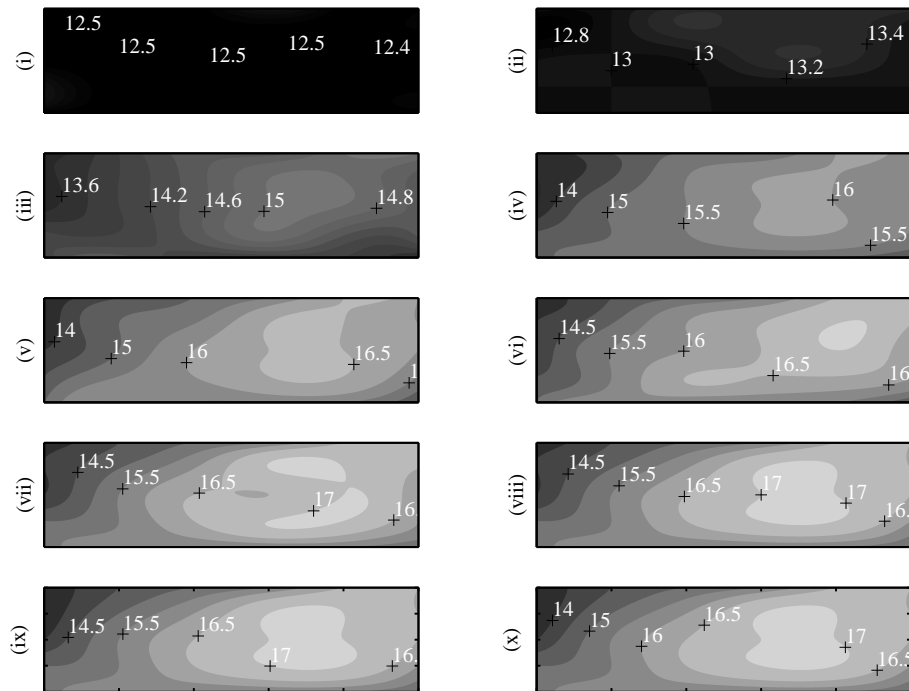
Figure 3.15: Transient response of temperature distribution in the growing area shown at 10 minute intervals from the moment the lights are switched on (i) through to 1.5 hours later (x). The height axis, length axis and legend (not shown) for each subplot are identical to those in Fig. 3.12. Numerical values are illustrative temperature point measurements, °C.

In this thesis, it was only possible to investigate this using a hot–wire air flow meter in an *ad-hoc* manner; the measurements of which shows that air typically enters the supply location with a velocity of 10 ms^{-1} but is dispersed into the growing area with an average velocity of 1.7 ms^{-1}. There is very little variation in airflow between the trays at different heights. Similar conditions occur during the later growth trials due to the relatively small size of the plantlets. Finally, the exhaust fan draws air at a velocity of 7 ms^{-1} and enhances the air velocity towards the outlet slightly, particularly for the lower levels, explaining the cooler temperatures in this region. On the other hand, one may argue that

3.9   Conclusions

This chapter has provided brief technical information about several key subsystems of the prototype grow-cell, with additional details provided in Appendices A, B, and D. The chapter has also shown how both laboratory and field tests can be used to help optimise some of these subsystems for particular plant types and growth scenarios. In general terms, the conveyor-irrigation and lighting systems can be adjusted to make the grow-cell more cost effective and sustainable (although operating costs and other economic considerations are beyond the scope of the present chapter). However, more specifically in the context of the present work, these subsystems have been adjusted for the particular requirements of the *Begonias semperflorens* growth trials reported in the following Chapter 4. Finally, analysis of interpolated temperature data presages likely challenges in respect to the stratification of environmental conditions within the grow-cell.

Chapter 4

Growth Trials

The growth trials took place between January-March and June-July 2015. The third party company that tested the pilot grow-cell is a nursery which grows edible and ornamental plants (Bordon Hill Nurseries)[1]. Of particular interest to this nursery, in the context of the grow-cell, is the propagation of three species: *Begonia tuberhybrida* (non-stop), *Impatiens divine* and *Begonia semperflorens*, all of which are potted in plugs and produced up to a young age for the commercial trade. The first trials were undertaken using only one layer of trays in order to reduce costs and initially prove that the concept works to the required standards of the nursery, while the second trials included one layer for each of the three species. These trials are considered in sections 4.1 and 4.2 respectively, while section 4.3 focuses on the micro-climate conditions arising inside the growth chamber for both sets of trails.

4.1   January-March 2015 Growth Trial

In the first trial, the begonia seeds (*Begonia semperflorens*) were sown in 240 cell seed propagation trays, prefilled with soil. Two of these trays fit into each grow-cell tray, making a total of 9600 seeds for the layer under trial. During irrigation, the grow-cell trays are filled to the top and then drained. In this manner, the plants' soil is kept moist until the next scheduled irrigation. Furthermore, plastic pieces of piping are mounted between the grow-cell and seed trays in order to air-prune

[1]As part of the PhD project, the present author took the opportunity of a placement in order to set up and monitor these growth trials.
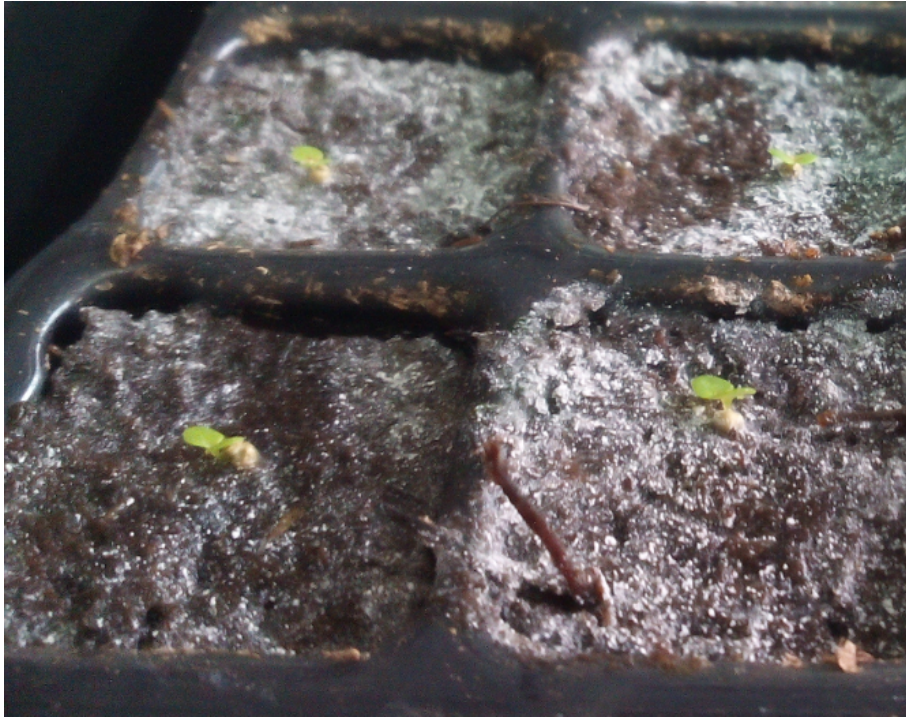
Figure 4.1: *Begonia semperflorens* plants germination period.

the plants. This is a technique which keeps an air gap in order to limit the plants' root development within their individual cells. Throughout the growth period the plants were irrigated every 30 hours, receiving a blend feed of Natrium, Phosphorus and Potassium. The temperature setpoint was 22 °C, with the RH 95% during the germination period and gradually lowered to 65 % RH over the course of the trial as follows: (i) 30/01/2015, 22 °C, 95 %RH; (ii) 12/02, 22 °C, 85 %RH; (iii) 16/02, 22 °C, 75 %RH; (iv) 06/03, 22 °C, 65 %RH; (v) 12/03, 16 °C, RH control off; and (vi) 16/03, 16 °C, 60 %RH.

Two weeks following germination (see Fig. 4.1), the vegetative stage of the seedlings showed fast development (Fig. 4.2). By the 5th week, the trials were officially complete, two weeks ahead of the scheduled (greenhouse-based) production. Naturally, generalised conclusions about the relative performance of the grow–cell cannot be made from this illustrative feasibility trial. Nonetheless, in consideration of the intended aim, it successfully demonstrates that *Begonia semperflorens* can be grown to the satisfaction of the nursery, with Fig. 4.3 showing the ready plantlets.
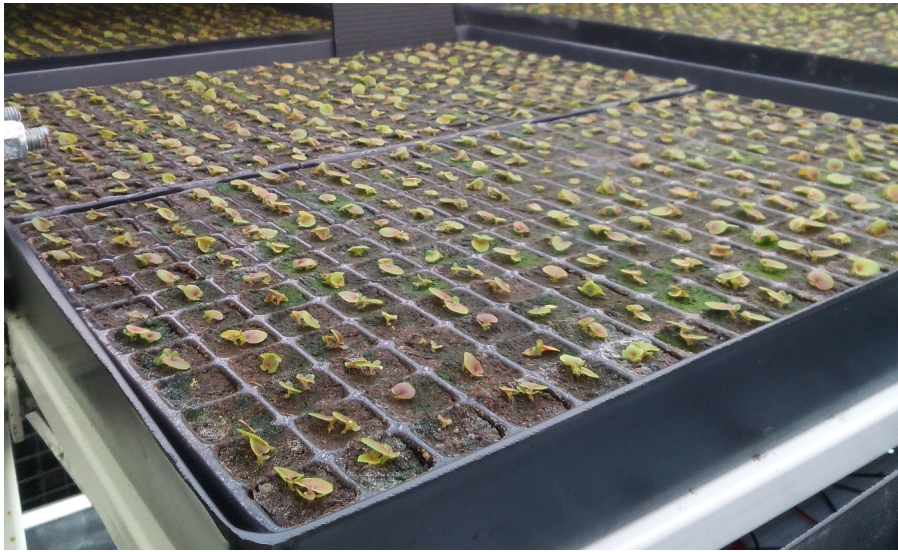
Figure 4.2: Three week old *Begonia semperflorens* plants.

Figure 4.3: Finished *Begonia semperflorens* plants before harvest.

4.2   June-July 2015 Growth Trial

For the second trial, three different kinds of plants were grown in dedicated layers, with a similar arrangement to the first trial in terms of seed quantity, feed and irrigation schedule. The delivery of light was continuous throughout the first 12 days and on a 16 hour interval for the rest of the growing period (12 am to 4 pm, to take advantage of lower costs during the night). Similarly, the temperature set-point was 22 and 23 °C during the night and day respectively, while humidity was not controlled during the first twelve days but was subsequently set to 80% RH and then reduced in an *ad hoc* manner by the nursery to 65% RH for the remaining period. During this second stage of the trial, the voltage to the lights was increased by 15%.

Impatiens Divine showed a growing rate similar to *Begonia semperflorens* in the previous trial. Both of these types were ready to harvest by week 5, as illustrated in Fig. 4.4 and Fig. 4.5 respectively. Moreover, root growth and leaf yield showed to be normal and near greenhouse production quality, as illustrated in Fig. 4.6 and Fig. 4.7.

By contrast, *Begonia tuberhybrida* normally takes 13 weeks to grow to the desired stage in a greenhouse and were expected to be ready by week 7 under LED lights. However, they had not grown to the expectations of the growers by week 5. In particular, they displayed a rather uneven growth profile as illustrated by Fig. 4.8. In the view of the growers, the cause for this failure was that the soil used was unsuitable for this type of plant. As a result, the growth trial for *Begonia tuberhybrida* finished earlier than planned.

4.3   Temperature and humidity observations

During both trials, micro-climate measurements were taken with a sampling rate of one minute, with the sensors mounted at the sides just above the growing trays. The collected data capture most of the periods listed above except for a few days, which were lost due to the process of downloading data from the sensors and setting them up to collect the next batch. During the first trial, for example, from the 30th of January until the 23rd of March, 1092 hours of temperature and humidity data were recorded (45.5 days) while 145 hours (6 days) were lost. Fig. 4.9 shows the

Figure 4.4: Finished *Impatiens divine* before harvest.

Figure 4.5: Finished *Begonia semperflorens* before harvest.

Figure 4.6: Root growth of *Impatiens divine.*

Figure 4.7: Root growth of *Begonia semperflorens.*

Figure 4.8: Unfinished *Begonia tuberhybrida*.

daily temperature variations along the length of the layer where begonias were grown during the first trial (see Fig. 3.5 for exact location of the sensors). Here, *Begonia semperflorens* were grown in the second layer from the top, with the other layers all empty (and with the LED lights switched off). Sensor 2, which is located at the front end of the layer of interest, is the only location on which the photo-period has negligible effect. This was expected as the air exchanges are more frequent at that location. Sensors 7 and 12 deviate by about 1 °C from the set-point (dashed black trace) during photo-periods, while further along the layer, sensors 17 and 22 reach 23.5 to 24 °C. In a similar manner to these, the back end sensor (27) deviates by about 1.5 °C from the set-point during lighting periods. The unused layers below the begonias are hardly affected by to the photo-periods. On the contrary, the top layer, which is above the begonias, did present a trend similar to Fig. 4.9 but at a smaller magnitude and only towards the back end of the growing area.

Again, for the first trial, the mean temperature and humidity distributions along the length of the grow-cell during light and dark periods are illustrated in Fig. 4.10 and (Fig. 4.11) respectively. These figures are generated using spline interpolation from the point measurements in MATLAB. As noted above, the begonia layer and the one immediately above it yield temperature levels up to 24 °C, while the temperature in the lower layers remain close near the set-point at all times. Furthermore, as
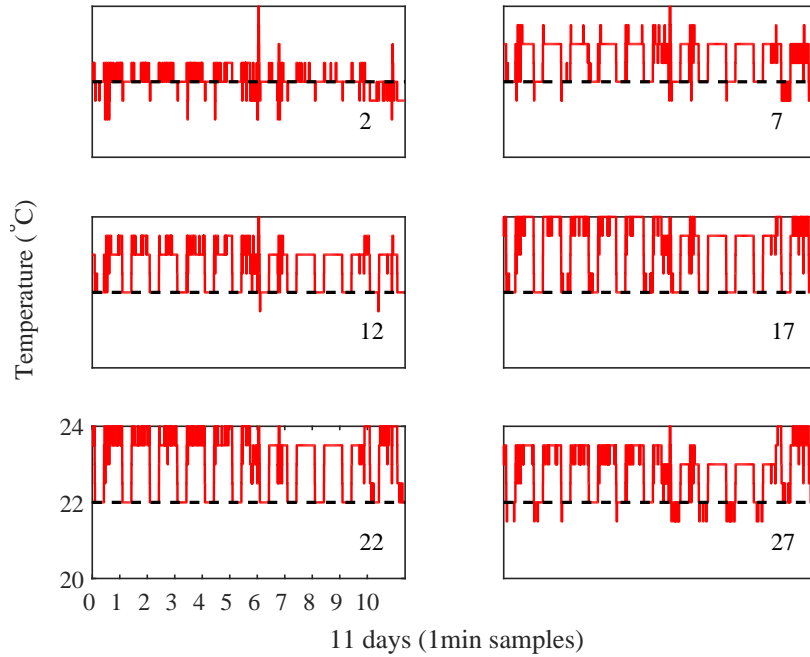
Figure 4.9: Selected temperature sensor readings from layer 2 during the first trial, January 30 to February 10. The numbers 2, 7, 12, 17, 22 and 27 refer to the sensor locations in Fig. 3.5.

previously seen in section 3.8, the temperature distribution is relatively uniform and close the set-point during dark hours but shows significant variation during the light periods. In a similar manner to the temperature, the humidity distribution (around the set-point of 95%RH) was uniform for the three layers below the growing layer. However, the growing layer humidity drops to as low as 85%RH during photo-periods and climbs to 92%RH during dark hours (Fig. 4.11) because of the plants. The overall deviation from the set-point lies in the range 11%RH and 5%RH.

Finally, Fig. 4.12 displays the average temperatures and humidities for each layer, together with set-point data, for the whole growing period of the second trial in three hour intervals. During the first twelve days with a continuous photo-period, the active growing layers are consistently warmer by 1 to 3 °C. This gradient increases throughout the remaining period due to the excess heat generated by the increasing the voltage to the lights. The conditions for the two inactive layers at the bottom of the grow-cell are shown by black traces. As expected, the inactive layer at the bottom yields conditions closest to the set-point while the upper one receives a significant amount of heat due to the lights operating above it. The humidity shows
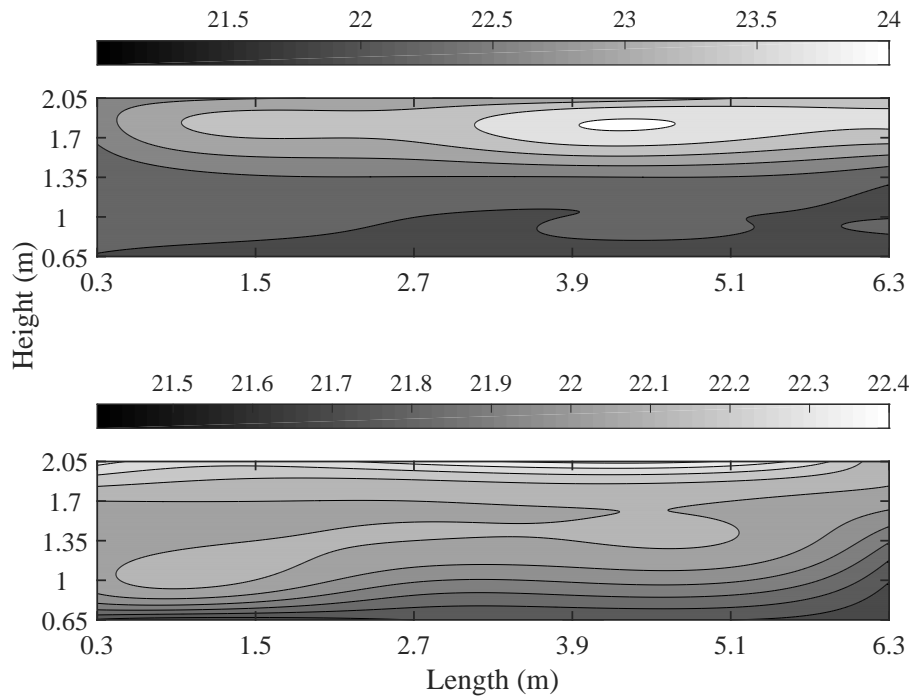
Figure 4.10: Interpolated temperature spatial distribution during lighting (upper plot) and dark (lower) hours, January 30 to February 10.

less variation in general.

4.4   Conclusions

The present chapter has briefly discussed the growth trials that took place between January-March and June-July 2015 by a third party company, a nursery which grows edible and ornamental plants. The discussion has largely focused on practical issues such as the feed system and micro-climate spatial variability. In fact, the primary objective of the growth trials within the scope of the present thesis was to test the entire prototype grow–cell system in an illustrative practical situation, to evaluate reliability of the developed feed, LED and conveyor system, and the ability to grow ornamental plants in a general sense.

In this context, the growth trials were regarded as a success by the industry partner and collaborating nursery. For *Impatiens divine* and *Begonia semperflorens*, the uniformity of the crop was reported as satisfactory, mainly due to light consistency, although plants were relatively smaller at the outer edges where the light intensity
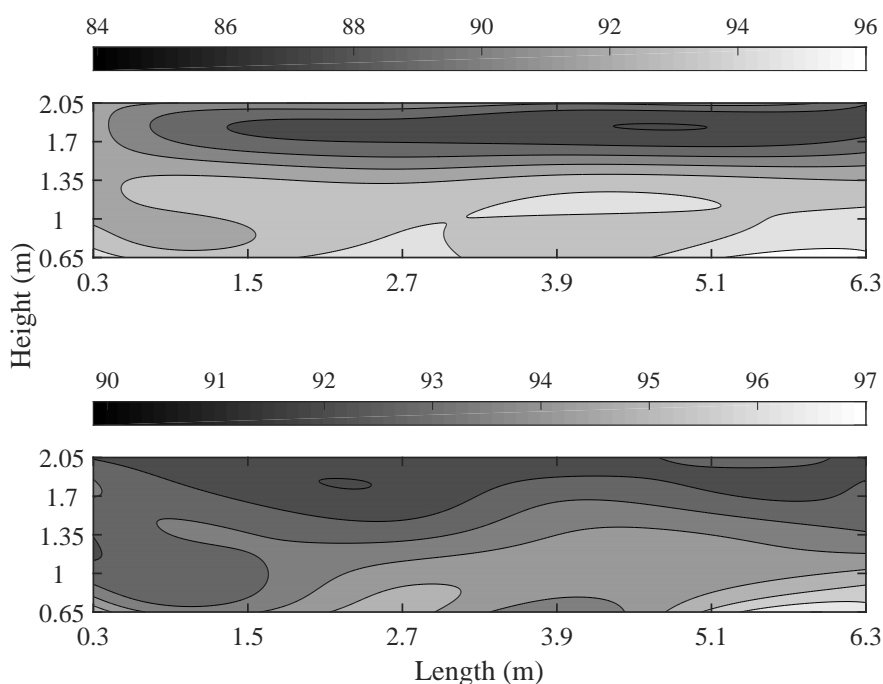
Figure 4.11: Interpolated humidity spatial distribution during lighting (upper plot) and dark (lower) hours, January 30 to February 10.
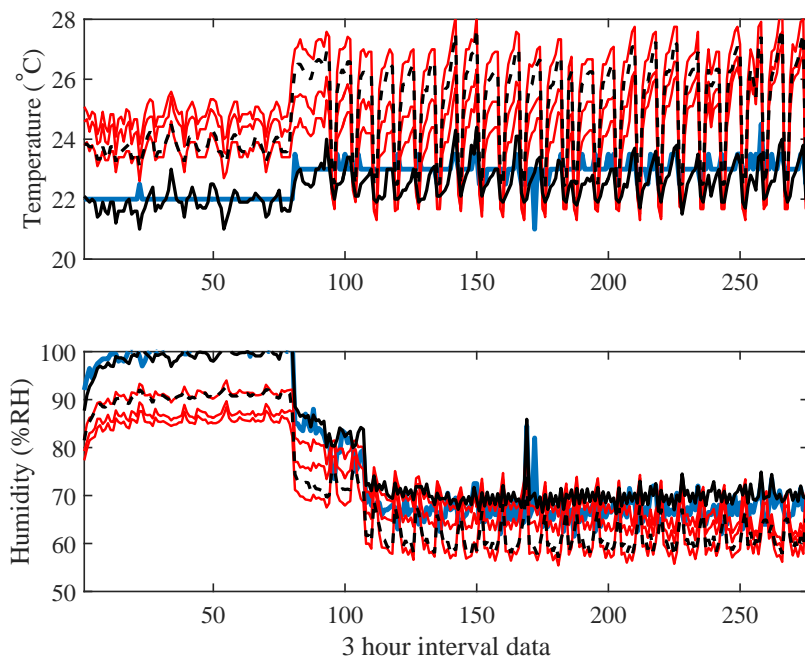
Figure 4.12: Temperature and humidity responses throughout the five week period of the second trial, plotted against sample number (3 hour samples). The set-points, active and empty layers are indicated by blue, red and black coloured traces respectively.

is lowest. Survival rate of plants was not formally quantified but is reported to be close to 100%. Growth of *Begonia tuberhybrida* was less successful and it is believed this relates to the soil used, although this requires further research.

More systematic experiments that use the grow-cell to rigorously investigate plant development, plant quality and whole system operating costs is an essential next step for future research. Indeed, this is the motivation for the development of the prototype in the first place. In this regard, the lessons learnt and some preliminary cost considerations are discussed in the following Chapter 5.

Chapter 5

Discussion and Conclusions

Based on the literature review, design considerations and laboratory work from Chapters 2 and 3, and the growth trial results from Chapter 4, a number of observations and recommendations can be made regarding the grow-cell prototype, particularly in relation to the control of micro-climatic variables within the airspace, subsystem design issues, energy consumption and operating costs. These are discussed in sections 5.1 through to 5.6 below, followed in section 5.7 by a brief summary and conclusion. In this manner, the present chapter provides the conclusions and suggestions for further research that are connected to Part A of the thesis.

5.1   Freight container and air-conditioning unit

The development of the test grow-cell was based on a freight container, for which the original Heating-Ventilation and Air-Conditioning (HVAC) unit had been been selected and optimized for food storage rather than plant growth. Hence, it has an energy cumbersome heating and cooling capacity to begin with. Partitioning the airspace into two sections changed the whole structure of the air-flow supply system, while the incorporation of lights added heat within the environment that is clearly not fully compensated for by the HVAC unit. This is evident in, for example, Fig. 3.12, Fig. 3.13, and Fig. 3.15. Added to the above is the empty space that the air has to travel before reaching the entrance of the growing area, at which point its flow reduces significantly. Despite these limitations, which will primarily impact upon the energy consumption costs, Chapter 4 showed that the unit was generally

sufficient in terms of providing the conditions required for plants to grow.

Two very simple future modifications, apart from re-sizing the HVAC's heating and cooling capacity, relate to the distribution of the airflow and the incorporation of sensors in the growing area. For the former, a horizontal airflow supply scheme, by utilising louvres and dampers at the entrance of the growing area would need less power to operate (in practice, plants need a ventilation rate as low as 1 ms^{-1}). With the current configuration, an unnecessary (by default) 10 ms^{-1} was used, decreasing to about 1.5 ms^{-1} at the entrance of the growing area. Furthermore, by utilising temperature, humidity and airflow sensors along the growing area, the HVAC unit would have more information in order to compensate for the heat gain induced by photo-periods and the humidity gain associated with this and the irrigation cycles. Control systems should be developed that utilise this information and so improve the homogeneity of the growing volume by acting upon the magnitude of the air-flow, dampers and louvres in an appropriate manner. Such a scheme would also reduce the conveyor system's energy usage as it would not need to carry out extra circulations to compensate for an irregular micro-climatic distribution; it would be used instead only for irrigation, inspection of the crop, and pre/post harvesting tasks.

5.2 Conveyor system

The industrial partner and the author jointly developed a novel system for circulating plants around the growing area. The straightforward mechanical design for the racking and conveyor can be adapted to fit differently sized containers, and offers a generic framework for future development. The incorporation of the conveyor system also proved to be useful in terms of compensating for the heterogeneity of the micro-climate, while fine tuning its circulation frequency allowed for balanced drying rates during the growth trials.

The conveyor system can further benefit from several modifications for the purpose of increasing its precision and ease of maintenance. For example, the crank and slotted lever mechanism that produces the horizontal movement does not guarantee precise displacement each time. Several alterations were carried out on the height of the pegs that pushed the tray carriers, in order to compensate for this inaccuracy.

During the growth trials, it was further noticed that the grooved circuit at the bottom of the conveyor that keeps the body of the tray carriers vertical also lacked mechanical precision, as it always sat still at a slight angle. This in turn affected the water's distribution within the trays, and more water had to be delivered in order to ensure that each soil bed gets appropriately wet.

Furthermore, although the tray hangers can be adjusted to change the distance between plants and lights, there are currently no marking points to indicate a certain distance (e.g. pre-drilled holes where the tray hanger can be mounted). These would significantly reduce the time it takes to readjust their position, and ensure precise levelling. Moreover, the top and the back sides of the structure were not accessible upon assembly and there was minimal space to work with. This made maintenance of the main motor, for example, rather difficult in practice. In this respect, it would be beneficial to create openings at key locations, where the user can have access from outside the container. Finally, pre and post harvesting automation, fitted adjacent to the grow-cell would save a lot of time for tasks like insertion and extraction of the trays. In fact, such a scheme is essential for multiple stacking grow-cells.

5.3 Irrigation system

The irrigation system was originally developed in order to facilitate plants in ebb and flow trays. This means that water would be filled to the top and drained to gutters for purification and re-use. However, the plants that were actually tested during the trials were grown from seedlings (this is because of the demands of the particular nursery that offered to collaborate on the growth trials within the time frame of this project). Hence, the latter irrigation approach proved incompatible and was revised as follows.

The practice followed for growing seedlings is typically the incorporation of a spraying boom that produces very thin droplets of water. Such an approach is essential as it increases the humidity of the growing environment, which is needed at germination stage, and it gently wets the soil upon which the seedlings sit without dislocating them from their sowing position. In order to bridge this incompatibility, the water delivery point was modified using angled plastic pipes, and diverted to

the corner of each tray. This minimized the risk of dislocating seedlings and the soil would get wet from the bottom to the top. Furthermore, the humidity set-point of the air-conditioning unit had to be constantly kept high. However, wetting the soil bed in this manner had problematic implications. Small lumps of soil beneath the plants would block the draining points, thus not allowing the water to drain, and in turn not allowing the air-pruning of plants. The measures taken to overcome this problem included use of a special type of soil, which contained a form of natural glue to keep the soil in place. In addition, small pipe filters were mounted at the drain points to further reduce this risk.

Another issue that was faced during the growth trials was the mains pressure variation. This resulted in a different length of time to deliver the same volume of water at each tray. Even though the author incorporated a standard batch control technique that ensured equal volumes of water at each tray, it was necessary to record the maximum times in order to set a safe circulation frequency of the conveyor system during irrigation. This limitation provides motivation for a unified conveyor-irrigation system to be considered in the future.

5.4 Lighting system

Naturally, the light conditions also have a significant impact on the performance of the grow-cell prototype as a whole. Mixed wavelength output is suitable for numerous plant species, mostly for propagation, and the presently installed system targets low and medium irradiance plants such as begonias. The prototype grow-cell encompasses the capacity to add and replace lights according to the target crop species. More generally, LEDs allow for previously unachievable agricultural applications, such as merging different wavelength outputs (see e.g. Fig. 3.6) to obtain the maximum photosynthetic utilisation by plants and the deployment of time–varying light outputs depending on the growth stage of the crop.

Section 3.6 showed how the PPFD output can be improved to find a satisfactory balance between costs and performance. Extrapolating from the shaded area in Fig. 3.9 and applying a 16 hour daily photo-period, it is feasible to save between 29 to 139 kWh per day. Such power consumption calculations, however, solely relate

to the particular LED units procured for the prototype and so should be treated with caution. Nonetheless, the generic concept is that the output can be straightforwardly varied for different species, and the spatial distribution and associated operational costs of the lighting system have to be considered on this basis. Further energy savings can be made by reducing the distance between the plants and light panels. For example, at a distance of 0.1 m, the PPFD magnitude increases by up to 50% in comparison to the 0.2 m utilised for the growth trial. Indeed, one benefit of LEDs is that low heat output allows for the lights to be placed very near the plant canopy and the heat generated can be utilised as a complementary heating source (potentially useful depending on the climatic region and time of year).

For this system, however, additional practical modifications should be undertaken. For example, the edges of the light units that sat on aluminium rods at each layer were hot glued instead of slotted, while waterproof car wire clips would make replacing the lights a much easier task than the present hard-wiring approach. In the present configuration, one would struggle to maintain the lights and even replace them with other light recipe units. Finally, the power supplies that drive the lights did not have a high mean-time-between-failure (MTBF) performance. In fact, several had to be replaced after just two-three weeks of use during the development work, while the author further repaired two more during the growth trials. A customized power supply on the other hand should prove to be more robust for this application.

5.5   Growth trials cost and energy usage

Table 5.1 shows the individual costs calculated for the five week growth period of *Begonia Semperflorens.* The equivalent is not calculated for the second growth trial as a more experimental growth regime was followed i.e. one that deviated from normal practice in the greenhouse. Regarding the seeds (9,600 were used in total), the average cost per 1000 is £9. For the feed, a pack of 80 kg costs £30 and can yield 150 litres, of which approximately 2.5 were used, hence accounting for £0.5. The average cost for a m^3 of water is £1.98. For a full irrigation cycle, 180 litres are needed to adequately water the soil bed. Multiplying 28 irrigation cycles throughout the trials yields a usage of 5 m^3, adding £10 to the overall cost. Finally a cost of

Cost index	
Plant species	*Begonia semperflorens*
Date sown	*February 5*
Date finished	*March 11*
Total production time	*5 weeks*
Seeds	£86
Soil	£112
Water	£10
Feed	£0.5
Lights	£47
HVAC	£147
Total	£403

Table 5.1: Growth trial information and cost list.

£2.8 per (pre-filled with soil) tray accounts for a total of £112. Splitting the total cost per unit (40 trays) yields £10 per tray. The HVAC unit is the main expense; the electricity cost is computed on the basis of the average power consumption over a five week period and an average cost of £0.05 per KWh. Using dedicated energy loggers for the HVAC unit and lights, it is possible to identify the individual energy consumed, i.e. 943 KWh for the lights and 2996 KWh for the air-conditioning unit, accounting for £47 and £147, respectively.

Assuming now that all five layers of the grow-cell are occupied with *Begonia semperflorens*, a potential reduction in production costs in comparison with Table 5.1 can be estimated. This scenario assumes a successful growth cycle and addresses some of limitations discussed above but is based on the currently available configuration of the prototype i.e. including the over-specified and inefficient HVAC unit. Here, the price of seeds, soil, feed and water will increase fivefold (total £1042.5). Such is not the case for the electricity cost, which will differ depending on the lighting level selected for operation and whether the HVAC unit is running in economy or normal mode. Should lights operate at 40 V, approximately 1 KW will be required (5 KW for all five layers), adding £210. Regarding the HVAC unit, Fig. 5.1 shows that the power consumption in both economy and normal mode is generally similar

regardless of the number of layers used. Hence the cost based on an average 4.9 KW and 1.2 KW per hour for normal and economy modes, is £206 and £50.4 respectively. The former would require a total of £1458.5 to produce 200 trays of plants (approx. £7.3 per tray), whereas using the economy mode of the HVAC unit will drop the overall price down to £1302.9 (£6.51 per tray). Effectively, even though the number of layers increased, the overall cost per growth cycle decreased from £10 per tray to £6.51-7.3 per tray. Further assuming that conventional soil may be used, the cost to fill one tray decreases from £2.8 to £0.8 (£160 for all five layers). This reduces the cost of the five layer growth cycle scenario to £4.5-5.3 per tray.

Finally, a cost comparison between greenhouse and grow-cell production could not be undertaken by the author as the third part company records overall energy data (i.e accumulated from all their facilities). However, one fact is that it takes 13 weeks for example to grow *Begonia Semperflorens* at the greenhouse facility of Bordon Hill Nurseries. Therefore, 3.7 growth cycles can take place per year, whereas 10 growth cycles a year may be achieved using the grow-cell. This itself makes the grow-cell interesting, yet a quantified comparison would need to be formulated in the future, for validation purposes.

5.6 Commercial grow-cell concept revisited

The economic viability of an industrial grow-cell depends on its design robustness, production cost, and energy efficiency. Here it is very important that the crop output, quality, and production time are satisfied to a level that compensates for the addition of the light energy costs to the overall cost of production (e.g. compared to a conventional greenhouse). In this regard, the prototype grow-cell understandably lacks optimality in several areas due to its research flexible design. For example, the current HVAC and the irrigation systems induce significant wasting of energy inputs, such as electricity and water. As a result, the cost to produce a tray of e.g *Begonia semperflorens* cannot be realistically compared with the reference greenhouse – the present configuration of the prototype is significantly more expensive. In its current configuration, the prototype represents a research facility that can be utilised for investigations into the various issues arising for a wide range of plant types.
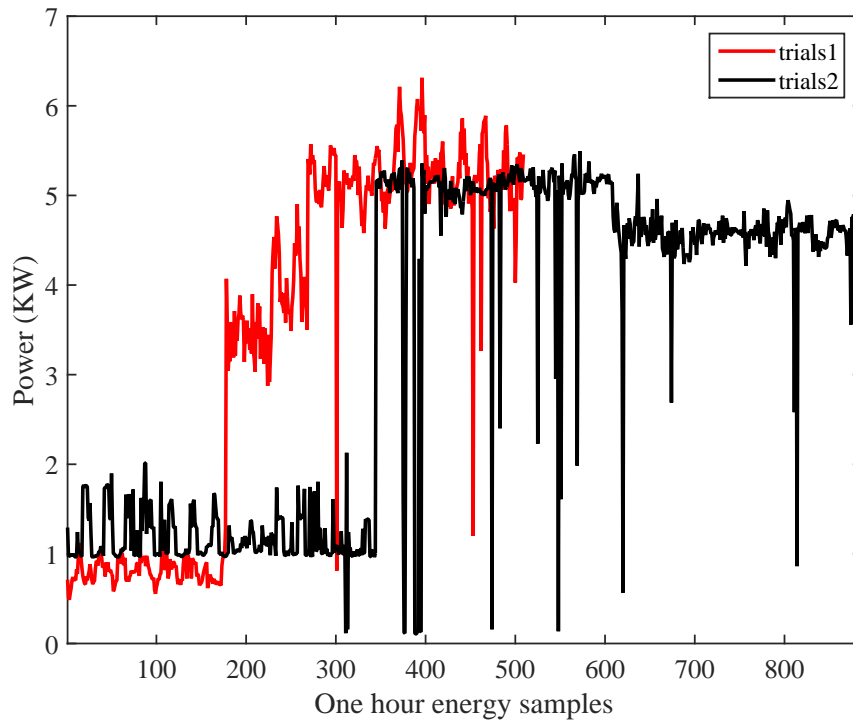
Figure 5.1: Instantaneous power used by the HVAC unit throughout both trials, with red and black traces depicting the first and second trials respectively.

Should the industrial partner wishes to develop a commercially orientated version of the grow-cell, the optimal approach would be to first identify a *specific* range of plants to be grown, as these will implicitly determine the type of irrigation, the lighting system, and the maximum layers based on their size. In turn, cooling and heating capacity, and the air flow system should be specified based on the external environmental conditions and the amount of light that is going to be used, and an appropriate HVAC system subsequently procured or developed. Finally, a central processing and power supply unit would be highly beneficial in terms of the robustness of the system. Appendix C lays out several recommended flow-charts developed by the author that could be used as a guide for the design of the future air handling unit, power supply, shelving, conveyor and irrigation system, and LED light system.

5.7   Conclusions

Part A of the thesis has described the development of a prototype grow-cell for research into closed environmental horticulture, namely a sealed building with LED

lights, mechanical rotation of plants and a controlled environment. A selective review of research in cognate topics has been used to develop the engineering requirements for the prototype. The subsequent research focus has been on the development of a conveyor system for moving the plant trays around, the arrangements for a single point irrigation/feed system, and the LED lighting system. Part A of the thesis has also considered measurements of micro-climatic variables inside the growing environment but this issue is discussed in much more detail in Part B. For example, a multi–zone controller that acts on the heating and ventilation devices in a manner such that the design requirement for each thermal 'zone' of the grow–cell is achieved, could potentially allow for improved growth regimes to be applied.

Chapter 3 has discussed the design, testing and optimisation of the subsystems prior to the plant growth trials, which were reported in Chapter 4. Based on these results, recommendations have been made in the present chapter for how the prototype should be adapted for particular requirements. Despite limitations in its present configuration, the grow-cell was successful in terms of growing and harvesting crops, including *Begonia semperflorens* and *Impatiens divine*. It is hoped that the prototype will now be utilised for practically orientated research and development, in which a range of horticultural, economic and environmental issues can be systematically investigated e.g. energy consumption and whole system running costs. There is also considerable scope for future quantitative research into the relative mass and quality (e.g. leaf size, root conditions etc.) of plants grown in different environments.

Part B

Data-Based Identification of Thermal Zones, Non-linear Modelling, and Control examples

Chapter 6

Introduction to Part B

Micro-climate measurements from the horticultural grow-cell, as discussed in Part A of the thesis, expose a lack of temperature homogeneity within the growing space. Current established heating and ventilation systems typically deal with micro-climate in an averaging manner; for instance, by utilising measurements from single locations and assuming these represent the micro-climate of the whole area (as is the case for the grow-cell air conditioning unit). However, it is evident that in facilities such as the grow-cell and fodder barn, there can emerge different thermal zones with similar characteristics (see, for example, Figure 2.3 in relation to the fodder barn discussed in Chapter 2). For glasshouses, crop output largely relies on the growers' experience and dealing with micro-climatic gradients generally leads to higher labour costs e.g as staff have to physically move plants around and/or introduce additional mechanical diversion of air flow [Kittas et al., 2003, Teitel et al., 2010].

A recent review [Duarte-Galvan et al., 2012] of control systems used in greenhouses, summarises numerous approaches to address the non-linear nature of controlled environment farming; although the studies mentioned in this review discuss various advantages in terms of model analysis and/or control efficiency, comparatively little information is given about the feedback terms used by the control algorithm and hence the extent to which each study has taken into consideration the volume and spatial variability of micro-climate. Of course, many authors do note the potential significance of spatial variation even when this is not explicitly addressed by the developed optimal control system [van Straten et al., 2011, Hamilton et al., 2016]. By contrast, a multi-zone approach to modelling and micro-climate control potentially

allows for the optimization of crop outputs and energy inputs. The ultimate goal is to act on the heating and ventilation devices in an optimal manner, such that the design requirement for each thermal zone is reached. An essential step towards the development of such a system is the identification of suitable thermal zones that may arise under different heating and ventilation scenarios.

Part B of the thesis investigates some of these issues, with a particular focus on the development of nonlinear statistical models for temperature in a forced ventilation test chamber, and on the use of these models to develop both single-zone and multi-zone temperature control systems. The test chamber provides a readily available facility for experimentation with different heating and ventilation settings in a laboratory environment, hence is ideal for the present research[1]. However, an obvious next step for the research is to apply the novel tools developed within Part B of the thesis to the grow-cell, and this is discussed further in Chapter 10.

In the present chapter, section 6.1 provides a brief review of how multi-zone models are usually thought of and utilised in the literature. Section 6.2 describes the laboratory scale forced ventilation chamber utilised for this research, followed in section 6.3 by a motivational example for zonal modelling, based on preliminary experimental data obtained from the chamber. Finally, section 6.4 lays out the objectives for chapters 7-9 of the thesis.

6.1   Multi-zone models

Physical, data-based or hybrid multi-zone models for control are commonly based on defined locations in a facility, for which there are relatively homogeneous environmental conditions; e.g. the inlet, outlet and different rooms of a building. Most commonly in literature, multi-zone approaches refer to studies that approximate the problem by considering a room or floor as one thermal zone, assuming uniform temperature [Outanoute et al., 2015, Joudi and Farhan, 2015, Taki et al., 2016, Espinosa and Glicksman, 2017]. Tashtoush et al. [2005] formulated a single zone

---

[1]Note that the commercial air conditioning unit used to develop the grow-cell, as reported in Part A of the thesis, was required for the on-going plant growth trials, and it was not possible to replace this with a more flexible system for research into modelling and control within the scope of the present project.

lumped parameter model under the assumption that it is perfectly mixed, while Goyal and Barooah [2012] developed a four zone lumped resistor-capacitor (RC) network for expressing the HVAC system of four rooms. Liao and Dexter [2004] treated a three-storey building by developing a three-zone physical model. Mossolly et al. [2009] regarded as one zone each room of a building, and Killian et al. [2015] partitioned a library floor into four conceptual zones based on cardinal points. In studies where one physical area is nonetheless divided into zones, a grid-like partitioning approach is usually taken *a priori*. For example, Gholami et al. [2010] developed a non-linear hybrid model using an Extended Kalman Filter, for three conceptual predetermined zones. Using bi-linear ordinary differential equations, the same approach is taken in De Persis et al. [2008]. Similar examples include Caponetto et al. [2000], Cortés and Quijano [2010] for greenhouse temperature and humidity, and Wu et al. [2008] for temperature variation inside livestock buildings. The present thesis proposes a different, data-driven approach, in which the zones of a single physical area are quantitatively determined using statistical tools.

Several other studies have resorted to multiple point measurements to describe the temperature distribution within an open airspace. For instance, using a forced ventilation test chamber at Katholieke Universiteit Leuven, Janssens et al. [2004], Desta et al. [2005a] developed a multivariable transfer function model with 36 sensor nodes to describe the temperature and humidity distribution, by combining physical modelling and data-based parameter estimation. Desta et al. [2008] extrapolate on those studies by focusing on a well-mixed sub-volume of the chamber from data generated by 2-Dimensional CFD models, while Thanh et al. [2007b, 2008] determine the interaction of the latter with a buffer zone outside the chamber. Van Buggenhout et al. [2006] developed a data-based model to describe the age of air, based on measurements of CO_2 concentration. Further studies that made use of the same KU Leuven forced ventilation chamber include [Price et al., 1999, Young et al., 2000, Thanh et al., 2007a, Desta et al., 2004b,a, 2005b, Van Brecht et al., 2005, Youssef et al., 2011]. Finally, Bleil De Souza and Alsaadani [2012] discuss some common strategies for thermal zoning, focusing on the human-built environment (specifically an office layout), including an approach based on temperature stratification that also provides some motivation for the present research.

The common theme in all of the aforementioned studies is the role of the air-flow. This is inherently coupled with micro-climatic variables since airflow magnitude largely determines the homogeneity and the quality of air within an enclosed space. Numerous applications address this and examples where the goal is to model ventilation effectiveness include Chen et al. [1969], Sandberg [1981], Davidson and Olsson [1987], Sherman [1989], Boulard and Baille [1993], Korthals et al. [1994], Peng et al. [1997], Taylor et al. [2004c], Desta et al. [2005b], Brande [2006], Cao et al. [2014], Gilani et al. [2016]; studies on the effect of ventilation within human and animal occupied buildings include: Barber and Ogilvie [1982], Berckmans and Goedseels [1986], Inard et al. [1996], Van Brecht et al. [2003], Chen [2009], Oldewurtel et al. [2010], Maddalena et al. [2015]; while for control of ventilation rate see e.g. Leigh et al. [1999], Leigh [2003], Taylor et al. [2004b,a], Stables and Taylor [2006], Nagaya et al. [2006], Wu et al. [2008].

In this regard, experimental data at various locations are useful because they can reveal the conditions created in the airspace for a given air-flow supply system. For example, selecting bespoke points for the airflow supply and exhaust gives rise to various airflow different patterns. Barber and Ogilvie [1982] present some types of incomplete mixing conditions created under different air inlet-outlet arrangements. Vox et al. [2010] suggest the installation of horizontal airflow fans as a medium to reduce the magnitude of incomplete mixing within a growing area. This arrangement and various others that take into consideration the need to equally distribute airflow, could result in better mixing but more data are required to allow for validation.

The research presented in this Part B of the thesis focuses on the temperature distribution based on multiple point measurements, and follows a data-based or statistical approach [Cunha et al., 1997, Pee and Berckmans, 1999, Taylor et al., 2013, Afram and Janabi-Sharifi, 2015, Cai et al., 2016]. As a result, experimental data are required, as discussed in the following section.

6.2 Laboratory scale forced ventilation chamber

All the experimental data utilised hereinafter have been obtained using a 2 m × 1 m × 2 m forced ventilation test chamber, originally built at Lancaster University by
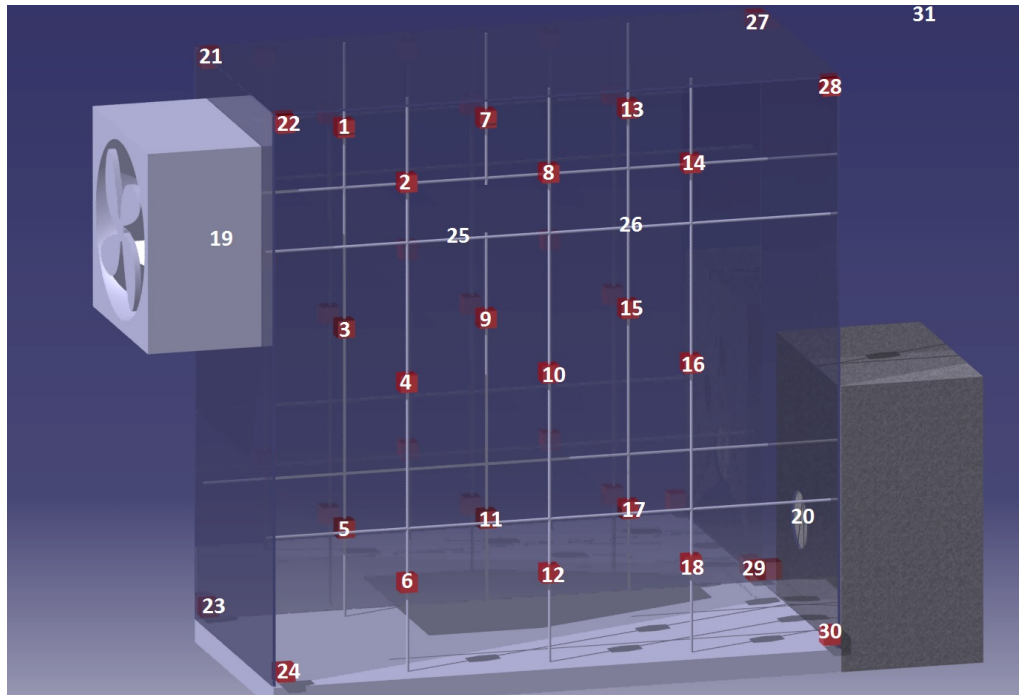
Figure 6.1: Layout of the sensor locations within the test chamber.

Philip Leigh [Leigh, 2003]. The chamber was more recently repaired and upgraded by the author as part of an MSc project [Tsitsimpelis, 2012] (however, it should be stressed that the experimental results and modelling approach that follow are all novel to the present thesis).

The forced ventilation chamber (Fig. 6.1 and Fig. 6.2) is equipped with 31 K-type thermocouples, 18 of which are laid out evenly in a grid arrangement around the main airspace, eight are located at the corners, two at the inlet and outlet openings, another two at the middle of the structure, and one outside of the chamber in order to capture the ambient laboratory temperature. The sensor outputs are conditioned by means of two National Instruments data acquisition cards (NI-USB-9213). Furthermore, two ventilation rate transducers (TSI-AVT8455) are placed at the inlet and outlet openings. These have dedicated signal conditioning circuitry that yield a variable DC voltage output range between 0 and 5 V, which corresponds to a ventilation rate range between 0 and 9 ms^{-1}. Both signals are captured by a NI-USB6008 data acquisition card.

Actuators include two 300 W axial fans and a 400 W heating element. The outlet fan extracts air from the chamber and forces outside air into it through the inlet

opening, where the heater also resides. The inlet fan forces air into the chamber and is used to replicate air disturbances under laboratory conditions, i.e. to represent pressure variations caused by changing wind speed outside a building. Both inlet and outlet openings have a six inch diameter. Furthermore, all three actuators are controlled via individual variable power supplies, which consist of a phase angle power control module (Semikron-SKPC200) and a thyristor pair. This allows to straightforwardly control the magnitude of their operation through a 0-5 V signal coming from another NI-USB6008 module. The operation of the chamber, for the purposes of both data collection and control implementation, is undertaken via LABVIEW software; with templates developed by the author covering various data collection and control scenarios for ventilation and temperature. Finally, the chamber envelope is made of transparent plexiglass sheets mounted in place via steel rods, while the flooring and the box that contains the inlet fan and heater are made of wood. The ambient laboratory conditions are free from solar radiation and other heat sources, and temperatures are generally kept daily between 18 to 21 $°C$.

6.3   Motivational example

An illustrative open-loop experiment for the Lancaster chamber is shown in Fig. 6.3. Here, the voltage input associated with the outlet fan is varied between different magnitudes. For this particular experiment, the heater input follows a standard pseudo-random binary signal (i.e. on–off). Temperature data were collected at a sampling rate of 1 second, from 30 locations within the test chamber, as shown in the upper subplot of Fig. 6.3. A careful visual inspection of the responses suggests that at periods with medium and low ventilation rates it may be possible to derive various 'zones' of relatively similar dynamic and steady state behaviour. Hence, following a similar approach to Agbi et al. [2012], the open space inside the chamber might be divided into a small number of (relatively) well-mixed zones for the purposes of modelling.

However, the utility of such a model for control system design is limited to the assumption of good mixing within each zone, and hence to the particular airflow patterns that emerge for a given experiment. Significantly, different input sequences yield
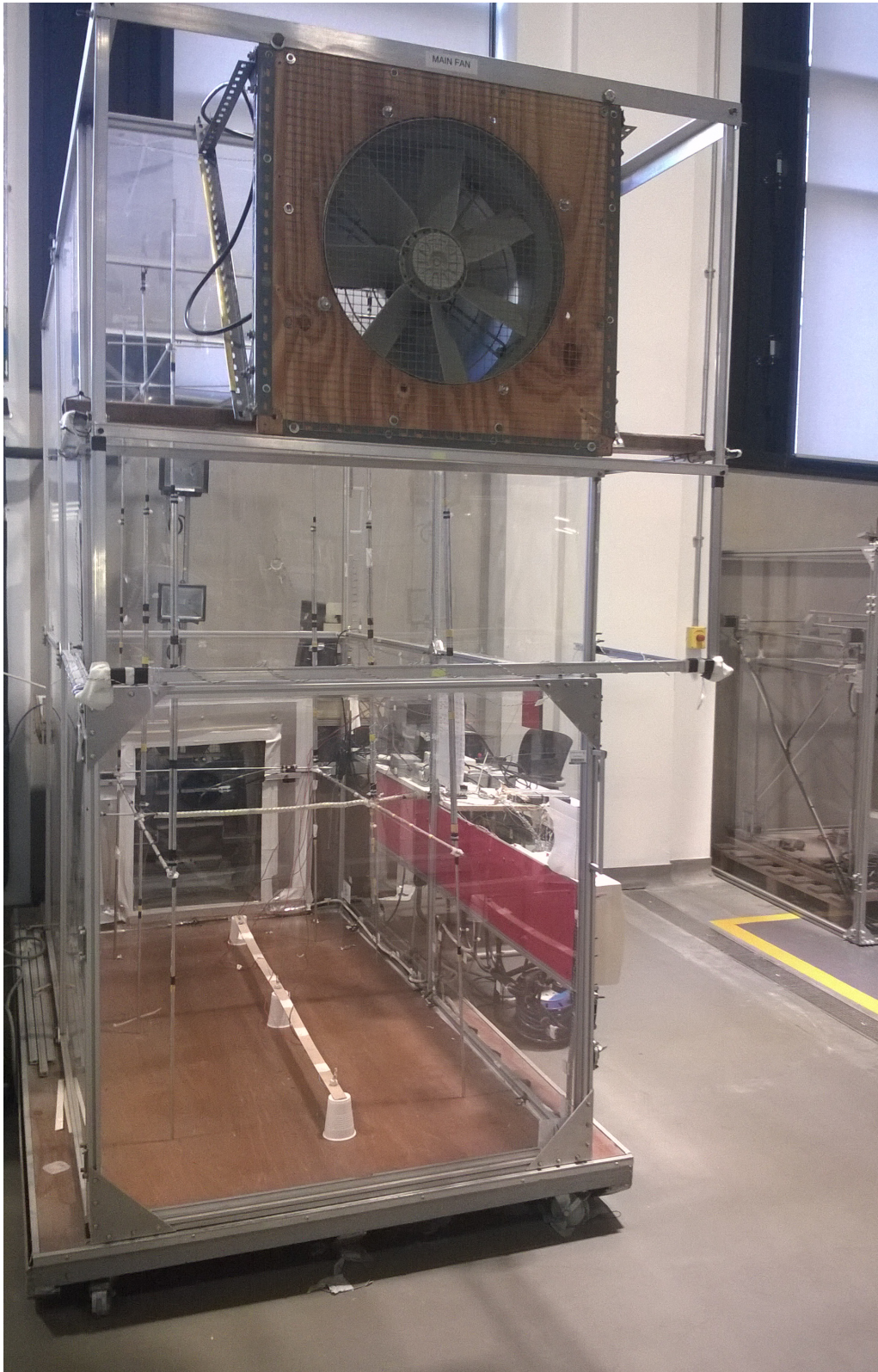
Figure 6.2: Laboratory forced ventilation test chamber [Leigh, 2003, Tsitsimpelis, 2012].

different airflow patterns and hence can suggest different zones (see later chapters). The experimental data shown in Fig. 6.3 are utilised to determine the resemblance between one thermocouple and all the other thermocouples. Fig. 6.4 shows the relationship between one particular thermocouple and all the other thermocouples, in terms of an estimated "accumulated distance" matrix. More generally, Fig. 6.4 is a schematic representation of the environmental test chamber, with the numerical values indicating the approximate location of (selected) thermocouples. The lower the numerical value shown, the more similar the response is to the reference thermocouple. The latter reference thermocouple (arbitrarily chosen for the purposes of this example) is represented by a zero, i.e. it is exactly correlated with itself.

Fig. 6.4 suggests one zone near the lower part of the chamber and another at the top layer. For this particular example, the correlation between thermocouples was measured by utilising dynamic time warping (DTW) [Petitjean et al., 2011]. DTW is an algorithm commonly used where two or more time series lead or lag each other, e.g. fingerprint and handwriting identification, speech recognition, and clustering spatial data [Kovacs-Vajna, 2000, Martin et al., 2001, Kadous and Sammut, 2005, Tanaka and Takahashi, 2016, Piburn et al., 2017].

6.4 Research Objectives

The present chapter has reviewed some of the literature in relation to the use of multi-zone models for describing micro-climate in an enclosed space, and has noted that the zones of such models are generally determined either arbitrarily or from the physical layout of the building. The first objective of Part B of the thesis, is to develop an alternative, data-based approach (DBM) to the identification of thermal zones in a building, and to evaluate the new approach using a laboratory forced ventilation chamber. Here, model structures are initially identified from measured data, collected from a distributed array of sensors, thus avoiding undue reliance on prior hypotheses and ensuring that the resulting models are identifiable from the available environmental data, notably temperature. In the DBM approach [e.g. Price et al., 1999], the identified model is only considered credible and, therefore, fully acceptable, if it is also capable of interpretation in a physically meaningful manner.
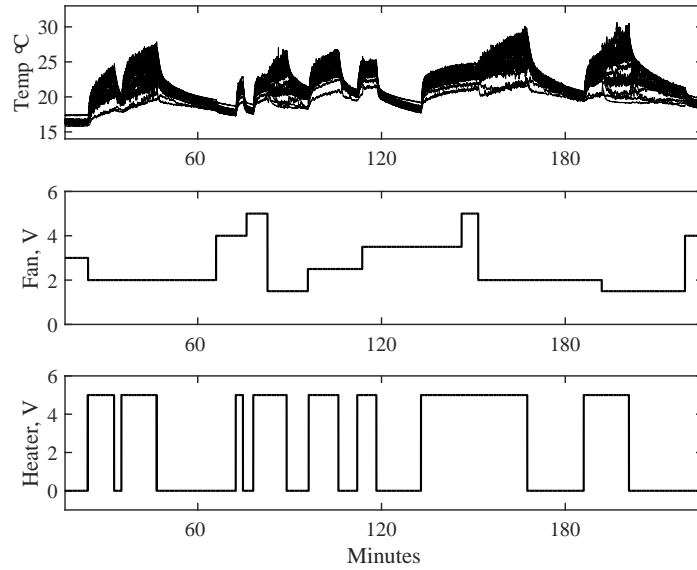
Figure 6.3: Open–loop experiment showing the fan and heater inputs (middle and bottom subplots), together with the temperature from each thermocouple (upper subplot).
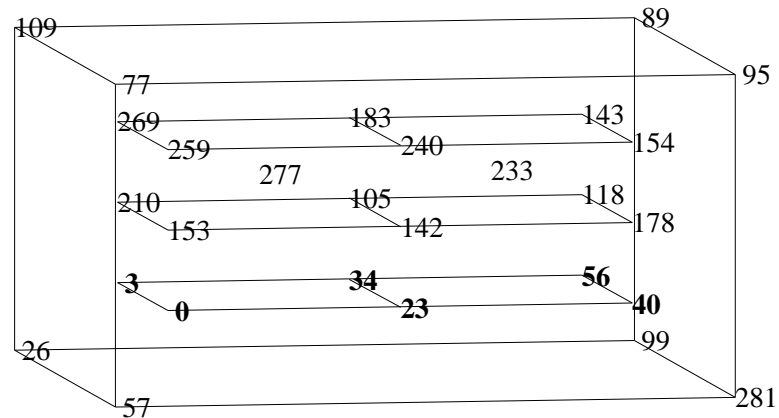
Figure 6.4: Resemblance between each thermocouple and an illustrative reference thermocouple, for the experiment in Fig. 6.3, with zone 1 highlighted in bold. The reference thermocouple has in this case a value of zero.

In the present context, this means the zones identified should make practical sense given the physical arrangement of the sensors (and hence also be useful for control purposes) i.e. the thermocouples in each zone should be clustered around a given physical location and not be distributed inside other zones. For a discussion of the broad–based concept of DBM modelling more generally, see e.g. Price et al. [1999], Young [2011, 2013] and the references therein.

Complementing the above research into zone identification, a second objective of the research is to identify suitable dynamic models for the temperature distribution, models that are again evaluated using experimental data from the laboratory chamber. Finally, these models will be used to develop both single-zone and multi-zone control systems for temperature. As discussed in later chapters, the steady state temperature distribution is related in a nonlinear sense to the different fan and heater inputs. As a result, the 'conceptual' zones identified from data vary over time (for example, for different experiments) depending on the the different air flow patterns that emerge for different input scenarios. Hence, a systematic approach is essential to identify thermal zones that are present in the airspace for a range of different heater and ventilation settings. The need for a quantitative approach to address this challenging problem is a key motivation for the development of the data-based zone identification tool.

To address these aims, Chapter 7 proposes use of statistical cluster analysis to quantitatively distinguish and group thermal zones within an open airspace for any given ventilation and heating setting. A data-based approach to thermal modelling that combines nonlinear static functions for steady state temperature with a dynamic model is subsequently presented in Chapter 8. The approach yields a two-dimensional Hammerstein type model, which is evaluated here under different heat and ventilation settings, for both individual sensor locations and exemplar thermal zones identified by clustering. Chapter 9 develops linear Proportional-Integral-Plus (PIP) control systems for the control of temperature in selected thermal zones.

The PIP approach is based on the definition of Non-Minimal State Space (NMSS) models, so that full state variable feedback control can be implemented directly from the measured input and output signals of the controlled process (Taylor et al. [2013]). The PIP controller can be interpreted as a logical extension of Proportional-Integral-

Derivative (PID) control, with additional dynamic feedback and input compensators introduced automatically, when the process has second order or higher dynamics or pure time delays greater than one sampling interval, as is the case for some of the temperature models. The new controllers are tested in simulation and experimentally in the ventilation chamber, for both conventional PIP control of a single thermocouple or single thermal zone; and for a novel multiple-input, multiple-output case, where the temperature of one zone, and its ratio to another, are both regulated using a multivariable PIP algorithm.

The conclusions to Part B of the thesis are summarised in the final section of Chapter 9, which also includes suggestions for further research into the robustness of the thermal zone identification and non-linear control methodology. Finally, Chapter 10 discusses the conclusions to the thesis as a whole, and suggestions for further research.

Chapter 7

Cluster Analysis

This chapter proposes the use of cluster analysis for distinguishing and formulating thermal zones of relatively well-mixed air, which may be subsequently utilised for single and multi-zone modelling and control. In particular, K-means and Agglomerative Hierarchical Cluster (AHC) analyses are used a) directly on experimental data and b) on the steady state gain and time constant of a preliminary linear Transfer Function model. In the second case, the model structures are identified from measured data, thus avoiding undue reliance on prior hypotheses and ensuring that the resulting dynamic models (developed more fully in the next Chapter 8) are fully identifiable from the available environmental data. Both clustering algorithms were selected in this analysis due to their computational simplicity and straightforward implementation.

This approach is an example of how data from multiple locations can be grouped for the purposes of reducing the dimensions of the modelling task (see e.g. Janssens et al. [2004], Desta et al. [2005a], who develop multivariable transfer function models). It also represents a novel example of the DBM modelling concept (Price et al. [1999], Young [2011, 2013]): guided by the results of the *data-based* clustering analysis, the final selection of zones for future modelling and control purposes is made by reference to the physical system under study i.e. the *mechanistic* part of the analysis. In other words, the model is only considered credible once the spatial location of each temperature sensor is taken into account.

Clustering algorithms have been extensively utilised in science, from genomics and clinicals, to engineering, earth and social sciences: see e.g. Eisen et al. [1998],

Fovell and Fovell [1993], Yun and Won [2012], Valenzuela et al. [2012], Zhou et al. [2013], Bürger et al. [2013], Wockner et al. [2014], Castaldi et al. [2014], Gocic and Trajkovic [2014], Cabieses et al. [2015], Rozental et al. [2015]. Further research work is dedicated to cluster assessment and validation indices [Sokal and Rohlf, 1962, Caliński and Harabasz, 1974, Davies and Bouldin, 1979, Rousseeuw, 1987], which are also used in this chapter; as well as studies comparing their performance for different circumstances [Milligan and Cooper, 1985, Fraley and Raftery, 1998, Arbelaitz et al., 2013, Saraçli et al., 2013, Murtagh and Legendre, 2014], particularly regarding the nature of the data being clustered.

Section 7.1 describes the clustering algorithms utilised in the chapter. Experimental data collected from the laboratory forced ventilation chamber are subsequently used to illustrate the issues involved and to help develop recommendations for how to apply clustering methods in this context. Hence, sections 7.2 and 7.3 discuss the data and the clustering set-up process, and section 7.4 introduces the Transfer Function modelling approach, which is used to estimate the time constant and steady state gain clustering objects. The results and discussion are presented in sections 7.5 and 7.6, followed by the conclusions in section 7.7.

7.1   Clustering Algorithms

7.1.1   AHC algorithm

The AHC algorithm starts with i clusters (i.e. the number of objects to be clustered; here the total number of temperature sensors), and finishes with a parent cluster, in which all the subgroups are contained. The clusters are formed on the basis of comparison between variables that characterise the measured data. The derived hierarchy can be then visualised by means of dendrograms.

The structure of data arranged as a $q \times p$ information matrix is shown in Table 7.1. Here, $q = 1, 2, ..., i$ refers to the location of each temperature sensor, or otherwise the number of data points to be clustered; and $p = 1, 2, ..., j$ is the number of clustering variables associated with each of these sensors.

The latter information matrix is converted into a triangular matrix, which contains the proximities between all pairs of temperature sensors, as shown in

	p			
	x_{11}	x_{12}	$\cdots$	x_{1j}
q	x_{21}	x_{22}	$\cdots$	x_{2j}
	$\vdots$	$\vdots$	$\ddots$	$\vdots$
	x_{i1}	x_{i2}	$\cdots$	x_{ij}

Table 7.1: Information matrix, where $q = 1, 2, ..., i$ refers to the location of each temperature sensor and $p = 1, 2, ..., j$ contains the values of the associated variables

q	1	2	3	$\cdots$	i
1	0				
2	d(1,2)	0			
3	d(1,3)	d(2,3)	0		
$\vdots$	$\vdots$	$\vdots$	$\vdots$	$\ddots$	
i	d(1,i)	d(2,i)	d(3,i)	$\cdots$	0

Table 7.2: Distance matrix that contains the pairwise difference between all temperature locations.

Table 7.2. This is achieved by means of a metric (also referred to as a proximity measure and distance function). For $p > 1$, the selected function yields unit-less values between the variables, since the contribution of each dimension is combined with the others [Aldenderfer and Blashfield, 2006]. Numerous proximity measures are available, and the choice of one typically depends on the data that are used for clustering. This aspect is covered later (section 7.3). For demonstration purposes however, assuming that one proceeds to compute the differences between $q = i$ temperature sensors that are characterised by $p = j$ dimensions using the Euclidean metric, the pairwise distance of e.g. $q = 1, 2.., i$ to itself and all other is calculated as follows,

$$d(q_1, q_i) = \sqrt{(x_{11} - x_{i1})^2 + (x_{12} - x_{i2})^2 + ... + (x_{1j} - x_{ij})^2} \qquad (7.1)$$

with the latter equation expressing the distance between $q = 1$ and $q = i$.

Every time the algorithm iterates, it merges the pair of temperature locations that has the minimum difference. The matrix is then reformulated with the new cluster replacing the merged individual objects. At this point, each distance between

the new cluster and each other temperature location is computed by using a function that is known as the linkage criterion,

$$d(12,3) = f(d_{1,3}, d_{2,3}) \qquad (7.2)$$

where $d(12,3)$ is the distance between the cluster that contains the exemplary here objects $q = 1$ and $q = 2$, and the individual object $q = 3$; this being determined by either distance $d_{1,3}$ or $d_{2,3}$, or both. There are typically three ways to calculate that distance: using either the single, or the complete, or the average linkage criterion. In the first two cases, the criterion gives full weight to the one distance that prevails over the other (minimum and maximum respectively), whereas in the third case, it is calculated as the average of the individual pairwise distances, i.e. $d(12,3) = mean(d_{1,3}, d_{2,3})$.

7.1.2 K-means algorithm

The k-means algorithm is essentially an optimisation routine, i.e. it iterates until it converges to an optimal solution. It also works around a pre-specified number of clusters and the $q \times p$ information matrix. At initialization, the algorithm randomly assigns $c = 1, 2, ..., k$ centroids (the centres of k clusters), with each having $p = 1, 2, ..., j$ coordinates (as many dimensions as the clustering variables). A distance metric is then utilised to formulate the proximity between each clustering object ($q = 1, 2, ..., i$) to each centroid. Using once again the euclidean distance as an example,

$$d(c_k, q_i) = \sqrt{(c_{k1} - x_{i1})^2 + (c_{k2} - x_{i2})^2 + ... + (c_{kj} - x_{ij})^2} \qquad (7.3)$$

In this manner, a $q \times k$ distance matrix is formulated, which contains the distance between each location to each centroid. On this basis, the algorithm assigns each $q = 1, 2, ..., i$ object to its nearest centroid. In this instance, each centroid is updated based on the clustering variables that characterise the objects it contains; and updating in turn the $q \times k$ matrix. This allows reassigning objects that were not properly assigned in the first iteration. This process then iterates until the centroids stop changing values, implying that all objects are truly assigned to their nearest centroid.

7.2   Data collection

As described earlier (section 6.2), the forced ventilation test chamber is equipped with a fan that draws the air off the chamber, and a heating element that introduces heat into it. Both actuators can be operated at various levels and hence there is great flexibility for carrying out open-loop experiments. The following two types of experiments are of particular interest in this analysis. One standard type is with a fixed applied voltage to the fan, a step change in the heater input is introduced, and data collection is carried out long enough until the temperatures have settled to a new steady state. Depending on the actuator settings, the temperature responses indicate different transient and steady state behaviours. For example, in Fig. 7.1, the upper plot shows data that have been collected under a fixed low ventilation rate setting, with a large step change in the heater input introduced after a minute; while in the bottom plot the data from the same locations are depicted under a fixed applied voltage to the fan and a small step change in the heater input. In the first case, the temperatures rise from an initial temperature of approximately 17 °C to a range of 20-33.5 °C, whereas in the second case the temperature increase is lower (around 3 °C), and settled there faster.

The second type of experiments address more complex scenarios, such as the dataset depicted in Chapter 6 (Fig. 6.3), where both the heater and fan vary randomly. Similar to the latter, the data shown in Fig. 7.2 depict an experiment where the heating element is fixed and the applied voltage to the fan is varied randomly (upper plot), whereas the opposite settings form the responses shown in the bottom plot of the latter figure.

7.3   Data processing

Hereinafter are presented three key aspects of the clustering task. These relate to a) which variables are best to characterise the objects one wishes to cluster, b) which function is more appropriate to formulate a matrix of differences between the objects, and c) the use of a complementary tool that assesses the quality of the produced clusters.
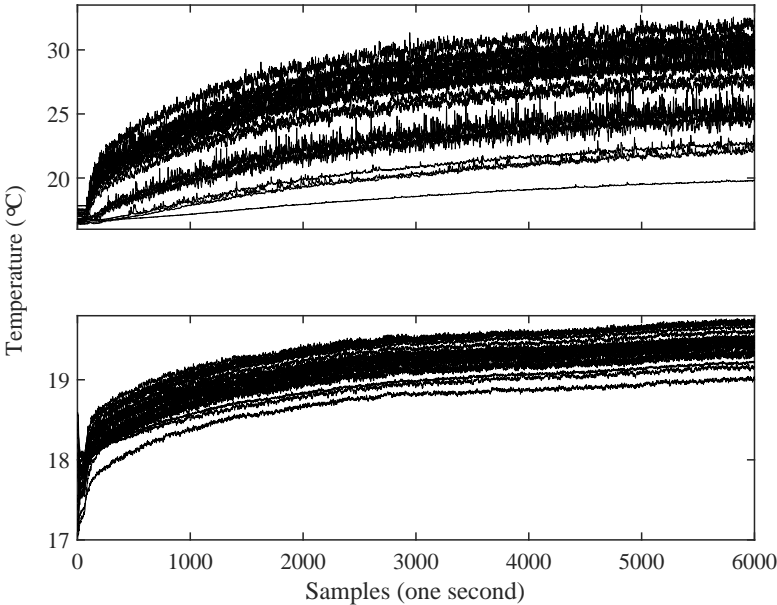
Figure 7.1: Typical responses for a step change in the heater input experiment. The upper plot depicts data that have been collected for a low fan setting and a high heater setting, whereas the bottom plot shows the same for a high fan setting and a low step change in the heater input.
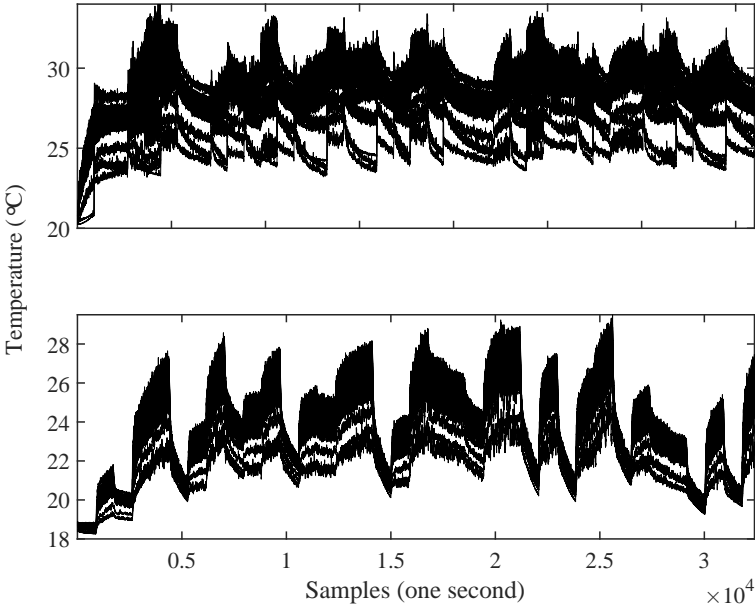
Figure 7.2: Two data-sets that have either the fan (ventilation rate) or the heater vary randomly; top and bottom plots, respectively.

7.3.1   Selection of clustering variables

Cluster algorithms need to be fed with a set of quantitative information that characterises the data described above. In this chapter, cluster analysis is undertaken with modelling and control design in mind; that is, to group measurement locations of similar dynamic and steady state behaviour. Intuitively, the time series of a dataset could be used in this regard. This means, however, that each measurement location would be characterised by its individual value at each sample, over a finite sampling time. For a rate of 1 sample per second, over a four hour experiment, the size of the information matrix would be q=i $\times$ p=14400. For step experiments, during which the actuators are fixed to one setting, this is unnecessary. For example, the temperature of one location at sample time k=100 and k=101 have a negligible difference. On the contrary, selecting values at different sampling instants (e.g. at the start, middle, and end of the dataset) dramatically decreases the dimensions of vector p, yet the information of how the temperature responses varied throughout an experiment is still captured.

An alternative way is to use the system parameters that are derived from the statistical estimation of discrete transfer function models, which describe the time series of each measurement location. In particular, the shapes of the individual responses are captured via their models. The parameters of these transfer function models could be utilised as clustering variables. However, they can provide more physically intuitive information, which is pertinent to the aims of this chapter, i.e. the time constant and steady state gain. This approach implies that a predetermined common model structure is imposed. However, it exploits information from data-based methods in a novel manner, and is thus interesting to utilize it.

For the more complex datasets, a series of step changes is applied in the input signals, the magnitude of which is chosen from a uniform random distribution. In this sense, using only e.g. three sampling instances will not be representative of how the temperatures varied throughout the experiment. Moreover, a single-input-single-output linear transfer function model cannot mathematically describe such open-loop experiments, and hence it is not meaningful to use them. Hence the approach of utilising all the instances of the raw data is implemented.

7.3.2 Selection of distance metric

In the first case, where the raw samples are used for clustering, the q locations are characterised by p dimensions of the same unit of measurement (i.e. temperature in $°C$). In these circumstances, literature advises the use of the "Cityblock" function to construct the $q \times q$ proximity matrix [Kaufman and Rousseeuw, 2009]. This function calculates the sum of absolute differences. On the contrary, where the system parameters are utilised ($p=2$), the time constant and steady state gain differ; the latter is unit-less and variable depending on the actuator settings, whereas the time constant can be expressed in seconds, minutes and so on. In addition, the two variables are different in terms of scale. This is known to cause one variable to prevail over the other, and unless this is desirable (in this study, it is not), there is the option of standardizing both variables [Kaufman and Rousseeuw, 2009]. The z-score, as it is known, computes the mean value of each clustering variable, and based on that it computes the mean absolute deviation (spread) for each value in the $q \times p$ information matrix.

7.3.3 Metaclustering

The hierarchical clustering results, are visualised by means of a dendrogram, which the user may exploit to decide on the number of clusters. Alternatively, most software packages allow one to automatically cut the dendrogram at different levels, which correspond to different k cluster solutions. The opposite applies for the k-means algorithm, as it seeks a new solution for a different k. For both algorithms, it is common to further assess the compactness (quality) of the produced clusters by resorting to validity indices [Liu et al., 2010, 2013, Milligan and Cooper, 1985]. Milligan and Cooper [1985], and more recently Arbelaitz et al. [2013] for example, assessed numerous validity indices for obtaining an optimal number of clusters under different types of data and algorithm approaches. For the present research, the Silhouette index [Rousseeuw, 1987] is used by the author in an *ad-hoc* manner, e.g when certain temperature locations may belong to more than one cluster. This is defined as,

$$s(i) = \frac{b(i) - a(i)}{max\{a(i), b(i)\}} \tag{7.4}$$

where $a(i)$ is the average difference of object $q=i$ to the other members allocated to the same group, while $b(i)$ represents the minimum average difference of datum i between the other groups. This also indicates the second best group to allocate to that datum, hence if it is much larger than $a(i)$ then $s(i)$ indicates that the datum is well allocated [Rousseeuw, 1987]. It takes a value in the range of 0 to 1, with unity indicating the optimal partitioning. The overall silhouette index is the average of the average of each group.

7.4 Transfer function models

As part of utilising the system parameters described earlier, for clustering, consider the following linear discrete-time system explaining temperature,

$$y(k) = \frac{b_1 z^{-1} + ... + b_m z^{-m}}{1 + a_1 z^{-1} + ... + a_n z^{-n}} u(k) + \frac{1}{1 + c_1 z^{-1} + ... + c_n z^{-n}} e(k) = \frac{B(z^{-1})}{A(z^{-1})} u(k) + \frac{1}{C(z^{-1})} e(k) \quad (7.5)$$

where $y(k)$ is the sampled output (temperature) and $u(k)$ is the input (heater voltage), while $A(z^{-1})$ and $B(z^{-1})$ are appropriately defined polynomials in the backward shift operator z^{-1}, i.e. $z^{-i}y(k) = y(k-i)$. For convenience, any pure time delay of $\delta > 1$ samples can be accounted for by setting the $\delta - 1$ leading parameters of the $B(z^{-1})$ polynomial to zero, i.e. $b_1, ..., b_{\delta-1} = 0$. Also note that, throughout this thesis, the noise model is not considered i.e. $C(z^{-1}) = 1$. The identification and estimation part in this thesis utilises the Refined Instrumental Variable (RIV) algorithm [Young, 2011, Taylor et al., 2013]. Note that, for a given physical system, an appropriate model structure first needs to be identified, i.e. the most appropriate values for the triad $[n, m, \delta]$. The two main statistical measures employed to help determine these values are the coefficient of determination R_T^2, based on the error between the measured and simulated responses; and Young's Identification Criterion (YIC), which provides a combined measure of model fit and parametric efficiency.

The CAPTAIN Toolbox (MATLAB) is used for the implementation of all these routines [Taylor et al., 2007, 2013, Young, 2011]. Note that the toolbox can also estimate Multiple-Input-Single-Output (MISO) models. For example, the following linear MISO Transfer Function model provides a reasonable fit to the experimental data captured in 6.3, as illustrated in Fig. 7.3,
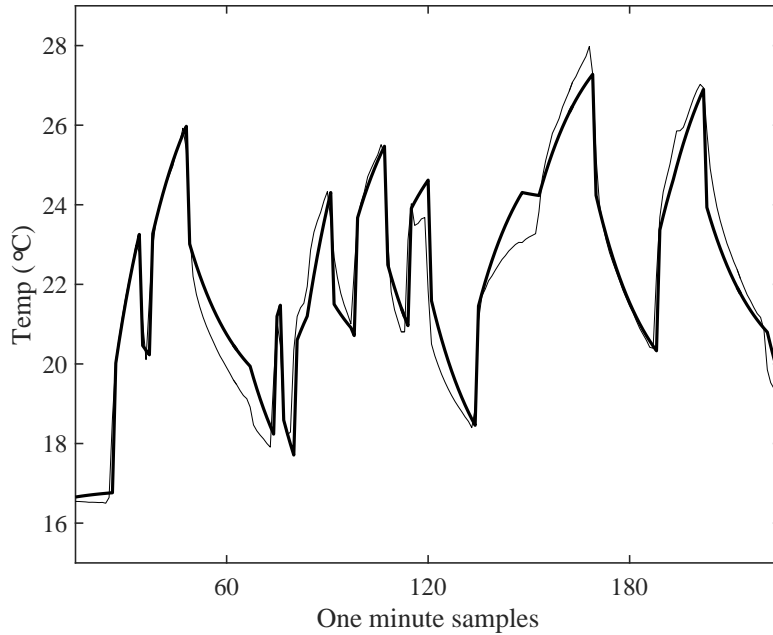
Figure 7.3: Model representation on one of the two zones that were derived by visual inspection of the data presented in section 6.3. The thick trace (equation 7.6) represents the model fit to the average zone data.

$$y_1(k) = \frac{b_1 z^{-1} + b_2 z^{-2}}{1 + a_1 z^{-1}} u_1(k) + \frac{d_1 z^{-1}}{1 + a_1 z^{-1}} u_2(k) \tag{7.6}$$

where $y_1(k)$ is the average temperature of one zone (the lower array of six temperature locations in Fig. 6.4), while $u_1(k)$ and $u_2(k)$ are the heater and fan inputs respectively. For the present example, the parameter estimates are $b_1 = 0.6296$, $b_2 = -0.5000$, $d_1 = -0.1023$, $a_1 = -0.9381$. This model explains 95% of the variance of the data, as indicated by the coefficient of determination ($R_T^2 = 0.9460$).

For both types of models (equations 7.5, 7.6) the parameters can be exploited to yield its time constant(s) and steady state gain (see e.g. Taylor et al. [2013]). The time constant is the time taken for the output to reach 63% of its steady state value. In the case of a first order Single-Input-Single-Output (SISO) model where $n = m = 1$, i.e.,

$$y(k) = \frac{b z^{-\delta}}{1 + a_1 z^{-1}} u(k) \tag{7.7}$$

the time constant is defined as follows,

$$\text{TC} = -\frac{\Delta t}{ln(-a_1)} \tag{7.8}$$

where Δt is the sampling interval. Note that as the order of the denominator increases, it has to be decomposed to first order models to derive the time constant of each order. The steady state response to a constant input u is given by,

$$y(k \to \infty) = \frac{b}{1 + a_1} \times u = \text{SSG} \times u \qquad (7.9)$$

where the steady state gain is obtained by setting $z^{-1} = 1$ (see Taylor et al. [2013], page 24). Furthermore, if a MISO model is utilised (e.g. equation 7.6), the individual steady state gains are added to form the final steady state gain.

7.5 Results

The following results are split in four subsections: the first three address experiments under a fixed fan setting and a step change in the heater input. In total, 12 step experiments are assessed; four for each of three fan settings. These are denoted as *f15*, *f25*, and *f45*. For each one, the heat settings are denoted similarly as *h15*, *h25*, *h35*, and *h45*. As described in section 6.2, the fan and heater are controlled individually via a 0-5 V DC signal, and hence the values that follow f and h imply for example a 1.5, 2.5, 3.5, or 4.5 V DC signal. Low ventilation rate (*f15*) corresponds to 1 ms^{-1}, whereas medium and high ventilation rate corresponds to 4.6 ms^{-1} and 8.8 ms^{-1}, respectively, at the outlet of the forced ventilation test chamber. The temperature locations that are used for clustering purposes are locations no. 1-18, as these represent the main grid of the chamber. The rest of the locations are not used so that the main grid resembles a study on an exemplary main growing area. The reader is encouraged to use Fig. 6.1 as a visual aid with regard to the locations referred hereinafter. The fourth subsection assesses three datasets: one where both the fan and the heater vary randomly, another one where the fan is fixed at *f25* and the heater varies; and a third one where the heater is fixed at *h45* and the fan varies.

K-means and hierarchical clustering is undertaken on the basis of a) raw data instances, and b) system parameters derived from linear transfer function models. For the former approach, the clustering variables are four; the individual average values at the minute the heat step is applied, and at instances that fall at 25%, 50%, and 90% of the length of the experiments (the average values of sixty samples amidst the selected instances). The first one relates to the initial state, the second and the

third relate to the transient part of the dataset, and the fourth (90%) relates to the part where temperatures have settled to a new steady state. The average values are calculated on the basis of 60 samples, with each sample representing one second. Using the second approach, the individual responses of each data-set are passed through the RIV algorithm in order to estimate the parameters of first order transfer function models with one sample of time delay (based on a one minute sampling rate). Such a structure was found to have a low response error for each data-set, with an average R_T^2 of 0.9811, 0.9657 and 0.9646 for low, medium, and high ventilation rates respectively; and characterised by good parametric efficiency (YIC: -12.3219, -10.4691, and -10.19). Based on the estimated parameters, the time constants and steady state gains are calculated (see equations (7.8) and (7.9)), and standardized in turn as described in section 7.3.2. For the non-linear datasets, both the k-means and hierarchical algorithms are utilised; but only using the raw data instances.

.

7.5.1   Low ventilation rate

For the lowest step change in the heater input, all four approaches yield the same result when $k = 2$; with one comprising four temperature locations (5, 6, 11, and 12) at the bottom layer, and another one containing the rest of the temperature locations on the main grid. Fig. 7.4 shows how the raw data instances are partitioned using both the k-means and hierarchical approaches; and Fig. 7.5 shows the partitioning using the standardized system parameters. In both plots, the two clusters are distinctively separated. For the former plot, the data structure show a more elongated structure than for the latter, and one could alternatively choose a $k=4$ cluster solution, which would split the big cluster in three. However, the heat step for this experiment is small and hence the overall difference between the temperature locations in the big cluster is also relatively small. Fig. 7.6 shows the relevant time-series for this open loop experiment, which confirms that the temperatures are clustered appropriately.

For the rest of the three heat step experiments, the existence of two clusters is overt; one group comprising the bottom layer temperature locations (5, 6, 11, 12, 17, and 18), and a second one comprising the locations of the middle and top layers. The partitioning depicted in Fig. 7.7, and Fig. 7.8; as well as the silhouette plot
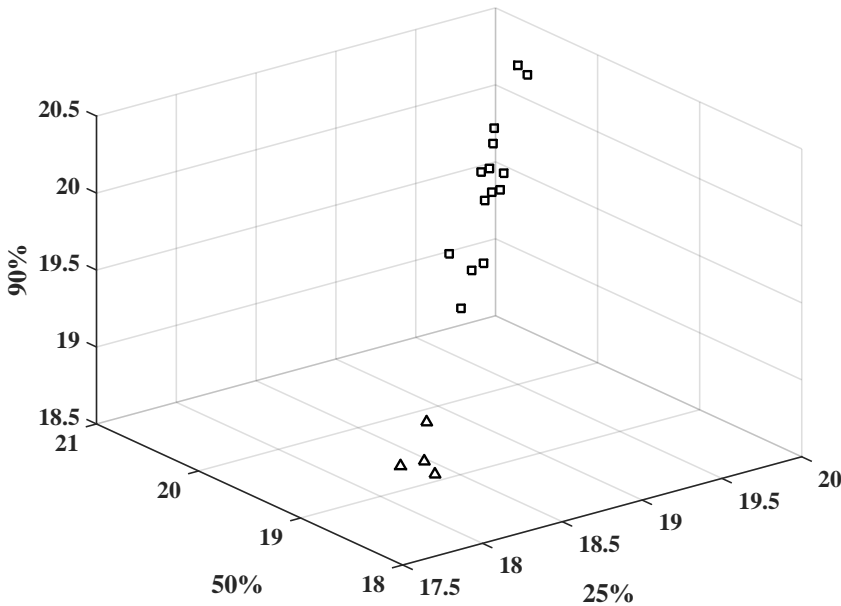
Figure 7.4: Three-dimensional plot that shows the structure of the data when plotted against 25%, 50%, and 90% average sample instances. Note that although the fourth clustering variable is used for clustering, it is simply omitted here for the sake of producing a meaningful graph. The two clusters are depicted in triangle and square shaped points.
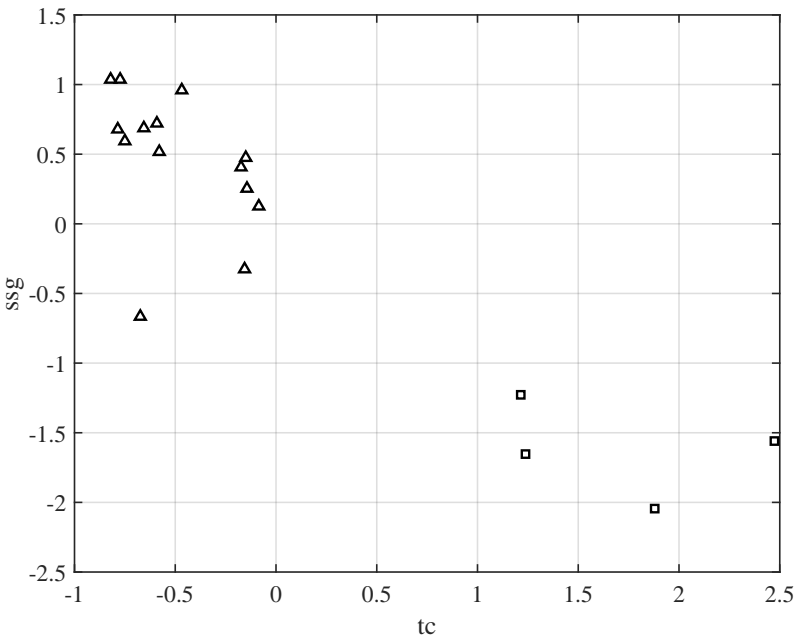
Figure 7.5: The structure of the partitioned data when plotted as standardized time constants (tc) against steady state gains (ssg). Similar to Fig. 7.4, the two clusters are depicted in triangle and square shaped points.
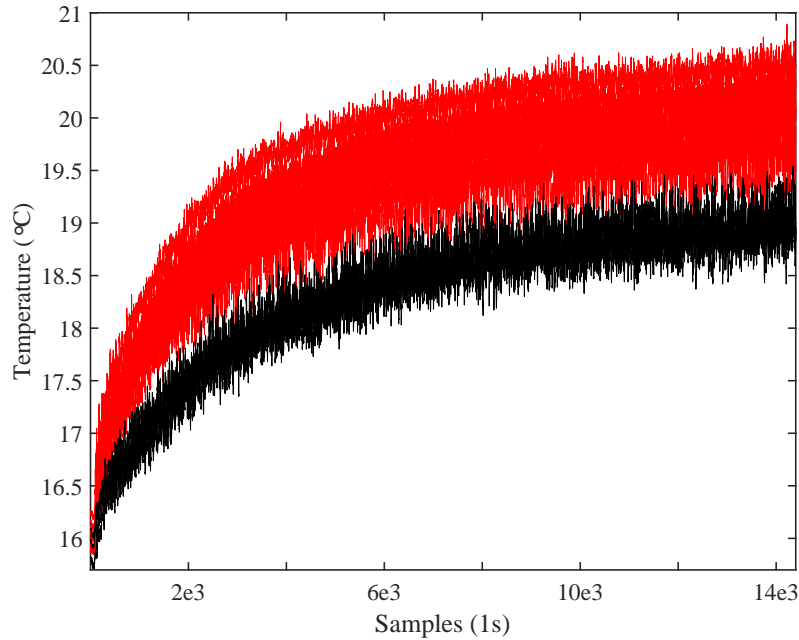
Figure 7.6: Temperature responses of heat step experiment *f15h15*, colour coded here, with the black trace representing the bottom layer temperature locations.

produced in Fig. 7.9, are all generated using the highest heat step experiment (*h45*) but are representative of the data structure in *f15h25* and *f15h35* (even though the actual temperatures are different for each one).

7.5.2   Medium ventilation rate

At a medium level of ventilation and using the lowest heat setting, the temperature gradient is less than 1 $°C$, and hence it is not meaningful to distinguish more than one clusters; i.e. the distribution is uniform. The same applies for a slightly higher heat step (*h25*). As it is seen from Fig. 7.10, the temperature gradient is no more than 2 $°C$ for all three time instances.

For a heat step of *h35*, the gradient is at all times around 3 $°C$, and hence it makes sense to assess a cluster solution of *k*=2. By using the raw data, both the *k*-means and hierarchical approaches yield two very similar spatially meaningful clusters. The *k*-means yields one cluster that comprises the front end locations near the outlet (i.e. 1-6, and location no. 7, which is next to location no. 1), and another one that contains the rest of the locations. The hierarchical approach yields the same results but allocates, in addition, location no. 12 to the front end group.
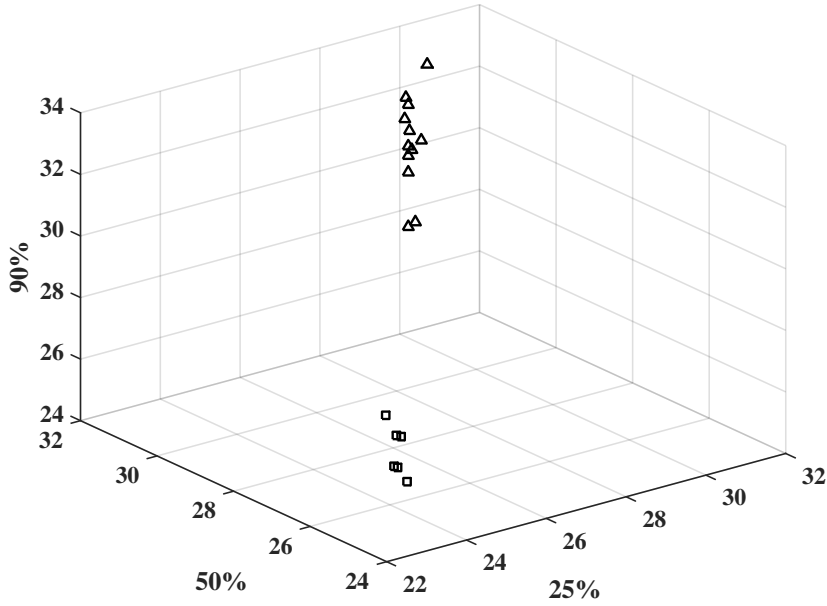
Figure 7.7: Structure of data for clustering based on the raw data instances of *f15h45*.
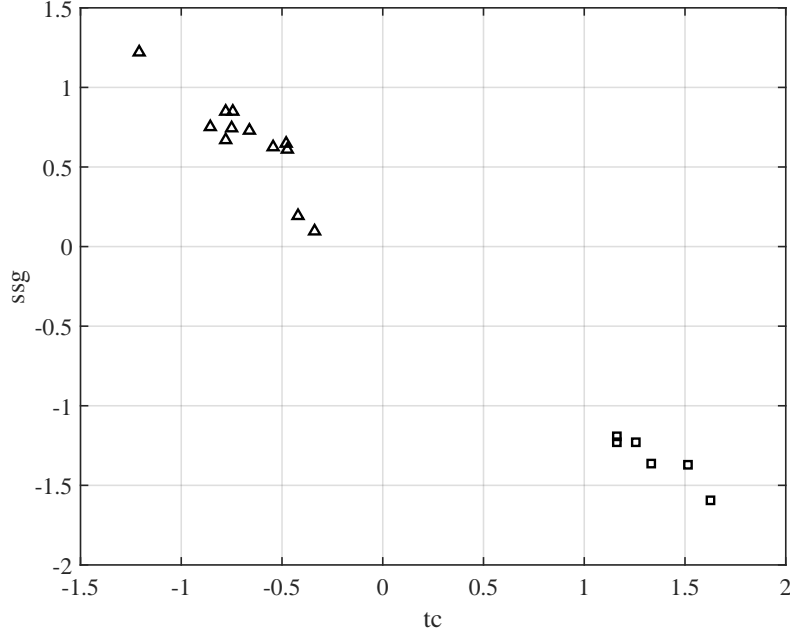
Figure 7.8: Two-dimensional structure of data for *f15h45*.
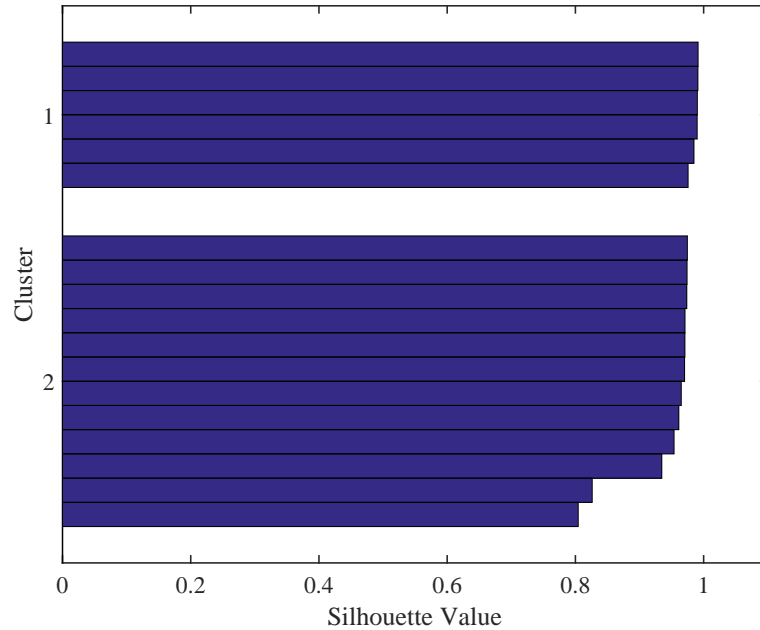
Figure 7.9: Silhouette plot for a clustering solution $k=2$, regarding *f15h45*. The high values suggest a good within cluster compactness and between cluster separation.

The three-dimensional plot in Fig. 7.11 highlights this location with a star symbol. As seen, it sits almost halfway between the clusters. The silhouette plots reveal that with k-means it has near zero value (bottom left plot), which indicates that it marginally belongs in one group; whereas its negative value in the silhouette plot produced after the hierarchical approach shows that it definitely does not belong in the other group. On the other hand, using the normalized system parameters yields different solutions. Again, there is a tendency to partition the space in a front to back manner, and thus the solutions are not entirely different, but they are not as clear as before; and the two algorithms disagree with each other. Finally, the exact same situation also describes the highest heat step (*h45*).

7.5.3   High ventilation rate

The three first heat step experiments with a high ventilation rate indicate that the temperature distribution is uniform as the overall gradient is at 0.4, 1.1, and 1.5 $°C$ respectively. The dataset with the highest heat setting is also a case where a cluster solution of $k=2$ is sensible as the overall gradient is approximately 2.6 $°C$. For this experiment, all four clustering approaches yield different solutions. For instance, the
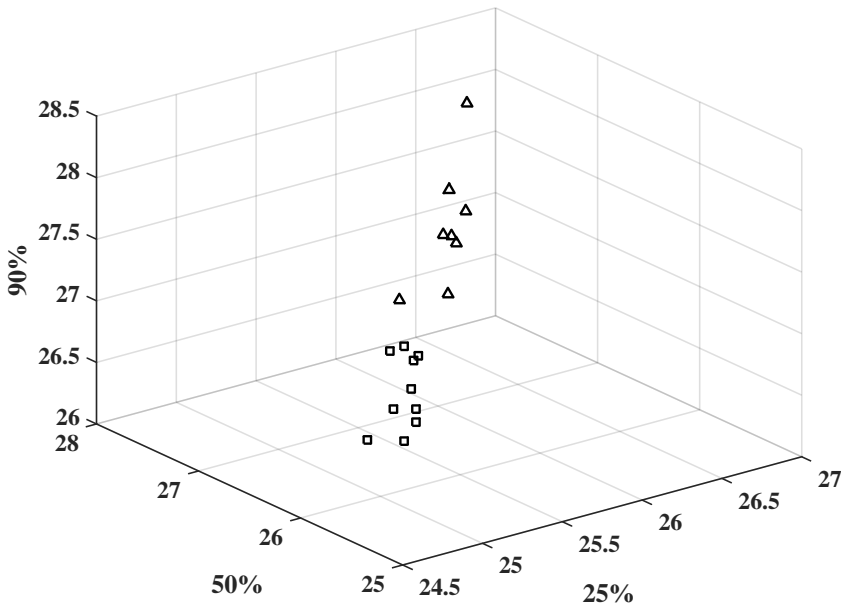
Figure 7.10: Clustered data structure for *f25h25*, which still shows elongated but compact enough to consider uniformity instead of the two zones shown here by triangular and square points. Note that the gradient is less than 2° C at all sampled instances.
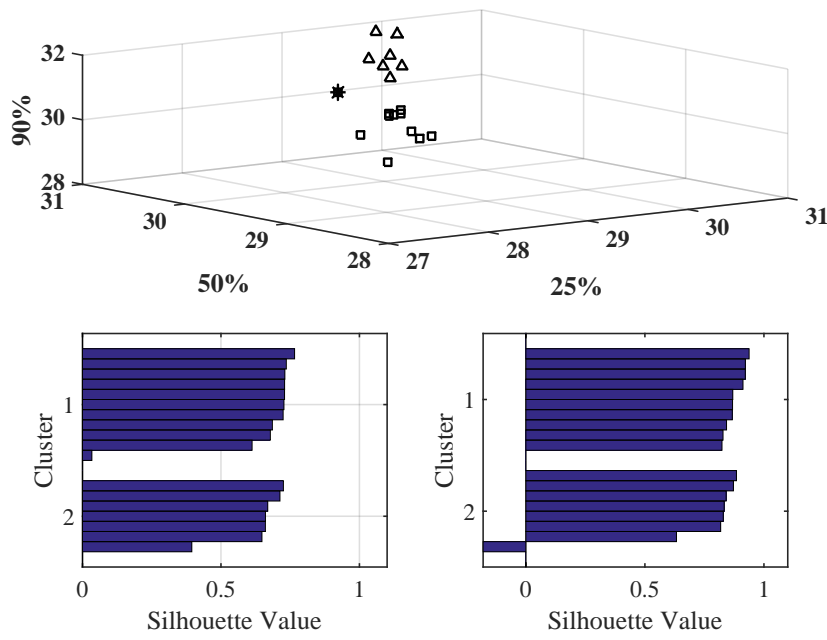
Figure 7.11: The top plot shows the data structure of *f25h35*, with location no.12 depicted here as a star symbol belonging marginally to both groups. However, the silhouette plots suggest that it belongs to neither for a cluster solution of *k*=2
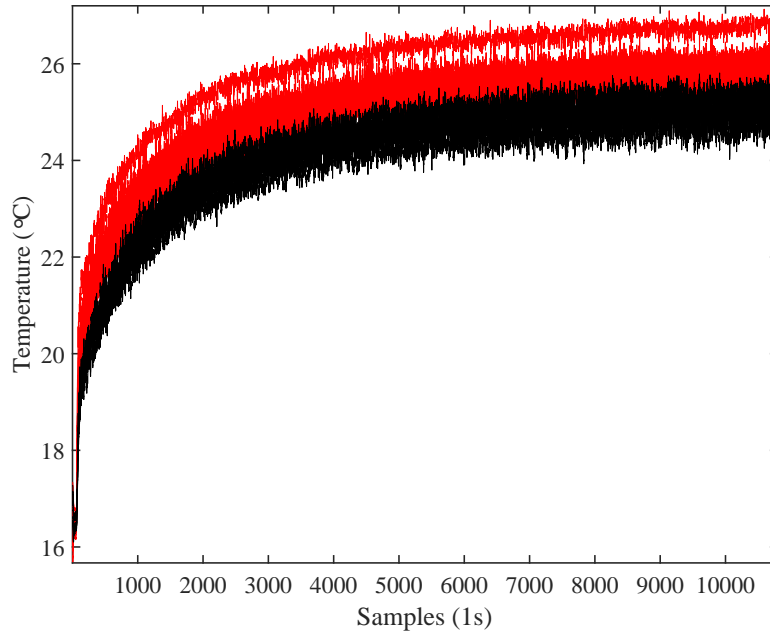
Figure 7.12: *f45h45* temperatures partitioned with respect to k-means (raw data). The first zone (red traces) contains the front end locations (1-4), together with the six locations of the bottom layer (5-6,11-12, and 17-18); the second contains the rest (upper and middle layer).

k-means that utilises the raw data creates one group that contains the front end locations (1-4), together with the six locations of the bottom layer (5-6,11-12, and 17-18), and another one grouping the rest. Fig. 7.12 shows this clear partitioning. The equivalent hierarchical on the other hand, creates one group with one temperature location (the highest temperature response that is visible in Fig. 7.12), and another one with the all the rest. The hierarchical algorithm that uses the normalised system parameters as clustering variables yields two groups that are identical to the ones observed in the low ventilation datasets, although in this case the bottom layer is warmer than the middle and the top ones. The corresponding k-means groups locations no. 7-8, 13-14 into one group (four locations next to each other at the top layer), and another one with the rest of the locations. The silhouette indices displayed for each approach in Fig. 7.13 suggest that the most robust solution is produced by utilising the hierarchical approach along with the system parameters as clustering variables.
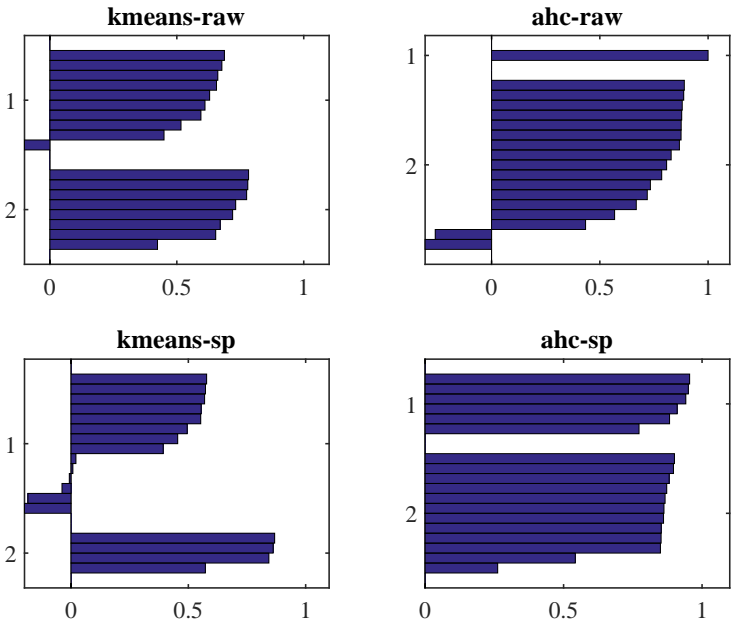
Figure 7.13: Silhouette plots produced by using the four different clustering approaches for the *f45h45* dataset.

7.5.4   Non-linear datasets

Each of the three datasets utilised here last 10 hours, originally with a sampling of one second. Here, each dataset is subsampled every 30 seconds, which corresponds to an information matrix of $q=18 \times p=1079$. For the dataset where both actuators vary, both algorithms agree that 2 clusters are sufficient to describe the temperature distribution. In particular, these are a) the bottom layer locations, and b) the middle and top layer locations. Fig. 7.14 depicts these two different types of behaviour. Note that the two clusters do merge for certain actuator signal combinations but the general behaviour of each cluster is well separated.

For the dataset where the fan is fixed at a setting of *f=25* and the heater varies, both algorithms agree that two clusters can sufficiently describe the temperature distribution. The results are consistent with the findings of section 7.5.2, i.e. one cluster towards the outlet (locations no. 1-7), and another one with the locations at the middle and the back of the main grid. Fig. 7.15 displays the behaviour of the two clusters. In this cases, the clusters tend to merge only when the fan setting is lowered (during cooling segments)

Finally, for a steady heat setting (*h45*) and with the fan varying, the clustering
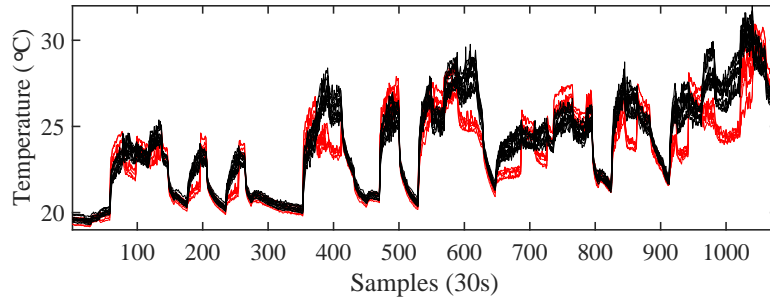
Figure 7.14: Colour coded cluster solution $k=2$. It can be seen that two types of behaviours are indeed present within the main grid, and that they are also meaningful; that is, they correspond in this case to the bottom layer (red traces) and the two other layers.
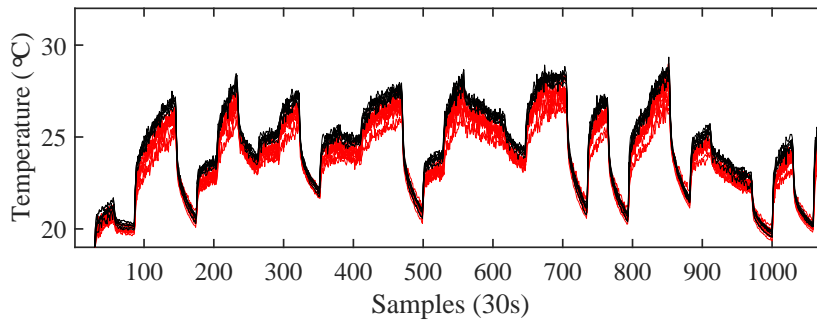
Figure 7.15: Two clusters again describing the temperature distribution. This solution confirms that for medium ventilation rate the test chamber is partitioned in a front to back manner within the main grid.

results are identical (and more apparent) as in the first case; i.e. the distribution can be described by two zones, the bottom layer, and the middle/top layers. Fig. 7.16.

7.6 Discussion

This chapter shows that clustering can be successfully applied in order to identify thermal zones from data-sets collected with different thermal and ventilation conditions by exploiting either information derived from average instances of the raw data, or from data-based modelling methods. In this manner, it is possible to model and undertake control design for single and multiple zones. Both clustering algorithms yielded physically meaningful thermal zones; derived without prior spatial informa-
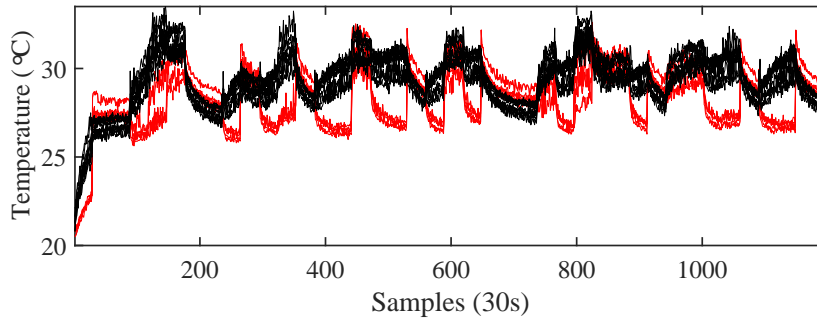
Figure 7.16: Two clusters describing the temperature distribution for a fixed heat setting and the fan varying.

tion about the measurement locations. The results from the step experiments hinted some form of consistency in terms of the zones created, while the results from the non-linear datasets confirmed the previous findings. For example, a fixed fan setting of *f25* does indeed produce a two zone structure with a front-to-back separation and the other two datasets show that a two zone structure with a bottom-to-top layer separation is prevalent when the fan varies randomly. The latter findings also confirm the assumption made in section 6.3 for the motivational example, but in a quantitative manner.

The basic limitation of clustering is that it requires significant user input in order to ensure that the results lack bias and reveal the natural dependencies that are present in the datasets under study. For example, the algorithm can be run on the basis of different settings: a) the type and pre-processing of clustering variables, b) the choice of distance metric, and c) the choice of linkage criterion (for the hierarchical approach). For the latter two, the author chose to use the recommended settings for the type of data that are utilised here, and the exploratory task was limited to producing results from two clustering algorithms and two different types of clustering variables. In general, the raw data were consistent in terms of producing meaningful zones, while the system parameters also mostly produced results that agreed with the latter; and any deviations could be accounted for the fact that a common model structure was essential for the clustering task.

The silhouette metaclustering index was finally advised where appropriate, and it was found to be particularly useful when locations marginally belonged to more than one group. Moreover, the number of zones sought after in a dataset depends on

the constraints of the application. For the datasets assessed here, the gradient was low enough to consider two zone solutions. If the corner locations were also used, formulating three of four zones would be more sensible.

7.7   Conclusions

This chapter proposed the use of cluster analysis to identify thermal zones for applications where multiple location measurements are available. Using a series of open-loop experiments, two different clustering algorithms with two different settings were assessed. Different machine learning algorithms have the potential to be used in such applications and hence it could be an interesting concept for future research. Chapter 9 presents two control examples that may be utilised based on these results. This analysis shows that it may be beneficial to undertake clustering for modelling purposes, as one may eventually utilise a single transfer function to express multiple locations. These zone representative models can be also used in block oriented structures, such as the non-linear thermal model that is presented in the following chapter.

Chapter 8

Thermal Modelling

This chapter considers mathematical models for describing temperature in buildings. In particular, a novel data-based approach is proposed, in which static nonlinear functions are used to describe the steady state temperature, in response to both heater and fan actuator inputs. These are combined in series with either linear Transfer Function (TF) or State Dependent Parameter (SDP) models to describe the dynamic response, with all the model components identified from experimental data. The particular form of SDP model utilised here, has a superficial similarity to the TF models introduced in the previous chapter, but the parameters of the model are functionally dependent on measured variables (here, the input or output signals). For an introduction to SDP models and for the algorithms used to estimate them, see e.g. Young [2011] or Taylor et al. [2013] (Chapter 9).

To illustrate the modelling concept, Fig. 8.1 represents a simplification of the full approach developed later in the chapter. Using temperature data from a series of straightforward experiments, with a range of time-invariant heater inputs, the steady state non-linear relationship between temperature and applied voltage to the heater is identified (ignoring in this initial model the applied voltage to the fan and associated ventilation rate). In turn, this allows for the formulation of a block-oriented model [Aguirre et al., 2005], with a Hammerstein structure, as illustrated in Fig. 8.1. Here, u_{heat} is the heater input (volts DC), whilst $\tilde{u}_e$ is the predicted steady state temperature, as calculated using the identified non-linear static function $\phi(\cdot)$; and u_{amb} is the external (laboratory or environment) temperature (degrees °C). In turn, $\tilde{u}_e$ acts on the input of a linear discrete time dynamic model, similar

to equation (7.5) in the previous chapter. Finally y_t is the resulting temperature response. Note that the dynamic model is modified appropriately to constrain the steady state gain to unity, thus allowing the steady state behaviour to be entirely determined by the non-linear static function $\phi(\cdot)$ [Pearson and Pottmann, 2000].

When the dynamic component is a straightforward linear TF, the above approach represents a type of Hammerstein model. However, section 8.6 of this chapter uses a SDP model to represent the system dynamics, which is arguably a type of Wiener-Hammerstein model. In fact, the literature seems somewhat ambiguous on the definition of these terms. Sometimes the Wiener-Hammerstein model is considered as an input nonlinearity (as here), followed by a linear model (the TF model component) and then an output nonlinearity (the SDP model component in this case) but on other occasions it is a single nonlinearity enclosed by two linear models. In any case, the overall modelling approach proposed in this chapter, has a certain similarity to that reported in the PhD thesis by Hitzemann [2013], who optimises polynomial functions to represent the coefficients of various steady state relationships for a DC-DC boost converter. In the present work, however, the concept is developed for the case of temperature in an enclosed space, with the models obtained linked to the clustering technique for zone identification developed in the previous chapter. The models obtained in this manner are evaluated using the forced ventilation test chamber for both (i) single thermocouple (sections 8.1 to 8.6) and (ii) single and multi-zone (section 8.7) scenarios.

Section 8.1 introduces the static function for the steady state response, followed by the initial linear dynamic model in section 8.2, and Hammerstein model in section 8.3. The limitation of this two-input model (as illustrated by Fig. 8.1) is demonstrated in section 8.4 and addressed in section 8.5, in which the applied voltage to the fan is introduced as a third input. The latter model is referred to here as a 2-dimensional Hammerstein model. This is because the coefficients of the static non-linear function are now functions of two variables, namely the heater and fan inputs (the ambient temperature enters the model as a straightforward additive component). Finally, the SDP extension of this modelling approach is considered in section 8.6 and 8.7, with the chapter conclusions presented in section 8.8.
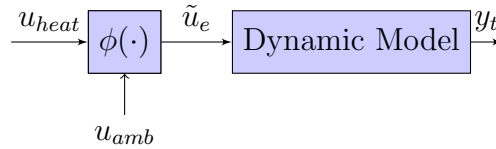
Figure 8.1: Exemplary Hammerstein Model

8.1   Identification of temperature steady state behaviour

Previous research [Stables and Taylor, 2006] has shown that the relationship between a time-invariant applied voltage to an axial fan u_{fan} and the steady state ventilation rate y_{vr}, can be conveniently described by the following flexible logistic growth function,

$$\phi(\cdot) = y_{vr\,\max}(1 + \mathrm{e}^{-\theta(u_{fan}-x_0)^{\frac{1}{c}}})^{-1} \tag{8.1}$$

where $y_{vr\,\max} = 8.8748$, $\theta = 0.0091$, $x_0 = 2.5170$ and $c = 0.0039$ are coefficients that determine the shape of the curve. These correspond to the maximum output, curvature factor, the inflection point and power, respectively. In other words, the steady state ventilation rate asymptotically approaches a maximum value $y_{vr\,\max}$ determined by the characteristics of the fan, as illustrated by Fig. 8.2.

Similarly, this non-linear static function $\phi(\cdot)$ is utilised in this chapter to characterise the steady state behaviour of the individual temperature locations in the chamber. In particular, the steady state temperatures of 48 step experiments (six fan/eight heat settings) are derived and then averaged for each temperature location. In turn, for each fan setting, the steady state average temperatures are plotted against heater voltage. For example, the black traces of Fig. 8.3 represent the steady state shape of temperature location no. 1 for six different fan settings. The shape of the curves is similar to that of ventilation estimated previously. Hence, the flexible logistic growth function is utilised again to explain the steady state behaviour of the overall model (red traces in Fig. 8.3). The relationship will be subsequently denoted for temperature as:
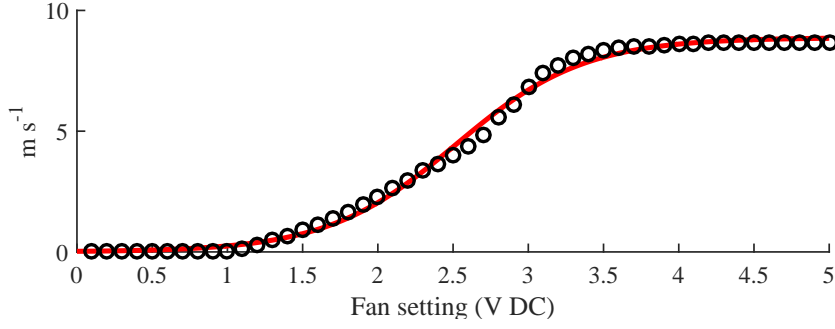
Figure 8.2: Steady state behaviour ventilation rate, with circles representing the data, and the red trace representing the model fit solved by equation (8.1).

$$\tilde{u}_e = \phi_1 \{u_{heat}\} = y_{t\max}(1 + \mathrm{e}^{-\theta(u_{heat}-x_0)^{\frac{1}{c}}})^{-1} \tag{8.2}$$

Note that for estimating a temperature power curve, u_{amb} is subtracted to bring the measured chamber location to its baseline. This is subsequently added back for model evaluation purposes (as shown in Fig. 8.1). For a given set of input (heat)/output (steady state temperature) data, and an initial set of parameters for equation (8.2) (i.e. x_0=20, $y_{t\max}$=6, c=0.07, and θ=0.09), the standard MATLAB® function fminsearch is utilised to calculate a set of parameters that minimizes the sum squared of residuals (SSR, equations (8.3), (8.4)), and fits equation (8.2) to the steady state data in a Least Squares sense (Nelder-Mead simplex method),

$$z(i) = \tilde{u}_{emeas}(i) - \phi_1 \{u_{heat}\}(i) \tag{8.3}$$

$$SSR = \sum_{i=1}^{n} z(i)^2 \tag{8.4}$$

where $i = 1, 2, ..., n$ corresponds to the step setting applied in the heater input, $z(i)$ is the fit error of each individual value , and $\tilde{u}_{emeas}(i)$ is the measured steady state temperature for a given time-invariant heat input. The initial selection of parameters is crucial towards converging to parameters that minimize equation (8.4). Choosing an initial value for $y_{t\max}$ is probably the easiest of four as one may derive this information from looking at the maximum value of the data-set. On the other hand, a more trial and error approach is followed for the other three coefficients. In general,
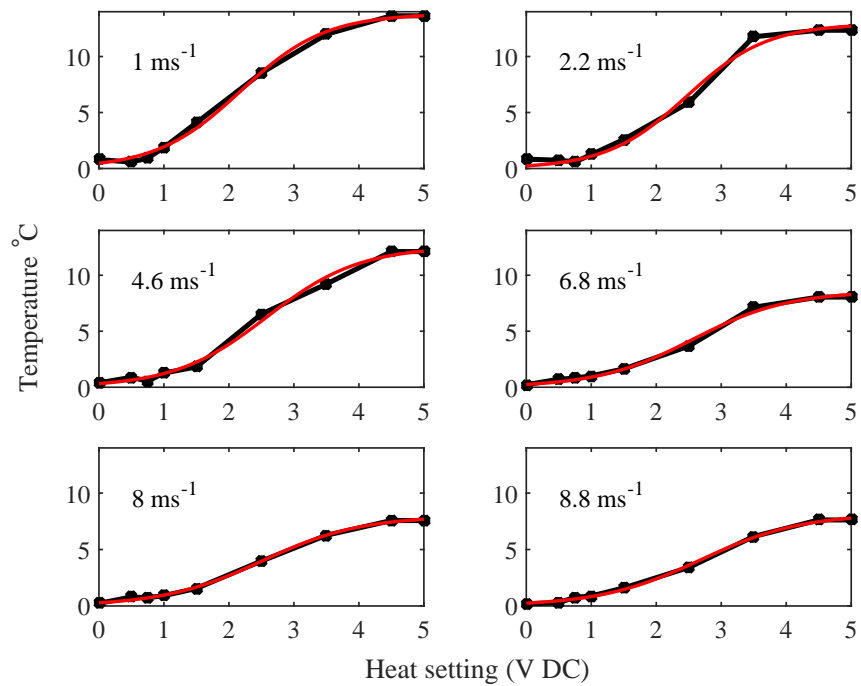
Figure 8.3: Steady state behaviour of exemplary temperature location no. 1 for six different fan settings. The points in this figure are the steady state temperatures derived from the experiments, whilst the solid traces result from solving equation 8.2.

x_0	$y_{t\,\max}$	c	θ
2.1795	13.8226	0.0670	0.1030
2.4702	12.9217	0.0416	0.0674
2.5860	12.5697	0.0216	0.0304
2.5666	8.5765	0.0631	0.0864
2.5105	7.9768	0.0807	0.1062
2.6838	8.1761	0.0911	0.1177

Table 8.1: Equation (8.2) optimised coefficients for each of the six power curves displayed in Fig. 8.3, with the first and last rows relating to the lowest and highest fan settings respectively

for these steady state data, x_0 values over 30 will not help to find any acceptable solutions while θ and c should be initialised with very small values. The set of initial parameters specified above works well in terms of estimating the temperature power curves of all temperature locations, and for all fan settings. Based on this initialisation for example, the set of parameters shown in Table 8.1 was found to satisfactorily fit the steady state data of Fig. 8.3.

8.2 Dynamic model

In order to identify the dominant heater-temperature dynamics, data were collected from all the thermocouples for level changes in the applied heater voltage, as illustrated in Fig. 8.4. The RIV algorithm, combined with the YIC and R_T^2 indices [Young, 2011], suggest that the following unit delay, discrete-time, second order model provides a good explanation of the of the measured data towards medium ventilation rates and moderate heat input,

$$y(k) = \frac{b_1 z^{-1} + b_2 z^{-2}}{1 + a_1 z^{-1} + a_2 z^{-2}} u_{heat}(k) \tag{8.5}$$

where $y(k)$ is the temperature of location no. 1 at sample k and the parameter estimates are $b_1 = 0.6051\ (0.0476)$, $b_2 = -0.5528\ (0.0420)$, $a_1 = -1.3963\ (0.0602)$, and $a_2 = 0.4198\ (0.0572)$, with the parameter standard errors included in brackets. This model explains 99% of the variance of the data, as indicated by the coefficient
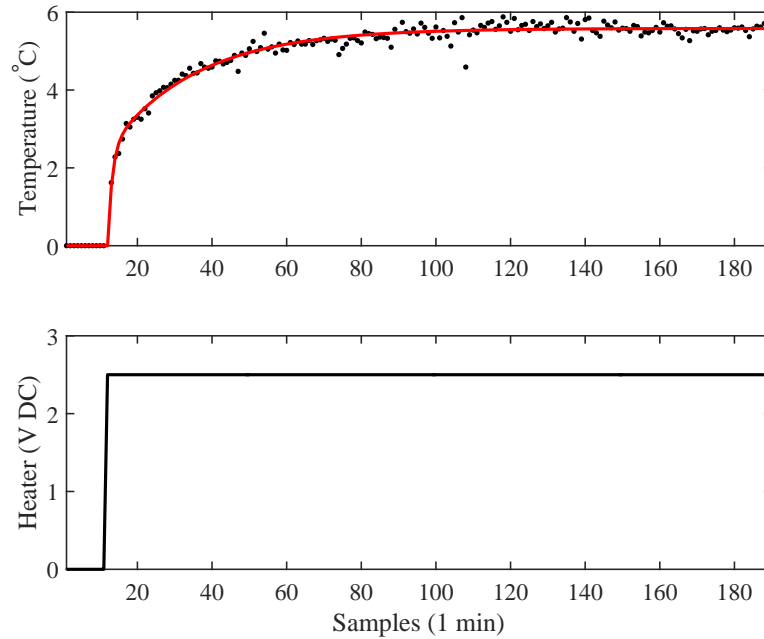
Figure 8.4: Open-loop experimental data and dynamic model for temperature, with time-invariant fan input of 2.5V. Upper subplot: temperature elevation (points) and linear model response (solid). Lower subplot: heater input.

of determination ($R_T^2 = 0.9881$). These parameter values are based on a sampling rate of 1 minute. For the illustrative results in Fig. 8.4, the operating level is defined by the fan and heater inputs at 2.5V DC (*f25h25*). Equation (8.5) is combined with the previously estimated steady state model, as discussed below.

8.3 Combined Model

A schematic diagram of the combined thermal model is given in Fig. 8.1. In this model, the steady state temperature is predicted using equation (8.2). The function $\phi(\cdot)$ generates an "effective input" $\tilde{u}_e(k)$, which is used to drive the dynamic model component as follows,

$$y(k) = \frac{b_1 z^{-1} + b_2 z^{-2}}{1 + a_1 z^{-1} + a_2 z^{-2}} \tilde{u}_e(k) \tag{8.6}$$

Note that because the utilised dynamic data of temperature location no. 1 are based on a fan operating level of 2.5 V, the coefficients of equation (8.2) are also

estimated based on the measured steady state data of the same temperature location, and the same fan setting; i.e. the third row from table 8.1. A scalar is imposed on (8.6), which is the TF's inverse, in order to ensure unity steady state gain (as calculated in e.g. equation (7.9)).

$$y(k) = \frac{1 + a_1 + a_2}{b_1 + b_2} \cdot \frac{b_1 z^{-1} + b_2 z^{-2}}{1 + a_1 z^{-1} + a_2 z^{-2}} \tilde{u}_e(k) \tag{8.7}$$

Dividing the denominator of the scalar and the numerator of the transfer function by b_1 yields

$$y(k) = \frac{1 + a_1 + a_2}{1 - p} \cdot \frac{z^{-1} - p z^{-2}}{1 + a_1 z^{-1} + a_2 z^{-2}} \tilde{u}_e(k) \tag{8.8}$$

where $p = -b_2/b_1$ is the zero of the linear model (8.6). The simulation model is then expressed in difference equation terms, in order to see how the predicted temperature changes based on its past values.

$$y(k) = -a_1 y(k-1) - a_2 y(k-2) + \left(\frac{1 + a_1 + a_2}{1 - p} \right) \cdot (\tilde{u}_e(k-1) - p \cdot \tilde{u}_e(k-2)) \tag{8.9}$$

Note that equation (8.9) has the same time constant and structure as equation (8.6) but has been adapted to ensure the required steady state gain of unity.

8.4 Preliminary evaluation

Evaluation results using an open-loop data set in which the heater level is varied and with a fan setting fixed at 2.5 V are shown in Fig. 8.5. Here, it can be seen that the transient and steady state behaviour of the data are well explained by the thermal model. The steady state temperature prediction is also shown in the lower plot of Fig. 8.5. Overall, the model explains the experimental data with an accuracy of 97%, calculated with the coefficient of determination (R_T^2). In contrast to a fixed fan input signal however, Fig. 8.6 reveals the model's incapacity to explain experimental data where both fan and heater inputs are varied, since the steady state non-linearity of the fan is not incorporated in it. For such a data-set the model fit drops down to 78%.
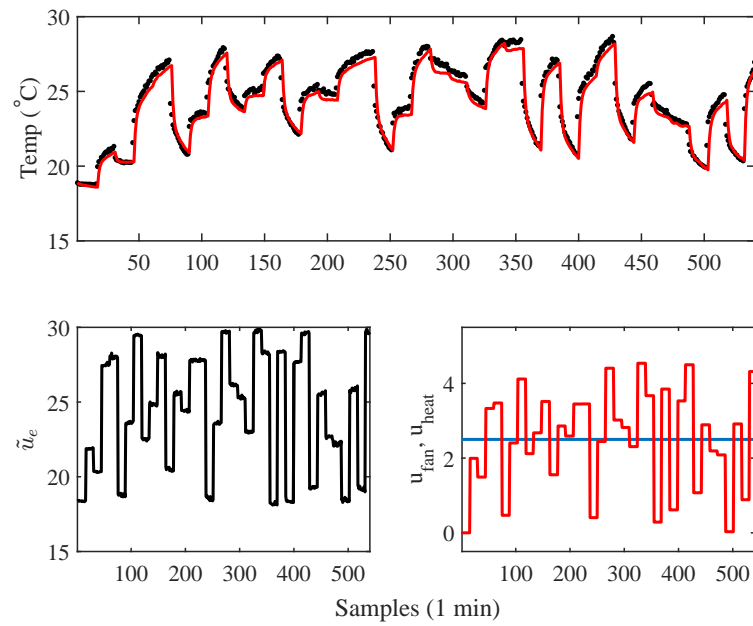
Figure 8.5: Open-loop evaluation experiment comparing the non-linear thermal model (solid trace) with experimental data (points). The lower plot on the left shows the predicted (effective input) steady state temperature, while the lower right shows the fan (blue trace) and heater input sequences.
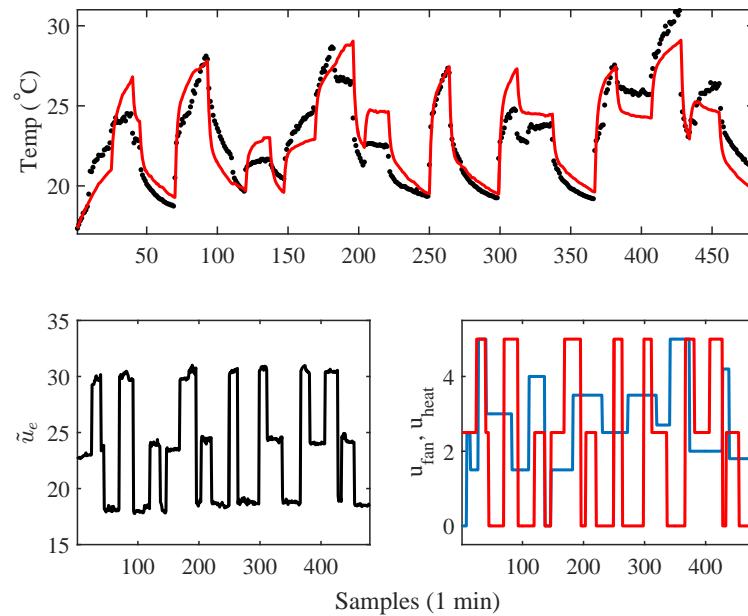
Figure 8.6: Open-loop evaluation experiment comparing the non-linear thermal model (solid trace) with experimental data (points). Here, both input signals are varied around their operating range. The lower plot on the left shows the predicted (effective input) steady state temperature, while the lower right shows the fan (blue trace) and heater input sequences.

8.5   2-dimensional Hammerstein model

As seen earlier by Fig. 8.3, given the steady state information of a temperature location it is possible to formulate its temperature power curves for various fixed fan settings, with the latter inherently weighing the coefficients of equation (8.2); evident also from table 8.1. In order to include this effect, an extension of the initial Hammerstein model is formulated in (Fig. 8.7). Here, u_{fan} is the fan input (Volts DC), whilst $\tilde{u}_{fan}$ is the steady state ventilation rate (ms^{-1}). Finally, ϕ_1 and ϕ_2 represent equations (8.1) and (8.2) for steady state ventilation rate and temperature, respectively.

Fitting polynomials to the logistic growth function coefficients, as shown in Fig. 8.8, yields a two-dimensional function for steady state temperature:

$$\tilde{u}_e = \phi_2 \left\{ u_{heat}, \tilde{u}_{fan} \right\} = y_{t\,\max}(1 + \mathrm{e}^{-\theta(u_{heat}-x_0)^{\frac{1}{c}}})^{-1} \tag{8.10}$$

where in this example, $\tilde{u}_e$ represents the predicted steady state temperature of temperature location 1; u_{heat} and $\tilde{u}_{fan}$ are the heater input and ventilation rate respectively; and the curve function ϕ_2 takes a similar form to equation (8.2). In this case, however, $y_{\max}$, θ, x_0 and c are all second-order polynomial functions of $\tilde{u}_{fan}$ in equation (8.10):

$$y_{t\,\max} \left\{ \tilde{u}_{fan} \right\} = p_1^{y_{t\,\max}} \cdot \tilde{u}_{fan}^2 + p_2^{y_{t\,\max}} \cdot \tilde{u}_{fan} + p_3^{y_{t\,\max}} \tag{8.11}$$

$$\theta \left\{ \tilde{u}_{fan} \right\} = p_1^{\theta} \cdot \tilde{u}_{fan}^2 + p_2^{\theta} \cdot \tilde{u}_{fan} + p_3^{\theta} \tag{8.12}$$

$$x_0 \left\{ \tilde{u}_{fan} \right\} = p_1^{x_0} \cdot \tilde{u}_{fan}^2 + p_2^{x_0} \cdot \tilde{u}_{fan} + p_3^{x_0} \tag{8.13}$$

$$c \left\{ \tilde{u}_{fan} \right\} = p_1^{c} \cdot \tilde{u}_{fan}^2 + p_2^{c} \cdot \tilde{u}_{fan} + p_3^{c} \tag{8.14}$$

where $p_i\,(i = 1, 2, 3)$ are coefficients. In equations (8.10), (8.11), (8.12), (8.13), and (8.14), $\tilde{u}_{fan}$ represents the estimated steady state airflow determined using equation (8.1), or alternatively the "present" measured ventilation rate. The former however is more fair to use in this manner, as no reference to measured data is utilised in the evaluation stage. Hitzemann [2013] similarly optimises polynomial
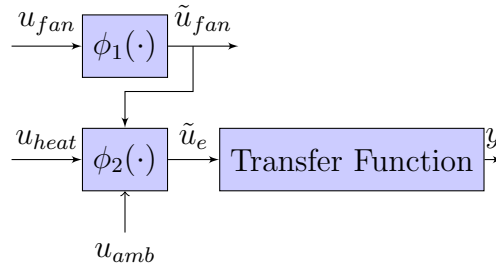
Figure 8.7: Schematic diagram of the 2-dimensional Hammerstein model.

Coefficient	$y_{t\max}\tilde{u}_{fan}$	$\theta\tilde{u}_{fan}$	$x_0\tilde{u}_{fan}$	$c\tilde{u}_{fan}$
p_1	-0.0102	-0.0309	0.0030	0.0042
p_2	0.1396	-0.4950	-0.0247	-0.0364
p_3	2.1434	14.2914	0.0809	0.1246
Fit error	0.1850	1.6097	0.0167	0.0258

Table 8.2: Polynomial coefficients that predict the values of $y_{t\max}\tilde{u}_{fan}$, $\theta\tilde{u}_{fan}$, $x_0\tilde{u}_{fan}$, and $c\tilde{u}_{fan}$ for different ventilation rate settings

functions to represent the coefficients of various steady state relationships, in order to develop a state-dependent model for a DC-DC boost converter. For illustrative purposes, Fig. 8.8 is based on temperature location 1 and the estimated polynomials for each logistic growth function coefficient in this case are listed in Table 8.2. However, as will be seen hereinafter, a similar approach can be taken for thermal zones.

The evaluation of the 2-dimensional Hammerstein model is based on equation (8.9) as before. Here, the same dataset depicted in Fig. 8.6 is explained better now as can be seen in Fig. 8.9, with a R_2^T value of 92.4%. Running the model for two more different data-sets, a similar quality of model fit is observed, with $R_2^T = 91.5\%$ for the dataset in Fig. 8.10; whilst an 86.6% is computed for the model fit in Fig. 8.11, which overestimates frequently the temperature change for a different fan input.
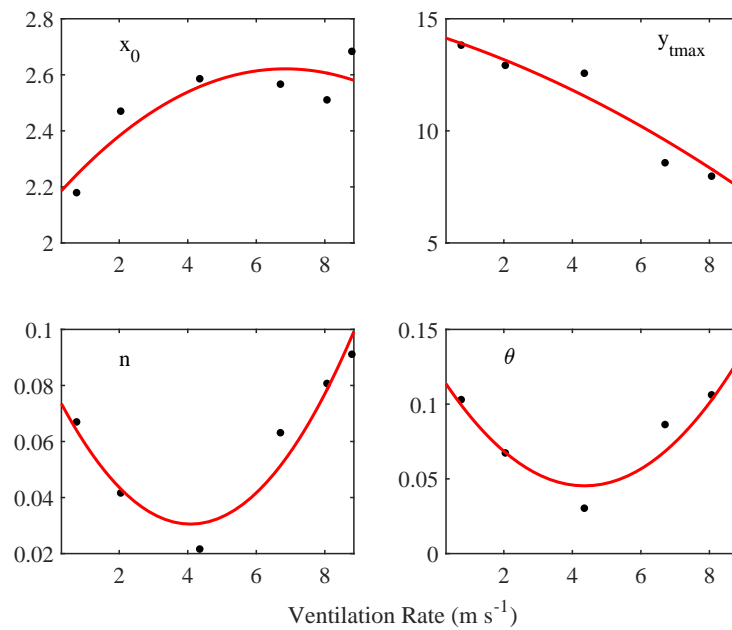
Figure 8.8: Logistic growth function coefficients (clockwise from top left) x_0, $y_{t\,\max}$, θ and c estimated from steady state temperature data collected at different ventilation rates (points), together with second order polynomial fit. The latter order was selected as it broadly yields curves that follow the trend observed from the measured data
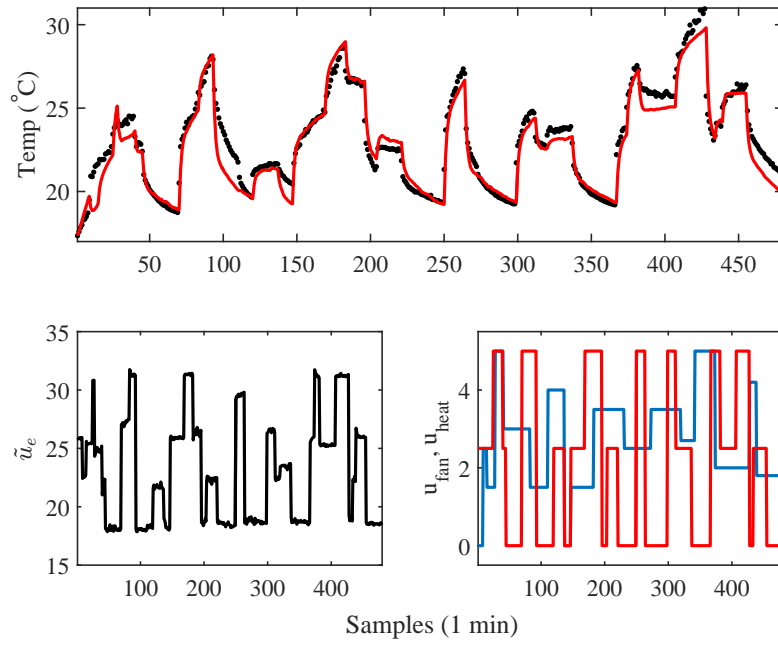
Figure 8.9: Evaluation of 2-dimensional Hammerstein model for the same dataset as in Fig. 8.6.
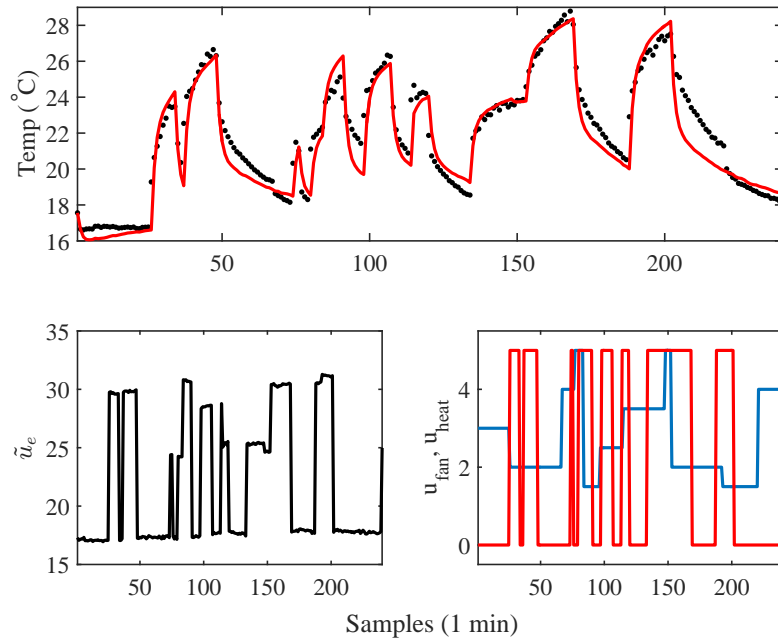
Figure 8.10: Evaluation of 2-dimensional Hammerstein model for a dataset where the heater shifts between 0, 50 and 100% and the ventilation rate is varied between medium and high levels.
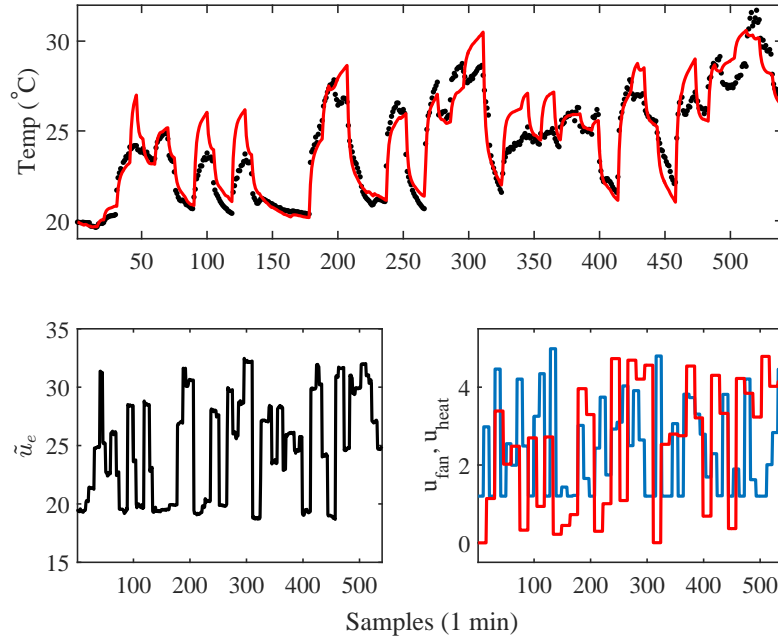
Figure 8.11: Evaluation of 2-dimensional Hammerstein model for a dataset where the fan input is varied to arbitrary levels every 10 minutes, and the heater input also changing every 15 minutes

8.6   State-Dependent-Parameter extension of the 2-dimensional Hammerstein model

For both aforementioned Hammerstein structures the parameters of the transfer function (8.5) are fixed, while its values are estimated around a limited heat operating range and a fixed fan setting. In this scenario the transfer function coefficients are estimated at every sampling instant k based on their relation to different ventilation rates. More specifically, the experimental open loop heat step experiments are used once more in order to reveal and model this relation.

Initially, a transfer function model is identified for temperature location no. 1, for each heat experiment (4 heat settings/6 fan settings); the structure of which is the same as in equation (8.5). The four parameters of the model for a fixed heat setting are then plotted against ventilation rate, where it can be seen that all of them follow a similar trend for medium and high heat settings (green, blue and red traces) except in the case of the lowest heat setting (Fig. 8.12). Averaging each parameter

against increasing ventilation yields trends that can be approximated by second order polynomial functions (Fig. 8.13). Hence, in this case, the steady state non-linearities are explained by the non-linear functions as before, and the temperature model's parameters change for different fan step changes, taking the following form,

$$y(k) = -a_1\{\tilde{u}_{fan}\}y(k-1) - a_2\{\tilde{u}_{fan}\}y(k-2)$$
$$+ b_1\{\tilde{u}_{fan}\}\tilde{u}_e(k-1) + b_2\{\tilde{u}_{fan}\}\tilde{u}_e(k-2) \quad (8.15)$$

with

$$a_1\{\tilde{u}_{fan}\} = 0.0031 \cdot \tilde{u}_{fan}^2 + 0.0488 \cdot \tilde{u}_{fan} - 1.7129 \quad (8.16)$$

$$a_2\{\tilde{u}_{fan}\} = -0.0029 \cdot \tilde{u}_{fan}^2 - 0.0461 \cdot \tilde{u}_{fan} + 0.7187 \quad (8.17)$$

$$b_1\{\tilde{u}_{fan}\} = -0.0106 \cdot \tilde{u}_{fan}^2 - 0.1232 \cdot \tilde{u}_{fan} + 0.1887 \quad (8.18)$$

$$b_2\{\tilde{u}_{fan}\} = 0.0100 \cdot \tilde{u}_{fan}^2 - 0.1138 \cdot \tilde{u}_{fan} - 0.1726 \quad (8.19)$$

thus yielding a State-Dependent-Parameter-type of model to be utilised with the 2- dimensional Hammerstein structure. The equivalent or rather time-step linear poles (not linearized) and zeroes of the SDP model, for the whole operating range, are depicted by pole-zero maps in Fig. 8.14. Each subplot depicts the poles (cross marks) and zeros (circles) for a fixed heat setting and six different fan settings. It can be seen that all the obtained poles are real and only one pole that lies on the negative real axis may cause oscillations. Furthermore, the average steady state gain for the whole ventilation rate operating range, as derived from Fig. 8.13 is depicted by Fig. 8.15. The steady state saturation for low ventilation rate is overt, however, due to parameter averaging, the same does not apply to very high ventilation rates. The combined evaluation model is expressed in difference terms as:

$$y(k) = -a_1\{\tilde{u}_{fan}\}y(k-1) - a_2\{\tilde{u}_{fan}\}y(k-2)$$
$$+ \left(\frac{1 + a_1\{\tilde{u}_{fan}\} + a_2\{\tilde{u}_{fan}\}}{1 - p\{\tilde{u}_{fan}\}}\right) \cdot \left(\tilde{u}_e(k-1) - p\{\tilde{u}_{fan}\} \cdot \tilde{u}_e(k-2)\right) \quad (8.20)$$

The latter combined model shows that the SDP TF's inverse is also updated at each sampling instant, thus ensuring steady state unity of the non-linear model. Running the simulation model for the same three different evaluation datasets shows a better fit for all (Fig. 8.16). In particular, the evaluation at the upper plot shows a negligible
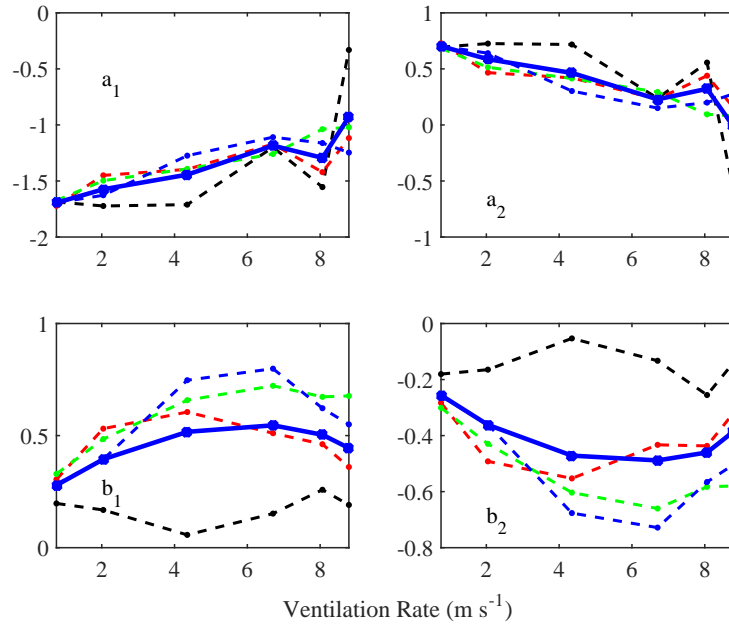
Figure 8.12: Second order parameter values against increasing ventilation rate; black trace corresponds to a fixed heat setting of 1.5 V, while red, green and blue traces correspond to fixed heat settings of 2.5, 3.5 and 4.5 V respectively. The thick blue trace depicts the heat setting average parameter values.

increase of the model fit (93%) as compared to that of Fig. 8.9. In comparison to the model fit of Fig. 8.10, the middle plot shows that with the sdp-configuration it increases up to 94%, whilst for the last evaluation data-set the model fit is also better (91%) than that of Fig. 8.11, which overestimates the effect of the ventilation rate. Table 8.3 summarises these results. Here, the R_T^2 and mean absolute error are laid out for each data-set that the three models were assessed with. The first three rows address data-sets where both actuators are varying; in the next two only the fan is varying, and in the last one only the heater is varying. The first row summarises the indices from Fig. 8.11 and the lower plot of Fig. 8.16; the second row relates to Fig. 8.6, Fig. 8.9, and the upper plot of Fig. 8.16; while the third row relates to Fig. 8.10 and the middle plot of Fig. 8.16. Moreover, it can be seen that for both data-sets where only the fan voltage is varied, all three models cannot represent the measured responses with a satisfying accuracy. On the contrary, the data-set where only the heater is varying, the results are much better. This data-set is also associated with Fig. 8.5.
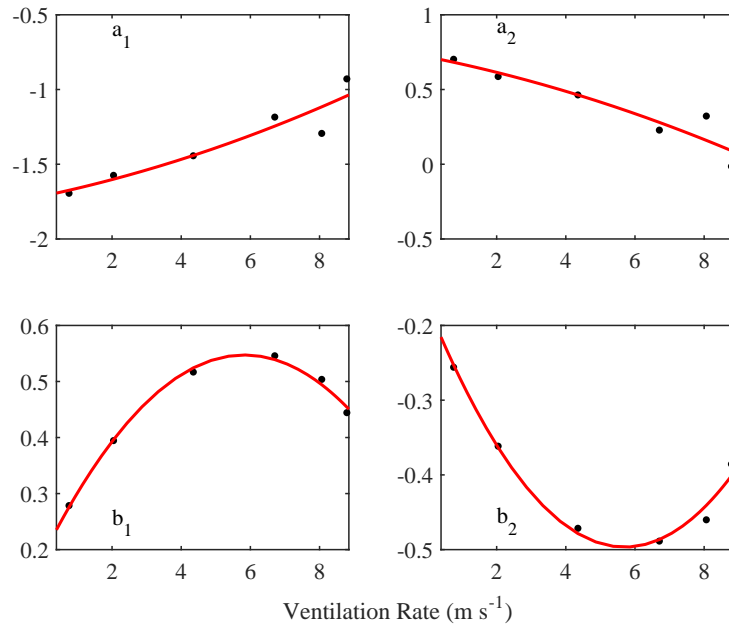
Figure 8.13: Second order polynomial functions explaining each average parameter of the sdp-model against ventilation rate.
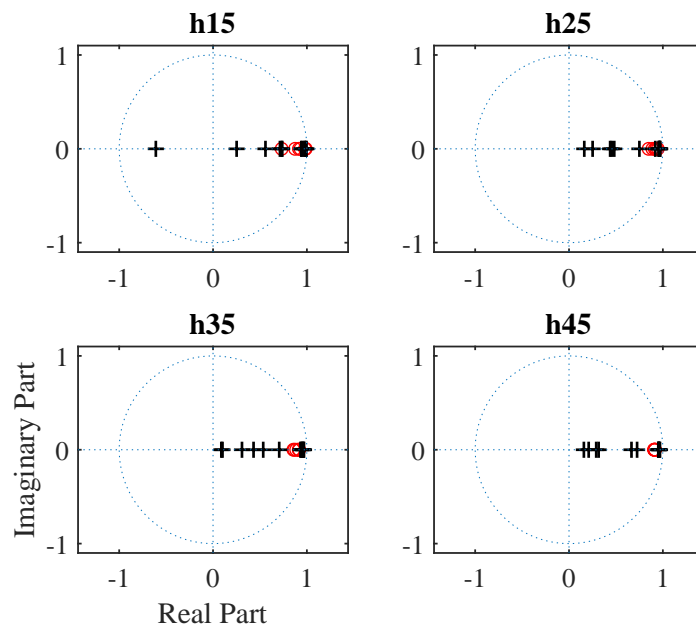
Figure 8.14: Pole-zero maps depicted for the whole operating range. The poles are depicted by cross marks. Each subplot shows the poles and zeros for six different fan settings under a fixed heat setting.
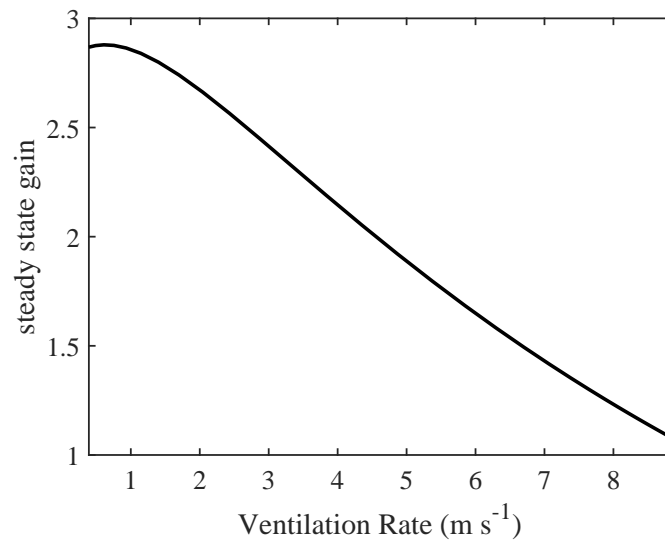
Figure 8.15: Average steady state gain of SDP model as derived from Fig. 8.13
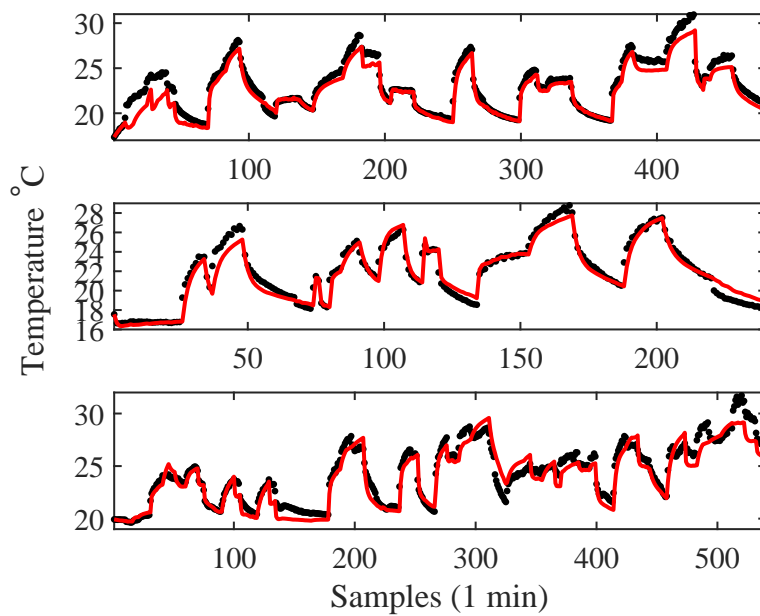
Figure 8.16: Evaluation of 2-dimensional sdp Hammerstein model for the three datasets previously utilised for evaluation. The top plot relates to Fig. 8.9, the middle relates to Fig. 8.10, and bottom plot to Fig. 8.11.

Type	1D (heat)		2D		2D-SDP	
——	R_T^2	MAE	R_T^2	MAE	R_T^2	MAE
Both	0.8672	0.8589	0.8660	0.7994	0.9068	0.7511
Both	0.7836	1.1171	0.9243	0.6105	0.9294	0.7463
Both	0.8017	1.0242	0.9149	0.7277	0.9385	0.5479
Fan	0.1706	1.0500	0.5811	0.5440	0.7482	0.4011
Fan	0.3864	1.2906	0.4448	1.0115	0.6800	0.9400
Heater	0.9762	0.3720	0.9712	0.7420	0.9700	0.7446

Table 8.3: Comparison table of fitting data-sets, using the 1-dimensional, 2-dimensional, and SDP extension Hammerstein model. The type implies which input was varying throughout a dataset. Red colour indicates the best model fits.
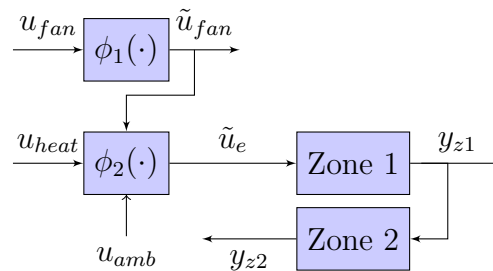
Figure 8.17: Schematic diagram of illustrative two-zone thermal model.

8.7   Non-linear multi-zone thermal model

The non-linear thermal model used to evaluate the new multi-zone identification approach takes the 2-dimensional Hammerstein structure with constant coefficients in the dynamic part. Illustrated in Fig. 8.17, it is a straightforward extension of the model identified from experimental data. Here, y_{z1} is the associated dynamic temperature response, used as an input variable for zone 2, for which the output temperature is denoted y_{z2}. Additional zones can be appended depending on the results of the clustering study.

Here, data from two open loop step experiments, similar to the ones used in Chapter 7 are displayed in Fig. 8.18. Zone 1 comprises the thermocouples located in the middle and top layers of the grid (labelled 1-4, 7-10 and 13-16) while zone 2
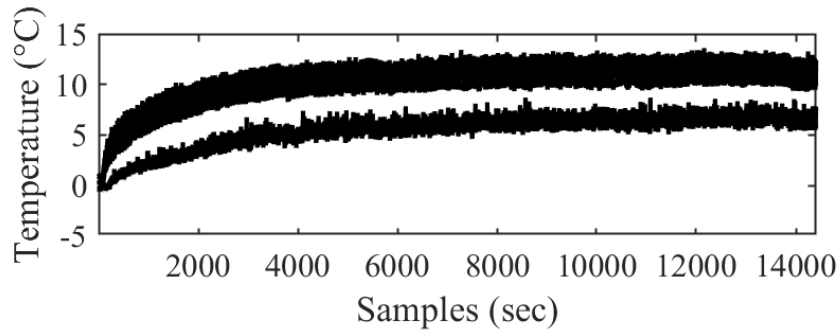
Figure 8.18: Temperature (elevation above ambient) distribution for *f15h35*. Measurements from all the thermocouples in the main grid are overlaid here.

includes the lower layer thermocouples (5, 6, 11, 12, 17, and 18). In particular, examination of the time-delays associated with the temperature response following a change in the heater input, suggests a causal relationship from zone 1 to zone 2.

The RIV algorithm, YIC, and R_T^2, suggest that the following second order model yields a suitable linear representation of zone 1 dynamic behaviour,

$$y_{z1}(k) = \frac{b_1 z^{-1} + b_2 z^{-2}}{1 + a_1 z^{-1} + a_2 z^{-2}} \tilde{u}_2(k) \tag{8.21}$$

The parameter estimates based on a sampling rate of $\Delta t = 1$ mins are $b_1 = 0.35$, $b_2 = -0.3215$, $a_1 = -1.6630$ and $a_2 = -0.9968$. The model response and experimental data are illustrated by Fig. 8.19–(i) and (ii). The output of zone 1 is subsequently used as the input to zone 2,

$$y_{z2}(k) = \frac{c_1 z^{-2} + c_2 z^{-3}}{1 + d_1 z^{-1}} y_{z1}(k) \tag{8.22}$$

where $c_1 = 0.3523$, $c_2 = -0.3348$ and $d_1 = -0.9714$, with the response shown in Fig. 8.19–(iii) and (iv). The model identified above is evaluated using the experimental data shown in Fig. 8.20. Here, Fig. 8.21 shows that the average temperature in both zone 1 and zone 2 are explained very well by the model ($R_T^2 = 0.9875$ and 0.9769 respectively). For comparison, Fig. 8.22 shows the response of a similar model structure but here based on selection of different zones. In this case, the zones are based on a group of 6 thermocouples close to the inlet and 12 thermocouples closer to the outlet. These zones might have been selected by a modeller based
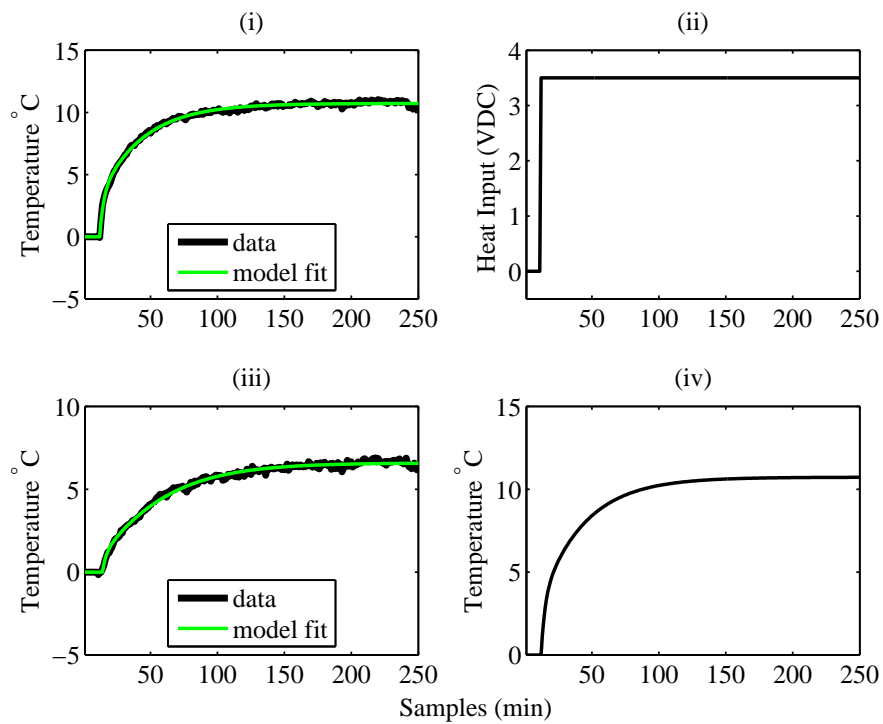
Figure 8.19: Upper subplots: (i) average temperature in zone 1 (noisy data) and model response (smooth), and (ii) heater input. Lower subplots: (iii) average temperature in zone 2 (noisy data) and model response (smooth), and (iv) zone 1 temperature used as the input.
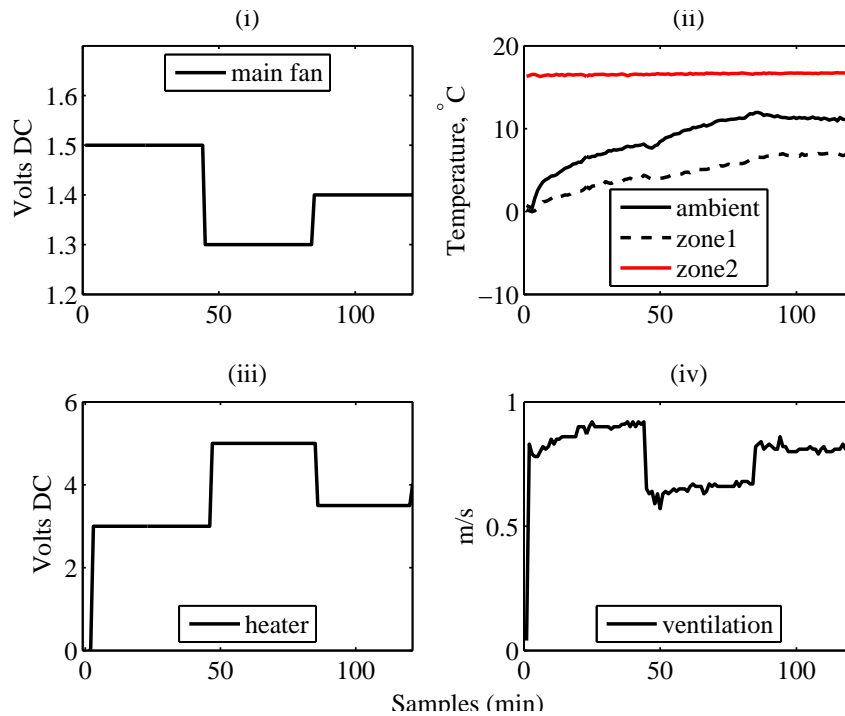
Figure 8.20: Input and output signals for evaluation experiment showing (i) fan input, (ii) temperatures, (iii) heater input and (iv) ventilation rate.

on consideration of the physical location of the thermocouples only. The model response deviates significantly from the measured data ($R_T^2 = 0.9306$ and 0.9164 for zone 1 and zone 2 respectively). Although representing a rather arbitrary example, Fig. 8.22 demonstrates the importance of objectively selecting suitable zones for the multi-zone model.

8.8   Conclusions

This chapter has developed a novel approach for modelling temperature in an enclosed space. Static nonlinear functions are used to describe the steady state temperature, in response to both heater and fan inputs, and are combined in series with either linear TF or nonlinear SDP models to describe the dynamic response. The coefficients of the static nonlinear functions are themselves identified from experimental data as being functions of the measured ventilation rate, as are the parameters of the SDP model. Hence, in future research, it would be useful to compare the combined static nonlinearity and SDP modelling approach, with models for temperature that are based only on the general form of the SDP model (i.e. in which the steady state
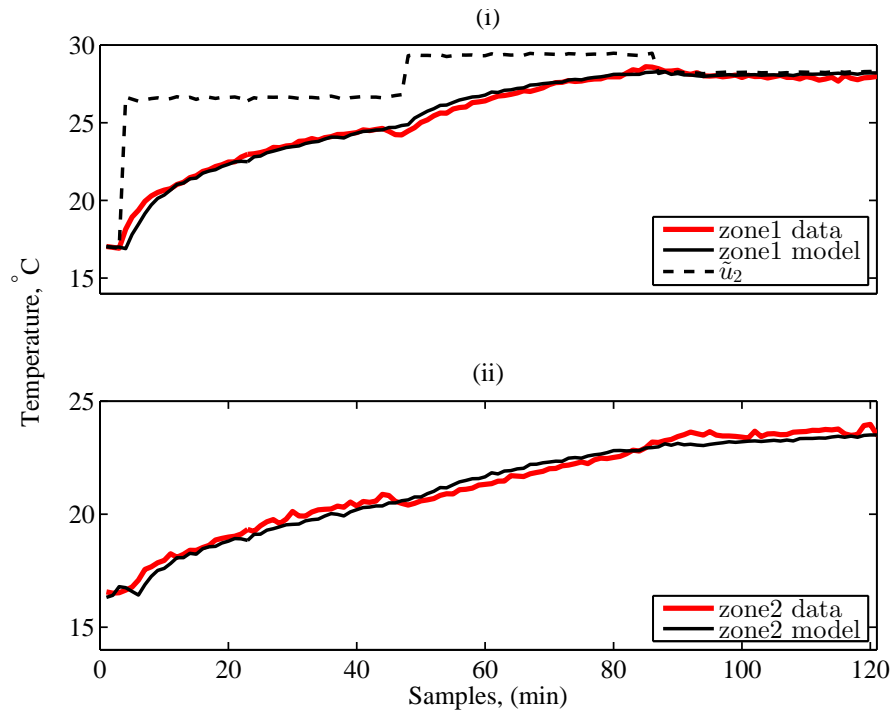
Figure 8.21: Evaluation experiment based on the proposed clustering approach, showing zone 1 (upper subplot) and zone 2 (lower).
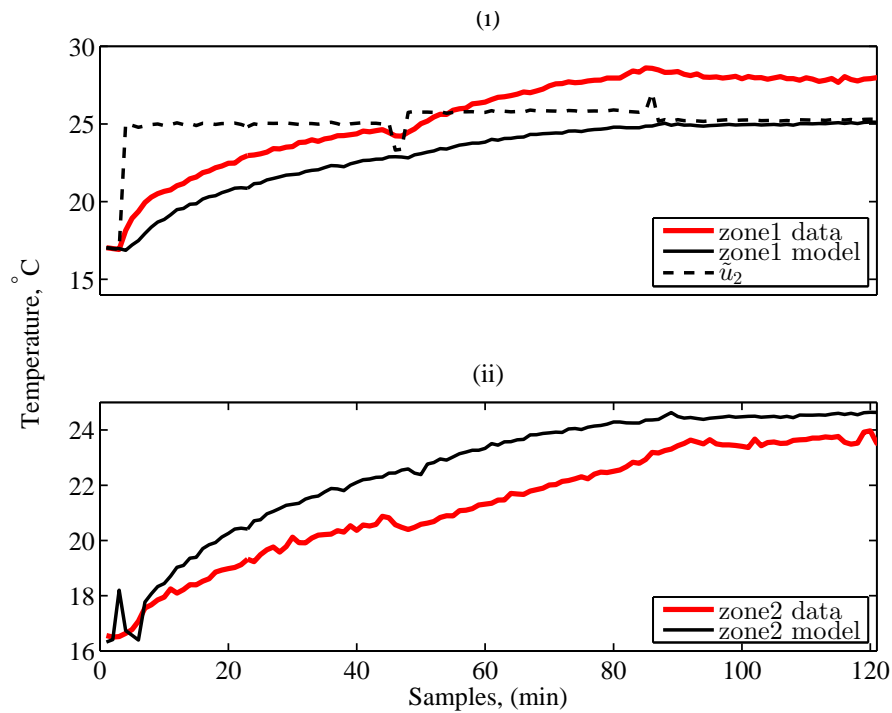
Figure 8.22: Evaluation experiment with user selected zones based only on the location of the sensors, showing zone 1 (upper subplot) and zone 2 (lower).

nonlinearity is embedded in the state-dependent parameters).

Although most of the chapter (Sections 8.1 though to 8.6) has utilised the response of a single thermocouple to illustrate the generic approach, it should be stressed that similar models are obtained for other thermocouples in the ventilation chamber and for the average temperature of a single zone identified using the clustering technique presented in the previous Chapter 7. However, in a second contribution of the chapter, section 8.7 has highlighted the potential of the new modelling approach within the context of a multi-zone model. The following chapter links to the present one by considering the simulation of a linear controller that utilises the 2-dimensional Hammerstein model.

Chapter 9

Temperature Control Examples

This chapter presents two examples of control system design, and evaluates these both in simulation and experimentally, with the latter using the laboratory ventilation chamber introduced in Chapter 6. The main aim is to illustrate use of the novel modelling contributions made in Chapters 7 and 8 within a control system design context. More specifically, these control designs are for: a) Single-Input, Single-Output (SISO) temperature control, acting upon a single thermal zone; and b) Multiple-Input, Multiple-Output (MIMO) control for simultaneously regulating (decoupling) the temperature of a single zone *and* the temperature difference between two thermal zones.

A True Digital Control (TDC) design methodology is followed [Taylor et al., 2013], with Proportional-Integral-Plus (PIP) controllers formulated for both the SISO and MIMO cases. PIP control is considered to be a logical extension of conventional Proportional-Integral (PI) control, with additional feedback and input compensators introduced for processes with second or higher order dynamics (as here for the control of a single thermal zone). It is based on the formulation of a Non-Minimal State Space (NMSS) model, in which the state vector consists of the present and past sampled input and output variables, together with integral-of-error state variables to ensure steady state tracking of the command inputs. The TDC approach is chosen for the present chapter, since it provides a readily available multivariable design approach that is straightforward to implement in practice [Taylor et al., 2013].

Sections 9.1 through to 9.3 develop the SISO temperature controller and evaluate its performance using both the non-linear model of Section 8.5 and the practical

ventilation chamber. Sections 9.4 and 9.5 introduce MIMO control design and present preliminary practical evaluation experiments, respectively. The two zones utilised for this research, are those identified earlier in Section 7.5.1 of the thesis (chosen here as an illustrative example of a multi-zone problem).

It should be pointed out that full details of the previously developed generic TDC and PIP/NMSS approach are omitted from the chapter, since these are not the focus of the thesis. Nonetheless, one novelty of the present work, is the proposal in section 9.4 to use a MIMO controller, acting on the heater and fan, to regulate the temperature of a selected zone *and* the degree of thermal stratification i.e. as represented by the temperature difference between two zones.

Finally, Section 9.6 presents both the chapter conclusions and the conclusions to Part B of the thesis more generally.

9.1 Single thermal zone control design

This chapter utilises linear control methods, hence the first step is to estimate a suitable linear TF model representing small perturbations of temperature around a desirable operating level. As discussed in Chapters 7 and 8, such TF models for temperature are typically second order: see e.g. equation (8.6). Hence, the model used for SISO control system design in the present section takes the following form:

$$y(k) = \frac{b_1 z^{-1} + b_2 z^{-2}}{1 + a_1 z^{-1} + a_2 z^{-2}} u(k) \tag{9.1}$$

where $y(k)$ represents the temperature elevation above laboratory temperature and $u(k)$ is the control input i.e. the applied voltage to the heater. The TF model is expressed difference equation form as follows,

$$y(k) = -a_1 y(k-1) - a_2 y(k-2) + b_1 u(k-1) + b_2 u(k-2) \tag{9.2}$$

The above model can be represented by the following non-minimal state space (NMSS) equations (see e.g. [Taylor et al., 2013] and the references therein):

$$\mathbf{x}(k) = \mathbf{F}\mathbf{x}(k-1) + \mathbf{g}u(k-1) + \mathbf{d}y_d(k) \; ; \; y(k) = \mathbf{h}\mathbf{x}(k) \tag{9.3}$$

where the non-minimal state vector $\mathbf{x}(k)$ consists of the present and past sampled values of $y(k)$ and the past sampled values of $u(k)$, together with an integral-of-error

state $z(k)$ introduced to ensure steady state tracking. For the present example,

$$\mathbf{x}(k) = \begin{bmatrix} y(k) & y(k-1) & u(k-1) & z(k) \end{bmatrix}^T \tag{9.4}$$

in which,

$$z(k) = z(k-1) + (y_d(k) - y(k)) \tag{9.5}$$

where $y_d(k)$ is the the temperature set point. The NMSS model (9.3) represents equations (9.2) and (9.5) as follows:

$$\begin{bmatrix} y(k) \\ y(k-1) \\ u(k-1) \\ z(k) \end{bmatrix} = \begin{bmatrix} -a_1 & -a_2 & b_2 & 0 \\ 1 & 0 & 0 & 0 \\ 0 & 0 & 0 & 0 \\ a_1 & a_2 & -b_2 & 1 \end{bmatrix} \begin{bmatrix} y(k-1) \\ y(k-2) \\ u(k-2) \\ z(k-1) \end{bmatrix} + \begin{bmatrix} b_1 \\ 0 \\ 1 \\ -b_1 \end{bmatrix} u(k-1) + \begin{bmatrix} 0 \\ 0 \\ 0 \\ 1 \end{bmatrix} y_d(k) \tag{9.6}$$

$$y(k) = \begin{bmatrix} 1 & 0 & 0 & 0 \end{bmatrix} \mathbf{x}(k) \tag{9.7}$$

The state variable feedback control law takes the following standard form: $u(k) = -\mathbf{k}^T\mathbf{x}(k)$ where, in this case, $\mathbf{k}^T = [f_0 \; f_1 \; g_1 - k_I]$, in which f_0 and k_I are the proportional and integral gains respectively, while f_1 and g_1 are additional control gains. In general block-diagram terms, the controller can be implemented as shown in Fig. 9.1 where, for the present example, $F_1(z^{-1}) = f_1 z^{-1}$, $G_1(z^{-1}) = g_1 z^{-1}$, $B(z^{-1}) = b_1 z^{-1} + b_2 z^{-2}$ and $A(z^{-1}) = 1 + a_1 z^{-1} + a_2 z^{-2}$. In difference equation form, the equivalent PIP control law is,

$$u(k) = -f_0 y(k) - f_1 y(k-1) - g_1 u(k-1) + k_I z(k) \tag{9.8}$$

However, PIP control is usually implemented in its incremental form as follows (see Chapter 6 in the book by Taylor et al. [2013] for details), and this is the form used for both the Simulink simulation experiments and Labview practical implementation in this thesis,

$$u(k) = u(k-1) + k_I(y_d(k) - y(k)) - f_0(y(k) - y(k-1))$$
$$- f_1(y(k-1) - y(k-2)) - g_1(u(k-1) - u(k-2)) \tag{9.9}$$

The control gains for the SISO controller below are computed via trial and error pole placement, to obtain a satisfactory smooth and relatively fast response, using the TDC toolbox in Matlab [Taylor et al., 2013].
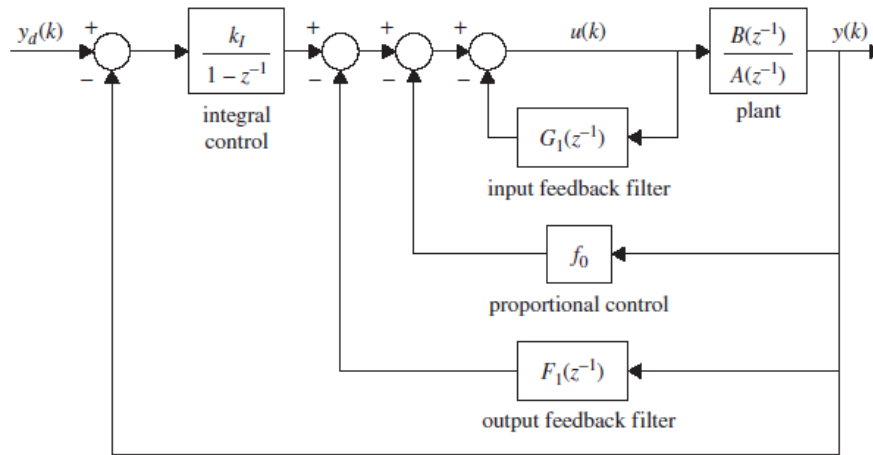
Figure 9.1: Proportional–Integral–Plus (PIP) control block diagram.

9.2   Evaluation using the non-linear model

In this example, the non-linear model developed in Section 8.5 is used for preliminary evaluation of the temperature controller. Here, the dynamic component's structure and parameters estimates are identified from simulated data, where the fan voltage is assumed to be 2.5 VDC and the heater voltage steps between 2.5 and 3.5 VDC. As in equation 9.1, the dynamic component is a second order model with two delay terms, and the parameter estimates are $b_1 = 0.7769$, $b_2 = -0.7570$, $a_1 = -1.6491$, and $a_2 = 0.6556$. The coefficients of the polynomials that find the static function's coefficients i.e. $y_{\max}$, θ, x_0 and c, are the same with the ones used in table 8.2. The structure of the controller is similar to the one shown in Fig. 9.1, however the control input goes through the non-linear static function defined by equation 8.10. The control simulation set-point $y_d(k)$ is also formulated by means of a second non-linear static function, which is the same as equation 8.10 again. Fig. 9.2 shows the block diagram that was used to run the simulation. The PIP control gains were calculated on the basis of trial and error pole placement. For this simulation, one pole was selected close to the origin i.e p_1=0.9744 and the second one was selected to be further away, p_2=0.85. Subsequently, the proportional and output feedback gains are f_0=0.1232, and f_1=-0.0534; the input feedback filter is g_1=-0.9744, and the integral gain is k_I=0.0043.

In the first simulation scenario, the command input $y_d(k)$ is formulated as follows:
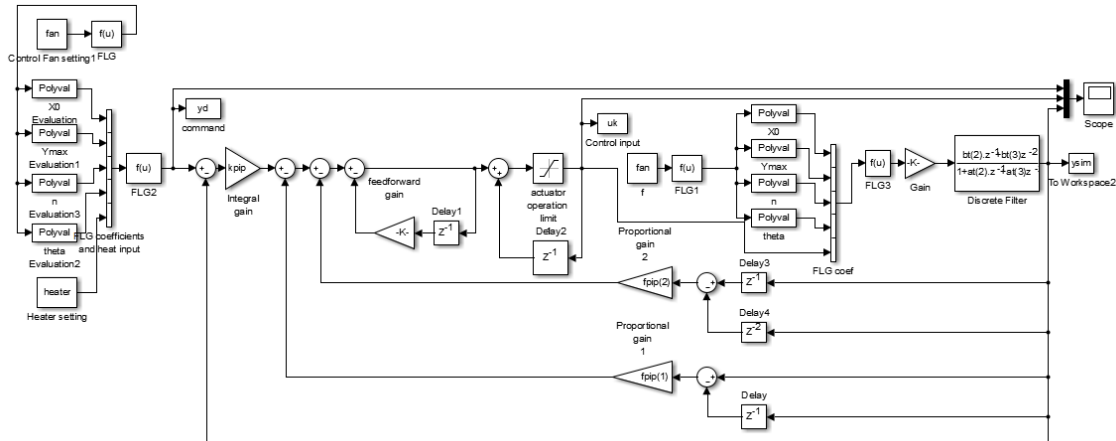
Figure 9.2: PIP controller implemented on a 2-dimensional Hammerstein model.

the voltage to the fan input is fixed at 2.5 VDC, while the voltage to the heater input is initially zero, stepped up in turn to 2.5 VDC; then stepped up again to 3.5 VDC, and finally stepped down back to 2.5 VDC. These signals are depicted at the lower plot of Fig. 9.3 by a dashed blue and a dashed green trace, respectively. Passing those two signals through equation 8.10 yields the command input to the controller, which is represented by a black trace at the upper plot of Fig. 9.3. The controlled temperature response (upper plot of Fig. 9.3, dashed red trace) shows that controller works well, while the control input (lower plot of Fig. 9.3, red trace) shows that for every step change of the set-point $y_d(k)$, it follows and eventually settles at a voltage, the value of which is the same as the heater input previously used to formulate the set-point.

For another scenario (Fig. 9.4), the command input is changed mainly due to the fan input changing. For example, at the 120th sample, the voltage to the fan is increased to 3.5 VDC, while the heater voltage remains at 2.5 VDC. The latter combination yields a lower temperature set-point. This results in a slower response as can been seen by the control input voltage, but the set-point is still tracked.

Finally, for a fixed fan setting and various step changes applied in the heater input (thus the set-point is only determined by the latter), this controller is compared with a PIP controller that uses a second order linear TF model. Its parameter estimates are $b_1 = 0.2855$, $b_2 = -0.2786$, $a_1 = -1.8737$, and $a_2 = 0.8754$. The following feedback gains f_0=0.5722, f_1=-0.4212, g_1=-0.8177, k_I=0.0125 are also calculated by pole placement, with p_1=0.9759, and p_2=0.85. The simulated response from the
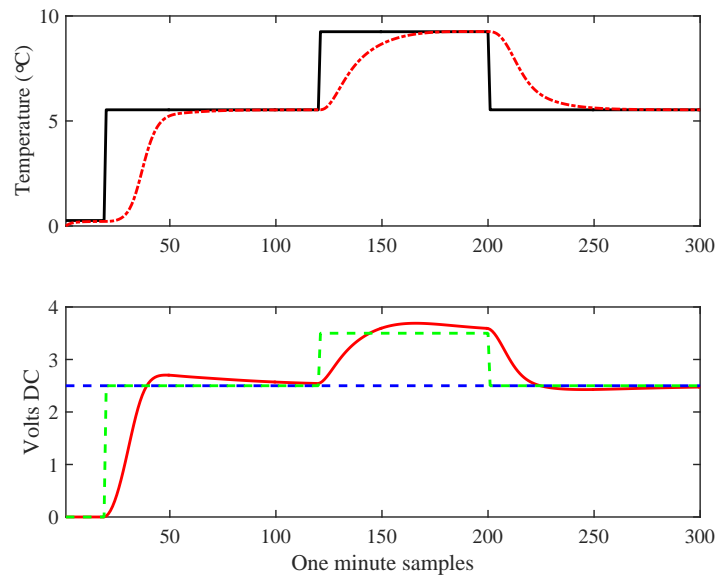
Figure 9.3: PIP control simulation on the non-linear thermal model. The upper plot shows the command input and temperature response with a black and a red trace, respectively. The lower plot depicts the control input with a red trace, whilst the fan and heater signals that eventually formulate the command input are represented by dashed blue and green traces, respectively.

PIP controller that uses the linear model is depicted in green colour. The first two plots show drastic step changes to the set-point; although the control with the linear model shows a consistent response, the control with the non-linear model is slower and overshoots in the upper plot; and it is slightly slower in the middle plot. On the contrary, for smaller set-point changes, the responses are almost identical; as seen in the lower plot of Fig. 9.5.

These simulations show that the responses are satisfactory when the set-points are near the operating point of the controller but somewhat slower for instances where the fan input is changed or drastic steps occur in the heater input. If a faster controller were to be used, with both poles closer to the origin, the simulation response would be highly oscillatory and unstable for certain step changes in the set-points that do not fall within its operating point. Hence, an SDP-PIP control approach may be more suitable in this regard.
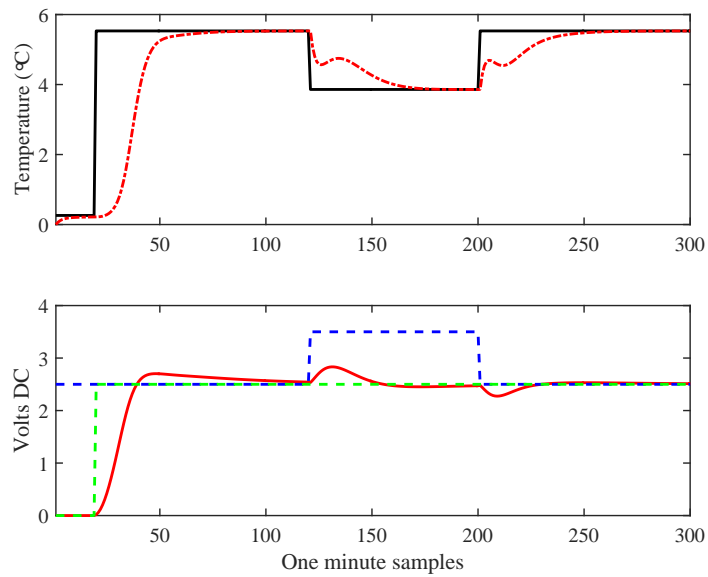
Figure 9.4: PIP control simulation on the non-linear thermal model. In this case, it is the fan that induces a change in the command input. The upper plot shows the command input and temperature response with a black and a red trace, respectively. The lower plot depicts the control input with a red trace, whilst the fan and heater signals that eventually formulate the command input are represented by dashed blue and green traces, respectively.
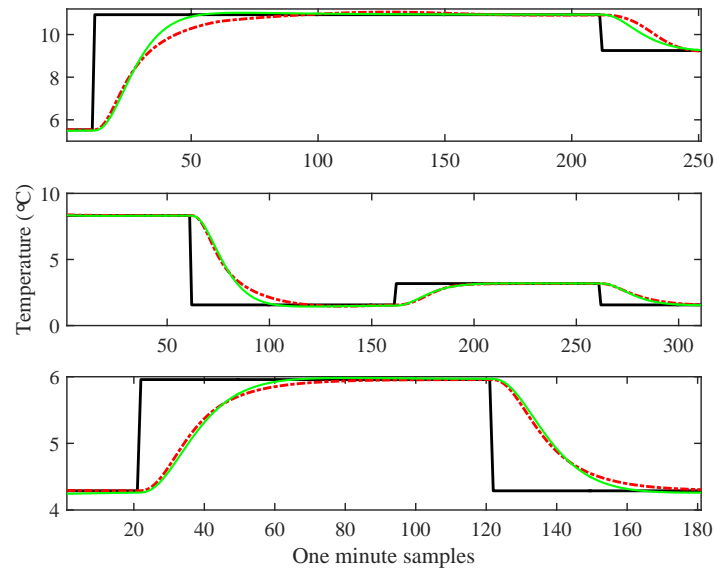
Figure 9.5: PIP control simulation on the non-linear thermal model (dashed red trace), compared with the PIP control simulation on the linear model, for three different set-point change scenarios.

9.3   Experimental results

Following the simulation study above, the SISO control approach is applied to the laboratory ventilation chamber. For these purposes, an appropriate linear control model is identified directly from experimental data as follows. An open loop experiment was undertaken, which involved a step increase and decrease applied to the heater input, under a low fan setting. In particular, the data-set used involves an initial moderate step applied in the heater input (not shown and utilised here), which increases after steady state is reached by the individual responses. From there onwards, the voltage to heater is increased to 3.5 VDC and dropped to 2.5 VDC, with each step lasting three hours. The fan setting was selected for convenience as it is known to create two thermal zones i.e. the bottom layer, and the middle-upper layer. The latter zone response is selected here for this example. The individual responses of the selected thermal zone is subsequently averaged and modelled using the RIV algorithm. Fig. 9.6 shows the average thermal zone response, model fit, and residual errors.

A second order model with one sample of delay explains the data satisfactorily
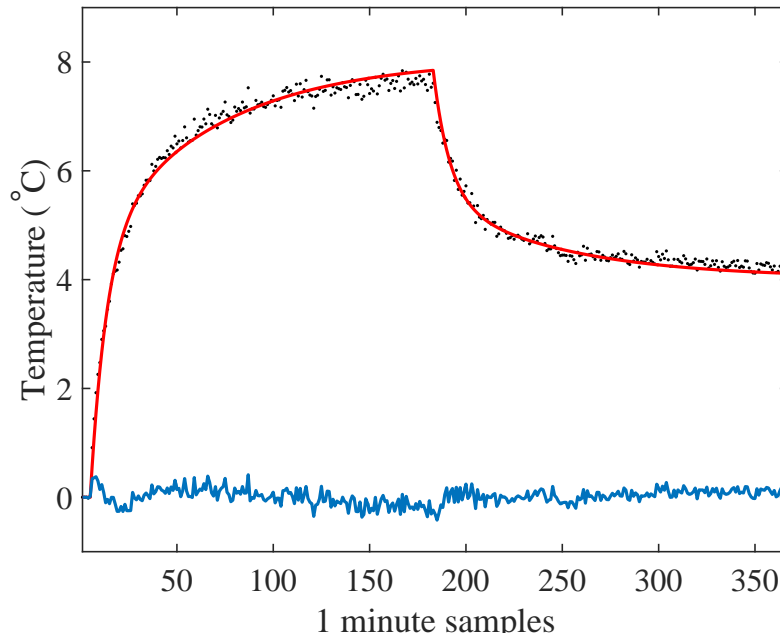
Figure 9.6: Middle-upper layer average temperature response (black dots), model fit (red trace), and residual errors (blue trace).

(R_T^2 =0.9919). The TF model 9.1 explains the data depicted in Fig. 9.6, and the parameter estimates are $b_1 = 0.2855$, $b_2 = -0.2786$, $a_1 = -1.8737$, and $a_2 = 0.8754$. Fig. 9.7 presents the simulated and actual performance of the controller. The average zone responses (black and green dashed traces for actual and simulation outputs respectively) are almost identical, while the control inputs are relatively similar. Finally, the red traces are the zone's individual responses during the tasks of control implementation kept within ± 1 $°C$ and ± 0.5 $°C$ for a 10 $°C$ and 6 $°C$ set point respectively. The individual responses show here that their transient behaviour is very similar, while they do show a 2 $°C$ gradient during their first steady state point. On the contrary, the gradient is more narrow (around 1 $°C$) for a 6 $°C$ set point.

9.4   Multiple-Input-Multiple-Output Control

In the Multiple-Input-Multiple-Output case the goal is to act on both fan and heater inputs in order to control the temperature and the homogeneity of the ventilation chamber. In this example, the first controlled variable is the temperature of one
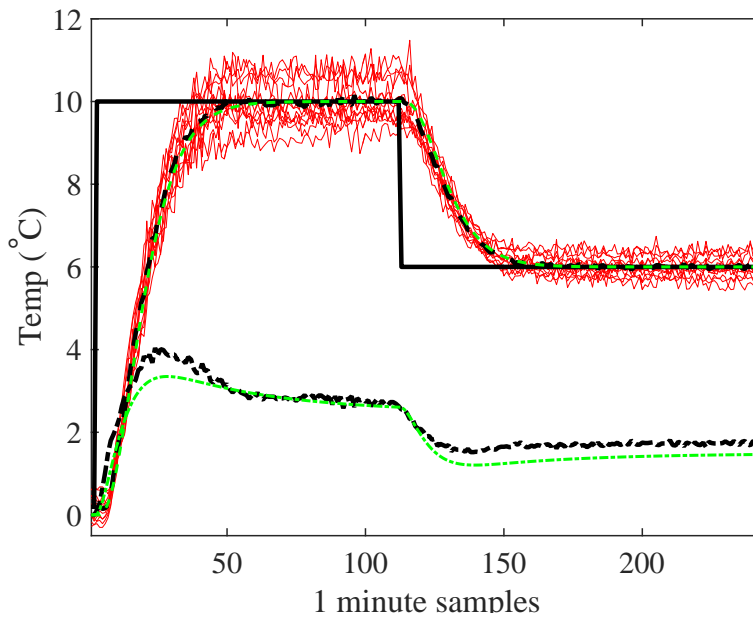
Figure 9.7: Proportional-Integral-Plus zone control simulation vs data. red trace: zone individual responses, dashed and dash-dotted black and green traces, are the system's and model's average zone temperatures and control inputs, respectively.

thermal zone and the second is the difference between the latter and another zone. The fan acts upon the difference between the zones, hence controlling the homogeneity, while the heater determines the temperature that is desired to achieve.

The two thermal zones that are present from the open loop experiment in Section 9.3 are utilised here, i.e. the lower layer and the middle-upper layer. These are the zones that were also identified in Chapter 7, page 82. Two different open-loop experiments were carried out in order to model how the individual step changes applied in the fan and heater inputs affect a) the temperature response of the middle-upper layer zone (which is the first controlled variable i.e. y_{z1}), and b) the temperature difference between the two thermal zones (second controlled variable, y_{td}). Fig. 9.8 and Fig. 9.9 show the temperature and zone difference model responses to individual steps changes applied to the heater and fan inputs. All four steps are explained by single order, unit time delay discrete models. First order models were chosen in this case for the purposes of simplifying the MIMO control design process, in terms of number of states in the NMSS model.

The two-input, single output models can be expressed in the following transfer
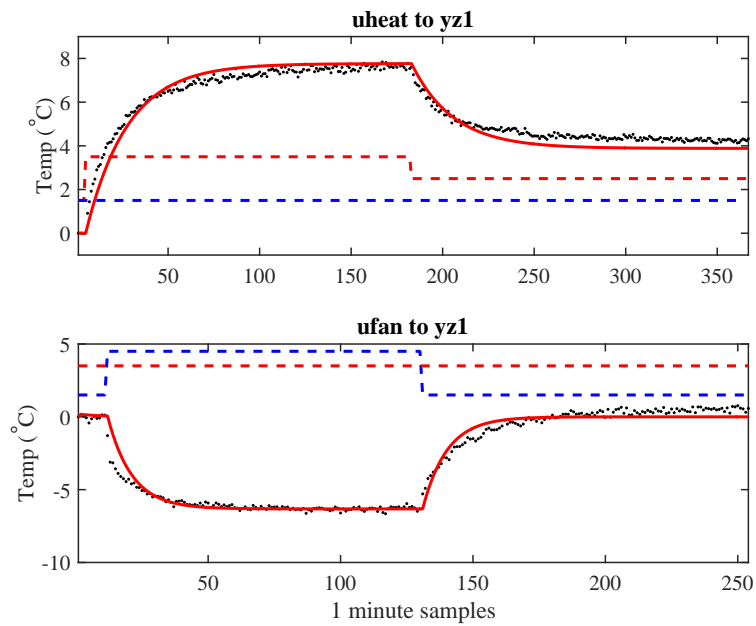
Figure 9.8: The upper plot shows the temperature response and model fit to a heat step, and the lower plot shows the same for a fan step. In both plots the dashed blue trace represents the fan setting and the dashed red trace represents the heat setting.
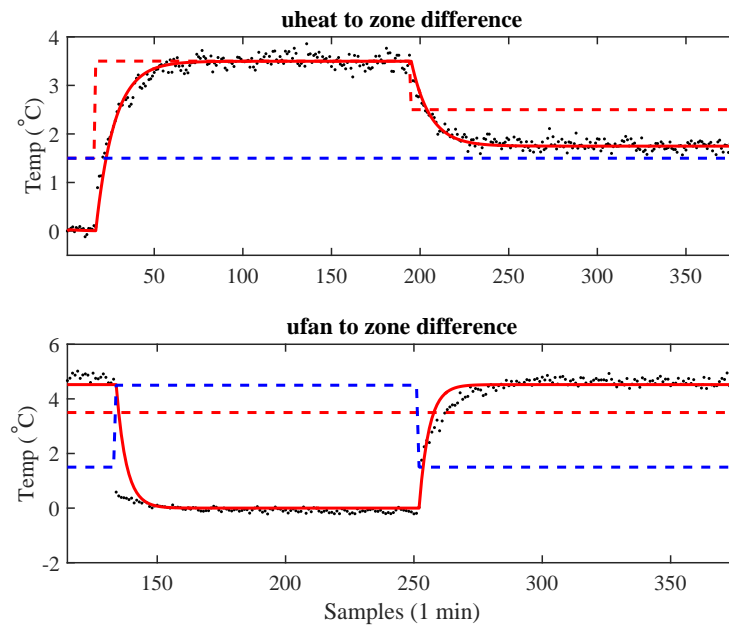
Figure 9.9: Temperature difference data and model fits between zone 1 and zone 2 for a heat step (upper plot) and a fan step.

function matrix form:

$$
\begin{bmatrix} y_{z1}(k) \\ y_{td}(k) \end{bmatrix} = \begin{bmatrix} \frac{0.1673z^{-1}}{1-0.9569z^{-1}} & \frac{-0.2193z^{-1}}{1-0.8959z^{-1}} \\ \frac{0.1588z^{-1}}{1-0.9092z^{-1}} & \frac{-0.3441z^{-1}}{1-0.7717z^{-1}} \end{bmatrix} \cdot \begin{bmatrix} u_{heat}(k) \\ u_{fan}(k) \end{bmatrix}
\tag{9.10}
$$

where $y_{z1}(k)$ is the temperature of zone 1 at sampling instant k, and $y_{td}(k)$ is the temperature difference between the two zones. Alternatively, equation (9.10) takes the following form:

$$
\begin{bmatrix} y_{z1}(k) \\ y_{td}(k) \end{bmatrix} = \begin{bmatrix} \frac{0.1673z^{-1}-0.1499z^{-2}}{1-1.8528z^{-1}+0.8573z^{-2}} & \frac{-0.2193z^{-1}+0.2099z^{-2}}{1-1.8528z^{-1}+0.8573z^{-2}} \\ \frac{0.1588z^{-1}-0.1226z^{-2}}{1-1.6809z^{-1}+0.7017z^{-2}} & \frac{-0.3441z^{-1}+0.3129z^{-2}}{1-1.6809z^{-1}+0.7017z^{-2}} \end{bmatrix} \cdot \begin{bmatrix} u_{heat}(k) \\ u_{fan}(k) \end{bmatrix}
\tag{9.11}
$$

From the common denominator transfer function matrix form, it is possible to derive the left Matrix Fraction Description form,

$$
\mathbf{A}(z^{-1}) \begin{bmatrix} y_{z1}(k) \\ y_{td}(k) \end{bmatrix} = \mathbf{B}(z^{-1}) \begin{bmatrix} u_{heat}(k) \\ u_{fan}(k) \end{bmatrix}
\tag{9.12}
$$

where,

$$
\mathbf{A}(z^{-1}) = \begin{bmatrix} 1 & 0 & 0 & 0 \\ 0 & 1 & 0 & 0 \end{bmatrix} + \begin{bmatrix} -1.8528 & 0 \\ 0 & -1.6809 \end{bmatrix} z^{-1} + \begin{bmatrix} 0.8573 & 0 \\ 0 & 0.7017 \end{bmatrix} z^{-2}
\tag{9.13}
$$

and

$$
\mathbf{B}(z^{-1}) = \begin{bmatrix} 0.1673 & -0.2193 & -0.1499 & 0.2099 \\ 0.1588 & -0.3441 & -0.1226 & 0.3129 \end{bmatrix} \mathbf{u}(k)
\tag{9.14}
$$

The derivation steps that yield Equations (9.13) and (9.14) involve usage of matrix algebra. In this case, these were automatically computed by calling the *mtf2mfd* Matlab function of CAPTAIN Toolbox. Similar to Section 9.1, the NMSS form is expressed as

$$
\mathbf{x}(k) = \mathbf{F}\mathbf{x}(k-1) + \mathbf{G}\mathbf{u}(k-1) + \mathbf{D}\mathbf{y}_d(k)
\tag{9.15}
$$

with the state vector $\mathbf{x}(k)$ being:

$$
\mathbf{x}(k) = \begin{bmatrix} y_{z1}(k) & y_{td}(k) & y_{z1}(k-1) & y_{td}(k-1) & u_{heat}(k-1) & u_{fan}(k-1) & z_{z1}(k) & z_{td}(k) \end{bmatrix}^T
\tag{9.16}
$$

Here, the lagged control input vector is $\mathbf{u}(k-1) = [u_{heat}(k-1)\ u_{fan}(k-1)]^T$ and the lagged command input vector is $\mathbf{y}_d(k) = [y_{dz1}(k)\ y_{dtd}(k)]^T$. The integral-of-error state variables are as in the SISO case,

$$
z_{z1}(k) = z_{z1}(k-1) + (y_{dz1}(k) - y_{z1}(k)) \ ; \ z_{td}(k) = z_{td}(k-1) + (y_{dtd}(k) - y_{td}(k))
\tag{9.17}
$$

The transition matrix $\mathbf{F}$ is in this example,

$$
\begin{bmatrix}
-1.8523 & 0 & 0.8573 & 0 & -0.1499 & 0.2099 & 0 & 0 \\
0 & -1.6809 & 0 & 0.7017 & -0.1226 & 0.3129 & 0 & 0 \\
1 & 0 & 0 & 0 & 0 & 0 & 0 & 0 \\
0 & 1 & 0 & 0 & 0 & 0 & 0 & 0 \\
0 & 0 & 0 & 0 & 0 & 0 & 0 & 0 \\
0 & 0 & 0 & 0 & 0 & 0 & 0 & 0 \\
1.8523 & 0 & -0.8573 & 0 & 0.1499 & -0.2099 & 1 & 0 \\
0 & 1.6809 & 0 & -0.7017 & 0.1226 & -0.3129 & 0 & 1
\end{bmatrix}
\tag{9.18}
$$

while the input $\mathbf{G}$ and command input vectors $\mathbf{D}$ are expressed as follows

$$
\begin{bmatrix}
0.1673 & -0.2193 \\
0.1588 & -0.3441 \\
0 & 0 \\
0 & 0 \\
1 & 0 \\
0 & 1 \\
-0.1673 & 02193 \\
-0.1588 & 0.3441
\end{bmatrix}
;
\begin{bmatrix}
0 & 0 \\
0 & 0 \\
0 & 0 \\
0 & 0 \\
0 & 0 \\
0 & 0 \\
1 & 0 \\
0 & 1
\end{bmatrix}
\tag{9.19}
$$

The SVF control law that is linked to the NMSS model defined by equation 9.15, and expressed by equations 9.18 and 9.19 is,

$$
\mathbf{u}(k) = \text{-}\mathbf{K}\mathbf{x}(k)
\tag{9.20}
$$

Different trial and error values are placed on the weighting matrices in order to solve a Linear-Quadratic (LQ) cost function. The weighting matrices that were utilised as an example here are $\mathbf{Q} = \text{diag}\,[0.5\ 0.25\ 0.5\ 0.25\ 0.5\ 0.5\ 0.01\ 0.001]$, and $\mathbf{R} = \text{diag}\,[0.5\ 0.5]$. As a result, the following control gains yielded a relatively slow closed loop response:

$$
\mathbf{k} =
\begin{bmatrix}
5.5960 & -1.0802 & -4.4520 & 0.8094 & -0.6371 & 0.7289 & -0.0691 & 0.0198 \\
-0.4783 & -1.0912 & 0.0279 & 0.6752 & 0.1228 & -0.3079 & 0.0478 & 0.0238
\end{bmatrix}
\tag{9.21}
$$

9.5   Evaluation

In the first simulation scenario, y_{dz1} is initially set to 7 °C, and $y_{dtd} =$3 °C. These setpoints are depicted in the upper plot of Fig. 9.10 by red and blue traces, respectively;
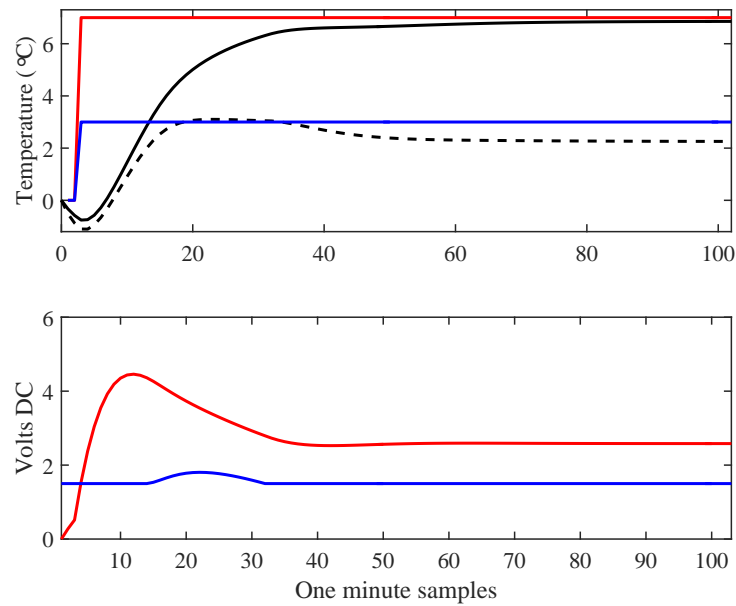
Figure 9.10: Simulation of MIMO controller with controller broadly achieving the setpoints. The lower plot shows the control inputs i.e. u_{heat} with a red trace, and u_{fan} with a blue trace

whilst y_{z1} and y_{td} simulation outputs are represented by a black trace and a black dashed trace, respectively. As can be seen, the temperature difference set-point is not achieved (off by 0.7 °C).

For a second exemplary simulation, y_{dz1} is initially set to 4 °C, and y_{dtd} is set to -0.5 °C (that is the lower layer being warmer than the middle/upper layer). In this case, both control inputs go high as expected; u_{fan} goes up to 5 VDC to push for uniform distribution, while u_{heat} reaches about 4.5 VDC to push the y_{z1} to reach this 4 °C elevation. Subsequently, y_{dz1} is set to 3 °C, which makes both inputs to decrease, and finally y_{dtd} is set to 0 °C. The latter change of set-point also temporarily affects the temperature response of y_{z1}, causing u_{heat} to slightly increase.

These simulation experiments were implemented in Labview, with a control input update rate of one minute. The results contrasted the simulations shown in Fig. 9.10 and Fig. 9.11. In particular, regarding Fig. 9.10, the response was initially similar, but as the fan control input slightly increased the temperature distribution was affected, causing a sudden heat rise to the middle-upper layer. In turn, this caused a dramatic drop of the voltage to the heater. The control signals ended up cascading
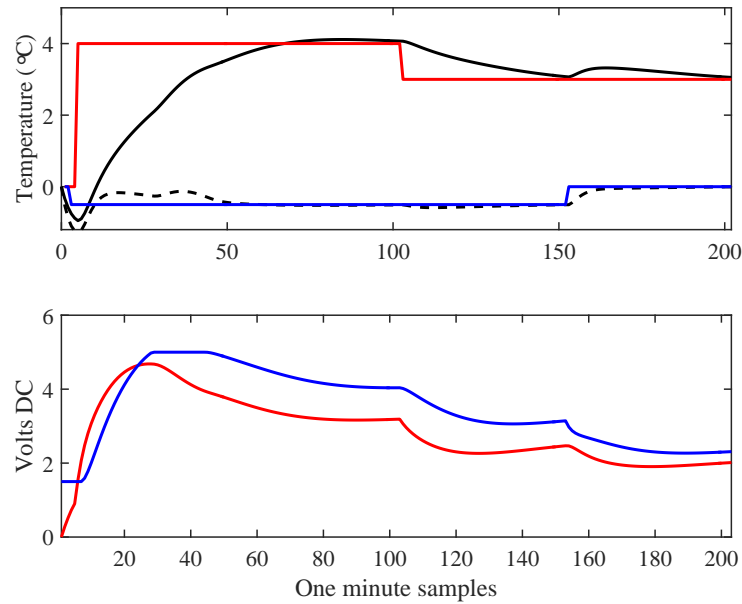
Figure 9.11: Second exemplary simulation of MIMO controller

between zero and maximum output, thus making the system unstable.

A third control implementation attempt of the real system is shown in Fig. 9.12. For this example, the system controller is designed to compute its action every 5 minutes, in an attempt to discard the cascading behaviour. However, this did not become possible until the control input of the fan was limited to operate within a very narrow operating level (i.e. 1.2-1.7 V DC). Even though this example showed to work, this MIMO controller cannot be used for a wide range of temperature distribution scenarios, and shows that future work should include an attempt to decouple the system and utilise filtering methods.

9.6   Conclusions to Part B of the thesis

This chapter has used a control system design context to illustrate the data-based modelling contributions made in Chapters 7 and 8 of the thesis. SISO and MIMO temperature controllers have been evaluated in simulation, followed by some preliminary implementation experiments. This research and that in Part B of the thesis more generally, was broadly motivated by the need to improve the micro-climatic conditions in indoor plant growing airspaces, where a relatively homogeneous en-
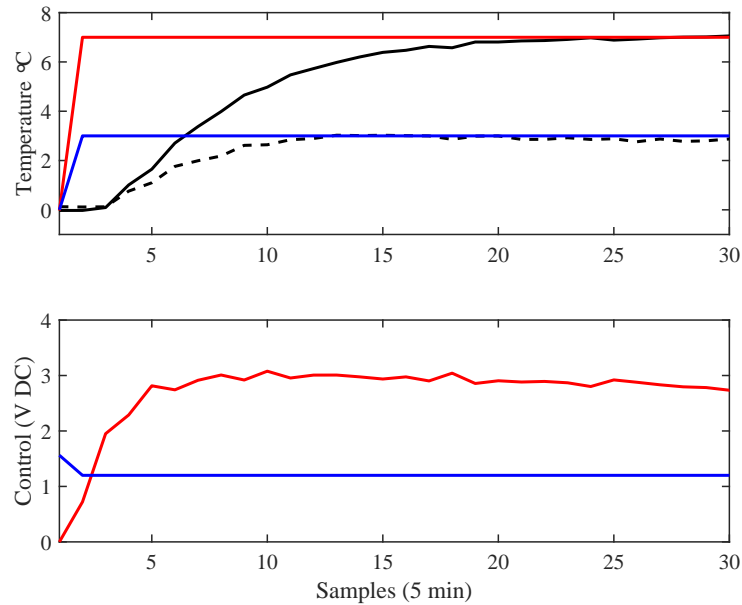
Figure 9.12: Mimo control experiment with limited control action achieving the desired temperature and temperature difference

vironment is desired. Experimental data for the grow-cell considered in Part A of the thesis, as well as the forced ventilation test chamber utilised as a research tool in Part B, shows that without adequate control, micro-climatic conditions vary significantly at different locations.

Hence, Chapter 7 presented a novel approach for objectively identifying relatively well-mixed zones in an airspace, by applying statistical clustering tools to multiple temperature measurements. The analysis provides a computationally straightforward way of partitioning an airspace into a number of zones that have a relatively uniform thermal behaviour, in terms of their steady state and dynamic response to the actuators. The research considered different clustering approaches to determine the most consistent way of systematically identifying the dominant behaviour that arises as a result of different ventilation rates, as illustrated by means of the 15 datasets considered in the chapter. For the particular case of the laboratory facility, the results quantitatively reveal that the distribution of temperature around the main grid of the chamber is explained well using just two zones, for which the temperature responses differ depending on the magnitude of the air flow. The advantage of a

multi-zone approach, is that it allows for a relatively simpler modelling and control design task, as considered in subsequent chapters.

Chapter 8 developed a novel non-linear thermal model. The single-input Hammerstein structure initially developed, proved useful to explain temperature variations for a wide range of time-invariant fan settings, while the extension of the model to a 2-dimensional structure allowed for experimental data in which the ventilation rate is also varied on–line. The best model fits are achieved by application of a state-dependent parameter approach for the dynamic component of the model. Whilst the above relates to models for a single thermocouple or thermal zone, the final part of Chapter 8 introduced a two-zone Hammerstein type model under the assumption of a causal relationship between the two zones. Although there is considerable scope for further research into both the static non-linearity and the dynamic component of the model, especially in the multi-zone case, evaluation experiments using the laboratory chamber demonstrate satisfactory model performance for subsequent use as a control system design tool.

In the latter regard, the Chapter 9 utilised the non-linear model as a simulation tool for preliminary evaluation of linear control systems, whilst the following Chapter 10 considers how it might be more directly utilised for nonlinear control design. More specifically, Chapter 9 has presented SISO and MIMO linear control systems for temperature in the ventilation chamber. The SISO controller simplified the control of the "upper-middle" part of the chamber, which was identified as being a single relatively well-mixed thermal zone, by representing the behaviour of all 12 thermocouples in this zone with a single linear Transfer Function model, subsequently successfully utilised for linear PIP temperature control.

The aim of the MIMO controller, by contrast, was to demonstrate how temperature distributions across the entire chamber can be controlled using a relatively straightforward scheme, here based on the information derived from several open-loop heater experiments (that were specifically designed to collect data for this purpose). The preliminary results presented, suggest that the homogeneity of the airspace may be controlled using the two dominant zones identified in Chapter 7: the temperature of one zone is primarily controlled by the heater, while the difference in temperature between the two zones is primarily controlled by the fan. In fact, the four input–

output pathways are clearly coupled, hence a multivariable PIP control approach was chosen in this chapter.

Evaluation experiments in simulation, together with selected successful practical experiments, demonstrate the veracity of the approach. However, it is also clear from the implementation experiments that further research is required, since the inherent non-linearities of the system make this a challenging problem, and the approach proposed might be limited to specific scenarios and conditions. For example, the tracking of the setpoints $y_{dz1} = 5$ °C and $y_{dtd} = 1$ °C (representing the zone temperature above laboratory temperature and the temperature difference between two zones respectively) can be achieved either by a combination of low fan/very low heat input, or a higher fan/high heat input. Moreover, the effect of a small change in the control voltage of the fan has a huge effect on the temperature distribution, causing the controller to fail in some of the practical implementation experiments. Nonetheless, the example demonstrates the wide scope for further control orientated research to utilise the models and zone identification schemes developed in Part B of this thesis.

Chapter 10

Overall Conclusions and Future Research

The research behind this thesis was motivated by an increasing interest in evolving the current established plant growing technologies, with a scope to shift horticulture to a more optimized and sustainable production. For example, reducing the use of pesticides and recycling of water are two very important aspects, from which the horticultural industry can benefit long term. In this respect, the present author has worked with an industrial partner to bring together a plant factory test rig i.e. the grow-cell. The first part of the thesis focused on this test rig and its evaluation via plant growth trials, whereas the second part utilised a laboratory scale forced ventilation chamber to experimentally investigate temperature distributions and novel modelling approaches. This was followed by the simulation and implementation of illustrative temperature control systems for the laboratory system.

Chapters 5 and 9 have already provided conclusions and recommendations for further research associated with Parts A and B of the thesis, respectively. The present chapter briefly summarises these in relation to the initial project aims (section 10.1) and provides additional suggestions for further research (section 10.2).

10.1 Summary

Chapter 1 set out the motivation and aims of the research. Chapter 2 outlined the three key engineering requirements for building a prototype grow-cell i.e. the

type of artificial lights, the mechanical movement of plants, and the distribution of the micro-climate. Chapter 3 presented the development of the test grow-cell. This included: a) the procurement of a container, equipped with an off-the-shelf HVAC system; b) the sourcing of suitable temperature and humidity sensors to monitor the growing area; c) the assessment of different LED light modules; d) the procurement of suitable LED lights and design of the associated variable power supply system; e) the design and construction of the conveyor control system for mechanical movement of the plants; f) the design and construction of the irrigation system; and h) the testing of the grow-cell in terms of the conveyor system and temperature distributions prior to the growth trials. The present author completed the above and actively participated in assembling the subsystems into the container, by means of hard-wiring, electrical testing and modifying the logic for operating the conveyor system.

Chapter 4 discussed the growth trials that were held at Bordon Hill Nurseries. During the two growth trial periods, the present author initiated modifications to the conveyor and irrigation systems to meet the emerging needs of these trials, and acquired temperature, humidity and energy data; as well as training members of the nursery staff to operate the conveyor system and set up appropriate irrigation and lighting periods. To conclude Part A of the thesis, Chapter 5 draws together various recommendations from the experience gained by building and testing the grow-cell. The research was based on a relatively low-cost design but nevertheless showed that the grow-cell can grow plants to growers' expectations. Similar facilities may be utilised in the future with the scope to grow crops in an environmentally friendly way. In this trajectory, the results that were derived for this thesis are not only useful to the industrial partner, who now has both the experience and the know-how to develop grow-cells that can be tailored for specific crops, but should also find interest to a wider audience in the horticultural industry.

All the tasks in chapters 2–4 took place between the first and the third year of the PhD project, and represent successful completion of four of the five objectives set out in Chapter 1 (section 1.3). Part B of the thesis concerns the remaining research objective (i.e. the fourth bullet point of section 1.3). It addresses the micro-climatic conditions of the growing area, since efficient control of the key

environmental variables is one way of optimizing enclosed growing airspaces, in the sense that all plants are receiving the same energy inputs. This research focused on temperature but other environmental variables are also important and interact with each other. For example, uniformity is also important in terms of watering the soil bed so that all plants receive the same amount of water and develop strong roots; and light uniformity encourages plants to have similar leaf size, issues that were both investigated to some degree in Part A.

Although motivated by the development of the grow-cell, Part B of the thesis specifically relates to a laboratory forced ventilation test chamber in the Engineering Department at Lancaster University. A data-based approach to modelling was followed throughout. Chapter 7 proposed the use of statistical clustering for utilizing data from multiple measurement locations in the ventilation chamber. The two standard clustering algorithms (k-means and AHC) yield meaningful thermal zones using raw measured data (i.e. based on data for specific time periods of a response) and from derived measures based on model parameter estimates. One conclusion to the investigation, is that it is beneficial to consider more than one object for the clustering (e.g. both time constant and steady state gain of an estimated model) but further research is required to determine how many such objects are optimal.

Chapter 8 made use of experimental data from the test chamber to develop a non-linear Hammerstein model for temperature. The modelling approach links together block oriented models and data-based linear TF models. This was further extended to a 2-dimensional case, in which the coefficients of a static non-linear function between steady state temperature and heater input are dependent on the state of the *fan* input; and the dynamic component of this model was extended to a state-dependent parameter form. Each increased complication improved the model fit but further research is required to determine if the state-dependent parameter model provides a significant increase in model fit compared to the simpler 2-d Hammerstein model. Finally, Chapter 8 also determines a causal relationship between two thermal zones and uses this to develop an associated two-zone model for temperature.

Chapter 9 developed both SISO and multivariable PIP control systems for temperature, primarily in order to highlight the contributions made in the previous two chapters of the thesis. More specifically, a SISO controller was simulated and

implemented for a single thermal zone identified in Chapter 7, and evaluated first using the non-linear model from Chapter 8, and finally using the laboratory facility. Secondly, the MIMO controller for regulating the temperature of two zones identified in Chapter 7 was assessed both in simulation and in practice. A novelty of the proposed MIMO controller is that it did not attempt to control the absolute level of temperature in two different zones, rather it considered the temperature of one zone and the temperature difference from another (i.e. representing thermal stratification). It would be true to say that Chapter 9 generated preliminary results that show there is considerable scope for further research into multi-zone control.

Even though the results of the second part of this thesis were based on a laboratory scale example, a future HVAC system design may borrow from the results of both parts of the thesis. For example, mechanical modifications that were suggested in the conclusions of the first part (e.g. a horizontal airflow supply scheme) may be employed; and repeat the modelling, clustering, and control design procedures but for measurements obtained within the grow-cell. This will be particularly useful to precisely characterise the capacity of the HVAC system and create a control scheme that improves the homogeneity of the growing volume by acting upon the magnitude of the heater, air-flow, dampers and louvres in an appropriate manner.

10.2 Future Research

The contributions made in this thesis may be utilised in the future for a range of tasks that relate both to the development of the grow-cell (and similar facilities) and to the modelling and control orientated research.

Grow-cell as a gold-mine for horticulture research

The development of the test grow-cell provided plenty of insight in terms of modernizing the horticultural industry. Several such types of facilities have been designed and tested, or are commercially operational, as noted in earlier chapters. The test facility developed here may similarly be used for the investigation of various aspects that relate to controlled environment agriculture. For example, there is considerable scope for research into the biological response e.g. to undertake various

experimental growth trials under different LED light settings, different LED light units, and perhaps develop a technology for producing tailored crops, in terms of flavour, aesthetics, nutritional content, and artificial pause and acceleration of growth cycles. All this brings in engineering contributions, including further work on a) the mechanical design of various subsystems, b) interfacing the grow-cell to renewable energy resources, and c) to develop a flexible and energy efficient HVAC system.

Regarding (a) for example, it would be interesting to develop a design that is modular but also adaptable to different types of light, with the aim to lower the production cost of different mechanical designs for different types of plants. Related to (b), a grow-cell that can survive by harvesting electricity from natural resources is also another feature that relates to improving its operational cost efficiency. Finally, an intelligent control system may allow researchers to investigate aspects of the system that relate to controlling the individual mechanisms of plants.

Temperature distribution identification and control

As mentioned earlier, Chapter 7 proposed straightforward clustering methods for distinguishing different temperature zones in an enclosed airspace, by utilising raw and model-based data. Even though this approach did reveal the dominant modes of the studied airspace, it remained an offline and exploratory tool. More sophisticated approaches may be evaluated in the future, which can also be applied online, hence trained upon receipt of output data and input settings. For example, artificial neural networks and genetic algorithms may be also assessed in this application. One may imagine a system that recognizes how e.g. the temperature distribution is changing over time, under different settings, and automatically instruct the actuators to create one or more different thermal zones. It could provide the means to control the distribution of a micro-climate by changing the angles of airflow inlet louvres, and hence the airflow direction. Such a concept is employed to a limited extent in some similar facilities by moving oscillating fans. Adding this extra variable (angle of airflow) to a MIMO control scheme would be therefore interesting to investigate using the laboratory chamber initially, and later in the grow-cell.

Thermal modelling

The thermal modelling chapter utilised one type of non-linear static function, which is exploited to yield the predicted steady state temperature (or the "effective input") to a modified TF linear model. The three variations of this scheme were evaluated by means of six different datasets, and the SDP approach yielded the best results as compared to the other two. There are several tasks that may be investigated in the future, in order to a) improve the non-linear model, and b) compare it with other non-linear models. Regarding (a), the flexible logistic growth functions that were utilised here for both temperature and ventilation rate were broadly sufficient to develop the non-linear model and test it. However, the total number of coefficients that need to be estimated, especially when combined with an SDP TF model, is quite large. In this manner, it is worth investigating other types of non-linear static functions and functions for fitting the TF parameters, and compare them all together in order to increase modelling accuracy. In addition, it would be also useful to compare such variations of the Hammerstein model with the performance of other non-linear models, not necessarily block-oriented type.

Control design

Control design ultimately aims for the deployment of a controller that can regulate the behaviour of a controlled variable. Even though, in the context of the grow-cell, the control problem may have minimal disturbances, the way the air-flow is transported into the air is non-linear, and hence all the micro-climatic variables behave according to that. With regard to creating a temperature distribution controller, it is essential to investigate the implementation of MIMO non-linear controllers. For example, the nonlinear model could be directly utilised to estimate an associated state-dependent control system. These could have features such as decoupling in order to cancel effects between interacting loops, filtering and e.g. feedforward control. The latter could be utilised, for instance, in an extension of the MIMO controller presented in Chapter 9. Assuming that a very accurate non-linear model is developed for these purposes, the addition of a feedforward path could also have a positive impact. Another important concept that needs to be addressed is that of sampling rate. Throughout this thesis, sampling has been set either at one or sixty per second,

for temperature. However, the response to a fan input is much faster than that of temperature, and hence at least ten samples per second are needed to accurately capture ventilation rate. Should both temperature and ventilation rate are to be controlled in the same loop, the control design must consider a suitable sampling rate.

Bibliography

A. Afram and F. Janabi-Sharifi. Black-box modeling of residential hvac system and comparison of gray-box and black-box modeling methods. *Energy and Buildings*, 94:121–149, 2015.

C. Agbi, Z. Song, and B. Krogh. Parameter identifiability for multi-zone building models. In *51st IEEE Conference on Decision and Control*, pages 6951–6956, Maui, Hawaii, December 2012.

L. A. Aguirre, M. C. S. Coelho, and M. V. Correa. On the interpretation and practice of dynamical differences between hammerstein and wiener models. *IEE Proceedings-Control Theory and Applications*, 152(4):349–356, 2005.

M. S. Aldenderfer and R. K. Blashfield. Cluster analysis. In M. S. Lewis-Beck, editor, *Sage University Paper Series on Quantitative Applications in the Social Sciences*. Sage, Beverly Hills, 2006.

C. C. Almeida, P. S. Almeida, N. R. C Monteiro, M. F. Pinto, and H. A. C Braga. LED-based electronic system to support plant physiology experiments. In *23rd IEEE International Symposium on Industrial Electronics (ISIE)*, pages 531–536, 2014.

O. Arbelaitz, I. Gurrutxaga, J. Muguerza, J. M. Pérez, and I. Perona. An extensive comparative study of cluster validity indices. *Pattern Recognition*, 46:243–256, 2013.

J. M. Arthur, J. D. Guthrie, and J. M. Newell. Some effects of artificial climates on the growth and chemical composition of plants. *American Journal of Botany*, 17 (5):416–482, 1930.

C. R. Ball. The relation of crop-plant botany to human welfare. *American Journal of Botany*, 8(7):323–338, 1921.

E. M. Barber and J. R. Ogilvie. Incomplete mixing in ventilated airspace. part 1. theoretical considerations. *Canadian Agricultural Engineering*, 24(1):25–29, 1982.

D. J. Barta, Tibbits T. W., R. J. Bula, and R. C. Morrow. Evaluation of light emitting diode characteristics for a space-based plant irradiation source. *Advances in Space Research*, 12(5):141–149, 1992.

D. Berckmans and V. Goedseels. Development of new control techniques for the ventilation and heating of livestock buildings. *Journal of Agricultural Engineering Research*, 33:1–22, 1986.

C. Bleil De Souza and S. Alsaadani. Thermal zoning in speculative office buildings: discussing the connections between space layout and inside temperature control. *Journal of Building Performance Simulation*, 2012.

T. J. Blom and Y. Zheng. The response of plant growth and leaf gas exchange to the speed of lamp movement in a greenhouse. *Scientia Horticulturae*, 119(2):188–192, 2009.

T. Boulard and A. Baille. A simple greenhouse climate control model incorporating effects of ventilation and evaporative cooling. *Agricultural and Forest Meteorology*, 65:145–157, 1993.

C. M. Bourget. An introduction to light-emitting diodes. *American Society for Horticultural Science*, 43(7):1944–1946, 2008.

D. Brande. Cleanroom cerification and particulate testing. In Anne Marie Dixon, editor, *Environmental Monitoring for Cleanrooms and Controlled Environments*, pages 1–223. CRC Press, 2006.

C. J. Brien, B. Berger, H. Rabie, and M. Tester. Accounting for variation in designing greenhouse experiments with special reference to greenhouses containing plants on conveyor systems. *Plant Methods*, 9(1):1–22, 2013.

C. S. Brown, A. C. Schuerger, and J. C. Sager. Growth and photomorphogenesis of pepper plants under red light-emitting diodes with supplemental blue or far-red lighting. *American Society for Horticultural Science*, 120(5):808–813, 1995.

E. M. Brown. Equipment for the growing of plants at controlled temperatures. *Plant Physiology*, 14(3):517–526, 1939.

R. J. Bula, R. C. Morrow, T. W. Tibbits, and Barta D. J. Light-emitting diodes as a radiation source for plants. *American Society for Horticultural Science*, 26(2): 203–205, 1991.

M. Bürger, D. Zelazo, and F. Allgöwer. Hierarchical clustering of dynamical networks using a saddle-point analysis. *IEEE Transactions on Automatic Control*, 58(1): 113–124, 2013.

B. Cabieses, H. Tunstall, and K. Pickett. Understanding the socioeconomic status of international immigrants in chile through hierarchical cluster analysis: a population-based study. *International Migration*, 53(2):303–320, 2015.

J. Cai, D. Kim, J. E. Braun, and J. Hu. Optimizing zone temperature setpoint excitation to minimize training data for data-driven dynamic building models. In *American Control Conference*, pages 6–8, 2016.

T. Caliński and J. Harabasz. A dendrite method for cluster analysis. *Communications in Statistics-theory and Methods*, 3(1):1–27, 1974.

G. Cao, H. Awbi, R. Yao, Y. Fan, K. Sirén, R. Kosonen, and J. J. Zhang. A review of the performance of different ventilation and airflow distribution systems in buildings. *Building and Environment*, 73:171–186, 2014.

R. Caponetto, L. Fortuna, G. Nunnari, L. Occhipinti, and M. G. Xibilia. Soft computing for greenhouse climate control. *IEEE Transactions on Fuzzy systems*, 8 (6):753–760, 2000.

P. J. Castaldi, J. Dy, J. Ross, Y. Chang, G. R. Washko, D. Curran-Everett, A. Williams, D. A. Lynch, B. J. Make, and J. D. Crapo. Cluster analysis in the copdgene study identifies subtypes of smokers with distinct patterns of airway disease and emphysema. *Thorax*, pages thoraxjnl–2013, 2014.

J. Chen, C. Guo, Z. Yang, T. Li, and J. Zhao. Li2srsio4: Ce3+, pr3+ phosphor with blue, red, and near-infrared emissions used for plant growth led. *Journal of the American Ceramic Society*, 99(1):218–225, 2016.

M. S. K. Chen, L. T. Fan, C. L. Hwang, and E. S. Lee. Air flow models in a confined space a study in age distribution. *Building Science*, 4(3):133–144, 1969.

Q. Chen. State of the art in building modelling and energy performances prediction: A review. *Building and Environment*, 44:848–858, 2009.

Andrés Cortés and Nicanor Quijano. Microclimate modeling and control: A multizone approach. In *American Control Conference (ACC), 2010*, pages 5910–5915. IEEE, 2010.

J. B. Cunha, C. Couto, and Ruano A. E. Real time parameter estimation of dynamic temperature models for greenhouse environmental control. *Control Engineering Practice*, 5(10):1473–1481, 1997.

L. Davidson and E. Olsson. Calculation of age and local purging flow rate in rooms. *Building and Environment*, 22(2):111–127, 1987.

D. L. Davies and D. W. Bouldin. A cluster separation measure. *IEEE: Pattern Analysis and Machine Intelligence*, 1:224–227, 1979.

A. R. Davis and Hoagland D. R. An apparatus for the growth of plants in a controlled environment. *Plant Physiology*, 3:277–292, 1928.

C. De Persis, J. J. Jessen, R. Izadi-Zamanabadi, and H. Schiøler. A distributed control algorithm for internal flow management in a multi-zone climate unit. *International Journal of Control*, 81(1):89–106, 2008.

D. Despommier. The rise of vertical farms. *Scientific American*, 301(5):80–87, 2009.

T. Z. Desta, K. Janssens, A. Van Brecht, J. Meyers, M. Baelmans, and D. Berckmans. Cfd for model-based controller development. *Building and Environment*, 39:621–633, 2004a.

T. Z. Desta, A. Van Brecht, J. Meyers, M. Baelmans, and D. Berckmans. Combining cfd and data-based mechanistic (dbm) modelling approaches. *Energy and Buildings*, 36:535–542, 2004b.

T. Z. Desta, A. Van Brecht, S. Quanten, S. Van Buggenhout, J. Meyers, M. Baelmans, and D. Berckmans. Modelling and control of heat transfer phenomena inside a ventilated air space. *Energy and Buildings*, 37:777–786, 2005a.

T. Z. Desta, S. Van Buggenhout, A. Van Brecht, J. Meyers, J.-M. Aerts, M. Baelmans, and D. Berckmans. Modelling mass transfer phenomena and quantification of ventilation performance in a full scale installation. *Building and Environment*, 40: 1583–1590, 2005b.

T. Z. Desta, M. Baelmans, and D. Berckmans. Behaviour of well-mixed zones (wmzs) in an imperfectly mixed ventilated room. *Building and Environment*, 43:2035–2045, 2008.

R. E. Dorland and F. W. Went. Plant growth under controlled conditions. VIII. growth and fruiting of the chili pepper (capsicum annuum). *American Journal of Botany*, 34(8):393–401, 1947.

R. J. Downs. Phytotrons. *The Botanical Review*, 46(4):447–489, 1980.

C. Duarte-Galvan, I. Torres-Pachecho, R. G. Guevara-Gonzalez, R. J. Romero-Troncoso, L. M. Contreras-Medina, M. A. Rios-Alcaraz, and J. R. Millan-Almaraz. Review. advantages and disadvantages of control theories applied in greenhouse climate control systems. *Spanish Journal of Agricultural Research*, 10(4):926–938, 2012.

M. B. Eisen, P. T. Spellman, P. O. Brown, and D. Botstein. Cluster analysis and display of genome-wide expression patterns. *Proceedings of the National Academy of Sciences*, 95(25):14863–14868, 1998.

F. A. D. Espinosa and L. R. Glicksman. Determining thermal stratification in rooms with high supply momentum. *Building and Environment*, 112:99–114, 2017.

FAO. World agriculture: Towards 2015/2030, summary report. Food and Agriculture Organization of the United Nations, Rome, 2002.

FAO. Towards a water and food secure future, critical perspectives for policy-makers. Food and Agriculture Organization of the United Nations (Rome), World Water Council (Marseille), 2015.

R. G. Fovell and M. C. Fovell. Climate zones of the conterminous united states defined using cluster analysis. *Journal of Climate*, 6(11):2103–2135, 1993.

C. Fraley and A. E. Raftery. How many clusters? which clustering method? answers via model-based cluster analysis. *The computer journal*, 41(8):578–588, 1998.

FreightFarms. Freight Farms. www.freightfarms.com, 2016. [Online; accessed 08/04/2016].

K. Fujiwara and T. Sawada. Design and development of an LED-artificial sunlight source system prototype capable of controlling relative spectral power distribution. *Journal of Light and Visual Environment*, 30(3):170–176, 2006.

M. Gholami, H. Schioler, M. Soltani, and T. Bak. Multi-zone hybrid model for failure detection of the stable ventilation systems. In *IEEE International Symposium on Industrial Electronics (ISIE)*, pages 262–267, July 2010.

S. Gilani, H. Montazeri, and B. Blocken. Cfd simulation of stratified indoor environment in displacement ventilation: Validation and sensitivity analysis. *Building and Environment*, 95:299–313, 2016.

M. Gocic and S. Trajkovic. Spatiotemporal characteristics of drought in serbia. *Journal of Hydrology*, 510:110–123, 2014.

G. D. Goins, N. C. Yorio, M. M. Sanwo, and C. S. Brown. Photomorphogenesis, photosynthesis, and seed yield of wheat plants grown under red light-emitting diodes (LEDs) with and without supplemental blue lighting. *Journal of Experimental Botany*, 48(312):1407–1413, 1997.

S. Goyal and P. Barooah. A method for model-reduction of non-linear thermal dynamics of multi-zone buildings. *Energy and Buildings*, 47:332–340, 2012.

GreenTech. Greentech Agro LLC. www.growtainers.com, 2016. [Online; accessed 08/04/2016].

E.-J. Hahn, T. Kozai, and K.-Y. Paek. Blue and red light-emitting diodes with or without sucrose and ventilation affect in vitro growth of rehmannia glutinosa plantlets. *Journal of Plant Biology*, 43(4):247–250, 2000.

J. Hamilton, M. Negnevitsky, and X. Wang. Thermal analysis of a single-storey livestock barn. *Advances in Mechanical Engineering*, 8(4), 2016.

E. M. Hardy and D. M. Blumenthal. An efficient and inexpensive system for greenhouse pot rotation. *Horticultural Science*, 43(3):965–966, 2008.

A. N. Harun, N. N. Ani, R. Ahmad, and N. S. Azmi. Red and blue LED with pulse lighting control treatment for brassica chinensis in indoor farming. In *IEEE Conference on Open Systems (ICOS)*, pages 231–236, 2013.

R. B. Harvey. Growth of plants in artificial light. *Botanical Gazette*, 74(4):447–451, 1922.

Y. Hendrawan, D. F. Al Riza, and H. Murase. Applications of intelligent machine vision in plant factory. In *19th IFAC Triennial World Congress*, pages 8122–8127, Cape Town, South Africa, August 2014.

E. Hendricks and R. B. Harvey. Growth of plants in artificial light. ii. intensities of continuous light required for blooming. *Botanical Gazette*, 77(3):330–334, 1924.

U. Hitzemann. *Extensions in non–minimal state–space and state–dependent parameter model based control with application to a DC–DC boost converter*. PhD thesis, Coventry University, UK, 2013.

C. J. Hughes. In newark, a vertical indoor farm helps anchor an area's revival. www.nytimes.com/2015/04/08/realestate/commercial/in-newark-a-vertical-indoor-farm-helps-anchor-an-areas-revival.html?_r=3, 2015. [Online; accessed 08/04/2016].

C. Inard, H. Bouia, and P. Dalicieux. Prediction of air temperature distribution in buildings with a zonal model. *Energy and Buildings*, 24:125–132, 1996.

K. Janssens, A. Van Brecht, T. Z. Desta, C. Booten, and D. Berckmans. Modeling the internal dynamics of energy and mass transfer in an imperfectly mixed ventilated airspace. *Indoor Air*, 14:146–153, 2004.

K. A. Joudi and A. A. Farhan. A dynamic model and an experimental study for the internal air and soil temperatures in an innovative greenhouse. *Energy Conversion and Management*, 91:76–82, 2015.

M. W. Kadous and C. Sammut. Classification of multivariate time series and structured data using constructive induction. *Machine learning*, 58(2):179–216, 2005.

G. Kang, J. Yoo, J. Ahn, and K. Kim. Transparent dielectric nanostructures for efficient light management in optoelectronic applications. *Nano Today*, 10(1): 22–47, 2015.

L. Kaufman and P. J. Rousseeuw. *Finding groups in data: an introduction to cluster analysis*, volume 344. John Wiley & Sons, 2009.

M. Killian, B. Mayer, and M. Kozek. Effective fuzzy black-box modeling for building heating dynamics. *Energy and Buildings*, 96:175–186, 2015.

H.-H. Kim, G. D. Goins, R. M. Wheeler, and J. C. Sager. Green-light supplementation for enhanced lettuce growth under red- and blue-light-emitting diodes. *American Society for Horticultural Science*, 39(7):1617–1622, 2004.

J.-J. Kim, J. Lee, S.-P. Yang, H. G. Kim, H.-S. Kweon, S. Yoo, and K.-H. Jeong. Biologically inspired organic light-emitting diodes. *Nano letters*, 16(5):2994–3000, 2016.

S. E. Kingsland. Frits went's atomic age greenhouse: The changing labscape on the lab-field border. *Journal of the History of Biology*, 42:289–324, 2009.

C. Kittas, T. Bartzanas, and A. Jaffrin. Temperature gradients in a partially shaded large greenhouse equipped with evaporative cooling pads. *Biosystems Engineering*, 85(1):87–94, 2003.

R. L. Korthals, S. L. Knight, L. L. Christianson, and L. Spomer. Chambers for studying the effects of airflow velocity on plant growth. *Biotronics: reports of Biotron Institute, Kyushu University*, 23:113–119, 1994.

Z. M. Kovacs-Vajna. A fingerprint verification system based on triangular matching and dynamic time warping. *IEEE Transactions on Pattern Analysis and Machine Intelligence*, 22(11):1266–1276, 2000.

T. Kozai, G. Niu, and M. Takagaki. *Plant Factory: An Indoor Vertical Farming System for Efficient Quality Food Production*. Academic Press, 2015.

W.-S. Lee and S.-G. Kim. Development of rotational smart lighting control system for plant factory. In *Proceedings of World Academy of Science, Engineering and Technology*, volume 62, pages 741–744, 2012.

P. Leigh, P. Young, A. Chotai, L. Price, J. Taylor, E. Vranken, and D. Berckmans. Modelling and control of forced ventilation in agricultural livestock buildings. In *5th International Congress of Biometeorology and Urban Climatology*, Sydney, Australia, November 1999.

P. A. Leigh. *Modelling and control of microenvironmental systems*. PhD thesis, Lancaster University, 2003.

H. Lewis and F. W. Went. Plant growth under controlled conditions. IV. response of california annuals to photoperiod and temperature. *American Journal of Botany*, 32(1):1–12, 1945.

K. Li, Z. Li, and Q. Yang. Improving light distribution by zoom lens for electricity savings in a plant factory with light-emitting diodes. *Frontiers in Plant Science*, 7, 2016.

Z. Liao and A. L. Dexter. A simpli!ed physical model for estimating the average air temperature in multi-zone heating systems. *Building and Environment*, 39: 1013–1022, 2004.

K.-H. Lin, H. Meng-Yuan, H. Wen-Dar, H. Ming-Huang, Y. Zhi-Wei, and Y. Chi-Ming. The effects of red, blue, and white light-emitting diodes on the growth, development, and edible quality of hydroponically grown lettuce (lactuca sativa l. var. capitata). *Scientia Horticulturae*, 150:86–91, 2013.

Y. Liu, Z. Li, H. Xiong, X. Gao, and J. Wu. Understanding of internal clustering validation measures. In *IEEE International Conference on Data Mining*, 2010.

Y. Liu, H. Xiong, X. Gao, J. Wu, and S. Wu. Understanding and enhancement of internal clustering validation measures. *IEEE transactions on Cybernetics*, 43(3): 982–994, 2013.

R. Maddalena, M. J. Mendell, K. Eliseeva, W. R. Chan, D. P. Sullivan, M. Russell, U. Satish, and W. J. Fisk. Effects of ventilation rate per person and per floor area on perceived air quality, sick building syndrome symptoms, and decision-making. *Indoor air*, 25(4):362–370, 2015.

D. Markham. This former semiconductor factory is now the world's largest indoor farm, producing 10k heads of lettuce per day. www.treehugger.com/clean-technology/former-semiconductor-factory-becomes-worlds-largest-indoor-farm.html, 2014. [Online; accessed 08/04/2016].

C. F. Martin, S. Sun, and M. Egerstedt. Optimal control, statistics and path planning. *Mathematical and Computer Modelling*, 33(1-3):237–253, 2001.

G. D. Massa, H.-H. Kim, R. M. Wheeler, and C. A. Mitchell. Plant productivity in response to LED lighting. *American Society for Horticultural Science*, 43(7): 1952–1956, 2008.

G. W. Milligan and M. C. Cooper. An examination of procedures for determining the number of clusters in a data set. *Psychometrica*, 50(2):159–179, 1985.

R. C. Morrow. LED lighting in horticulture. *American Society for Horticultural Science*, 43(7):1947–1950, 2008.

M. Mossolly, K. Ghali, and N. Ghaddar. Optimal control strategy for a multi-zone air conditioning system using a genetic algorithm. *Energy*, 34(1):58–66, 2009.

D. P. D. Munns. "the awe in which biologists hold physicists": Frits went's first phytotron at caltech, and an experimental definition of the biological environment. *History and philosophy of the life sciences*, 36(2):209–231, 2014.

F. Murtagh and P. Legendre. Ward's hierarchical agglomerative clustering method: Which algorithms implement ward's criterion? *Journal of Classification*, 31(3): 274–295, 2014.

S. Muthu, F. J. Schuurmans, and M. D. Pashley. Red, green, and blue LED based white light generation: Issues and control. In *37th IEEE Industry Applications Society (IAS) meeting*, pages 327–333, October 2002.

K. Nagaya, Y. Li, Z. Jin, M. Fukumuro, Y. Ando, and A. Akaishi. Low-temperature desiccant-based food drying system with airflow and temperature control. *Journal of food engineering*, 75(1):71–77, 2006.

D. T. Nhut, T. Takamura, H. Watanabe, K. Okamoto, and M. Tanaka. Responses of strawberry plantlets cultured in vitro under superbright red and blue light-emitting diodes. *Plant Cell, Tissue and Organ Culture*, 73:43–52, 2003.

B. Oguntoyinbo, M. Saka, Y. Unemura, and J. Hirama. Plant factory system construction: Cultivation environment profile optimization. *Environmental Control in Biology*, 53(2):77–83, 2015.

H. Ohara, T. Hirai, K. Kouno, and Y. Nishiura. Automatic plant cultivation system (automated plant factory). *Environmental Control in Biology*, 53(2):93–99, 2015.

F. Oldewurtel, D. Gyalistras, M. Gwerder, C. N. Jones, A. Parisio, V. Stauch, B. Lehmann, and M. Morari. Increasing energy efficiency in building climate control using weather forecasts and model predictive control. In *10th REHVA World Congress CLIMA*, May 2010.

M. Outanoute, A. Lachhab, A. Ed-dahhak, A. Selmani, M. Guerbaoui, and B. Bouchikhi. A neural network dynamic model for temperature and relative humidity control under greenhouse. In *Third International Workshop on RFID And Adaptive Wireless Sensor Networks (RAWSN), 2015*, pages 6–11. IEEE, 2015.

J.-E. Park and K.S Nakamura. Automatization, labor-saving and employment in a plant factory. *Environmental Control in Biology*, 53(2):89–92, 2015.

M. W. Parker. Environmental factors and their control in plant experiments. *Soil Science*, 62:109–119, 1946.

C. Payne. Toshiba's clean factory farm produces 3 million bags of lettuce a year without sunlight or soil. http://inhabitat.com/toshibas-clean-factory-farm-produces-

3-million-bags-of-lettuce-a-year-without-sunlight-or-soil, 2014. [Online; accessed 08/04/2016].

R. K. Pearson and M. Pottmann. Gray-box identification of block-oriented nonlinear models. *Journal of Process Control*, 10(4):301–315, 2000.

M. V. Pee and D. Berckmans. Quality of modelling plant responses for environment control purposes. *Computers and Electronics in Agriculture*, 22:209–219, 1999.

S.-H. Peng, S. Holmberg, and D. Davidson. On the assessment of ventilation performance with the aid of numerical simulations. *Building and Environment*, 32 (6):497–508, 1997.

F. Petitjean, A. Ketterlin, and P. Gançarski. A global averaging method for dynamic time warping, with applications to clustering. *Pattern Recognition*, 44:678–693, 2011.

N. E. Pfeiffer. Microchemical and morphological studies of effect of light on plants. *Botanical Gazette*, pages 173–195, 1926.

J. Piburn, R. Stewart, and A. Morton. Attribute portfolio distance: A dynamic time warping-based approach to comparing and detecting common spatiotemporal patterns among multiattribute data portfolios. In *Advances in Geocomputation*, pages 197–205. Springer, 2017.

H. W. Popp. A physiological study of the effect of light of various ranges of wave length on the growth of plants. *American Journal of Botany*, 13(10):706–736, 1926.

L. Price, P. C. Young, D. Berckmans, K. Janssens, and C. J. Taylor. Data–based mechanistic modelling (DBM) and control of mass and energy transfer in agricultural buildings. *Annual Reviews in Control*, 23:71–83, 1999.

P. J. Rousseeuw. Silhouettes: a graphical aid to the interpretation and validation of cluster analysis. *Journal of Computational and Applied mathematics*, 20:53–65, 1987.

A. Rozental, E. Forsell, A. Svensson, D. Forsström, G. Andersson, and P. Carlbring. Differentiating procrastinators from each other: A cluster analysis. *Cognitive behaviour therapy*, pages 1–11, 2015.

J. C. Sager and J. C. McFarlane. Radiation. In R. W. Langhans and T. W. Tibbits, editors, *Plant Growth Chamber Handbook*, pages 1–29. Iowa Agricuture and Home Economics Experiment Station, 1997.

M. Sandberg. What is ventilation efficiency. *Building and environment*, 16(2): 123–135, 1981.

S. Saraçli, N. Doğan, and İ. Doğan. Comparison of hierarchical cluster analysis methods by cophenetic correlation. *Journal of Inequalities and Applications*, 2013 (1):1–8, 2013.

M. H. Sherman. On the estimation of multizone ventilation rates from tracer gas measurements. *Building and Environment*, 24(4):355–362, 1989.

A. Shimada and Y. Taniguchi. Red and blue pulse timing control for pulse width modulation light dimming of light emitting diodes for plant cultivation. *Journal of Photochemistry and Biology B: Biology*, 104:399–404, 2011.

SkyGreens. Sky Greens Pte Ltd. www.skygreens.com, 2016. [Online; accessed 08/04/2016].

R. R. Sokal and F. J. Rohlf. The comparison of dendrograms by objective methods. *Taxon, International Association for plant taxonomy*, 11(2):33–40, 1962.

J.-W. Song. Grow light for plant factory using quantum dot led. *Journal of International Council on Electrical Engineering*, 6(1):13–16, 2016.

M. A. Stables and C. J. Taylor. Nonlinear control of ventilation rate using state dependent parameter models. *Biosystems Engineering*, 95(1):7–18, 2006.

M. Sugano. Elemental technologies for realizing a fully-controlled artificial light-type plant factory. In *12th IEEE International Conference & Expo on Emerging Technologies for a Smarter World (CEWIT)*, pages 1–5, 2015.

M. Taki, Y. Ajabshirchi, S. F. Ranjbar, A. Rohani, and M. Matloobi. Heat transfer and mlp neural network models to predict inside environment variables and energy lost in a semi-solar greenhouse. *Energy and Buildings*, 110:314–329, 2016.

Y. Tanaka and M. Takahashi. Dynamic time warping-based cluster analysis and support vector machine-based prediction of solar irradiance at multi-points in a wide area. In *Proceedings of the ISCIE International Symposium on Stochastic Systems Theory and its Applications*, volume 2016, pages 210–215. The ISCIE Symposium on Stochastic Systems Theory and Its Applications, 2016.

B. Tashtoush, M. Molhim, and M. Al-Rousan. Dynamic model of an hvac system for control analysis. *Energy*, 30:1729–1745, 2005.

C. J. Taylor, P. Leigh, L. Price, P. C. Young, D. Berckmans, K. Janssens, E. Vranken, and R. Gevers. Proportional–integral–plus (PIP) control of ventilation rate in agricultural buildings. *Control Engineering Practice*, 12(2):225–233, 2004a.

C. J. Taylor, P. A. Leigh, A. Chotai, P. C. Young, E. Vranken, and D. Berckmans. Cost effective combined axial fan and throttling valve control of ventilation rate. *IEE Proceedings: Control Theory and Applications*, 151(5):577–584, 2004b.

C. J. Taylor, M. A. Stables, and P. C. Young. Identification of a multivariable state dependency for airflow rate in a forced ventilation test chamber. In *5th UKACC International Control Conference*, Bath, UK, September 2004c.

C. J. Taylor, D. J. Pedregal, P. C. Young, and W. Tych. Environmental time series analysis and forecasting with the Captain Toolbox. *Environmental Modelling and Software*, 22(6):797–814, 2007.

C. J. Taylor, P. C. Young, and A. Chotai. *True Digital Control: Statistical Modelling and NMSS Design*. John Wiley & Sons, 2013.

M. Teitel, M. Atias, and M. Barak. Gradients of temperature, humidity and co¡ sub¿ 2¡/sub¿ along a fan-ventilated greenhouse. *Biosystems Engineering*, 106(2): 166–174, 2010.

D. J. Tennessen, E. L. Singsaas, and T. D. Sharkey. Light-emitting diodes as a light source for photosynthesis research. *Photosynthesis research*, 39:85–92, 1994.

V. T. Thanh, A. Van Brecht, E. Vranken, and D. Berckmans. Modelling of three-dimensional air temperature distributions in porous media. *Biosystems Engineering*, 96(3):345–360, 2007a.

V. T. Thanh, E. Vranken, A. Van Brecht, and D. Berckmans. Data-based mechanistic modelling for controlling in three dimensions the temperature distribution in a room filled with obstacles. *Biosystems Engineering*, 98:54–65, 2007b.

V. T. Thanh, E. Vranken, and D. Berckmans. Data-based mechanistic modelling of three-dimensional temperature distribution in ventilated rooms filled with biological material. *Journal of Food Engineering*, 86:422–432, 2008.

T. W. Tibbits and T. T. Kozlowski. *Controlled Environment guidelines for plant research. Proceedings, Controlled Environments Working Conference, University of Winsconsin, Madison, 12-14 March.* Academic Press, 1979.

T. W. Tibbitts and D. T. Krizek. History of the ashs working group on growth chambers and controlled environments, 1969-96: A case study of involvement. *Horticultural Science*, 32(1):16–20, 1997.

W. E. Tottingham. Temperature effects in the metabolism of wheat. *Plant Physiology*, 1(4):307–336, 1926.

I. Tsitsimpelis. Data based modelling of temperature distribution in a forced ventilation test chambers. Master's thesis, Lancaster University, 2012.

A. Valenzuela, F. J. Olmo, H. Lyamani, M. Antón, A. Quirantes, and L. Alados-Arboledas. Classification of aerosol radiative properties during african desert dust intrusions over southeastern spain by sector origins and cluster analysis. *Journal of Geophysical Research: Atmospheres (1984–2012)*, 117(D6), 2012.

C. H. M. Van Bavel. Precision and replication. In T. W. Tibbits and T. T. Kozlowski, editors, *Controlled Environment guidelines for plant research. Proceedings, Controlled Environments Working Conference, University of Winsconsin, Madison, 12-14 March*, pages 321–330. Academic Press, 1979.

A. Van Brecht, J.-M. Aerts, P. Degraeve, and D. Berckmans. Quantification and control of the spatiotemporal gradients of air speed and air temperature in an incubator. *Poultry science*, 82(11):1677–1687, 2003.

A. Van Brecht, S. Quanten, T. Z. Desta, S. Van Buggenhout, and D. Berckmans. Control of the 3-d spatio-temporal distribution of air temperature. *International Journal of Control*, 78(2):88–99, 2005.

S. Van Buggenhout, T. Z. Desta, A. Van Brecht, E. Vranken, S. Quanten, W. Van Malcot, and D. Berckmans. Data-based mechanistic modelling approach to determine the age of air in a ventilated space. *Building and Environment*, 41:557–567, 2006.

G. van Straten, G. van Willigenburg, E. van Henten, and R. van Ooteghem. *Optimal Control of Greenhouse Cultivation*. CRC Press, 2011.

G. Vox, M. Teitel, A. Pardossi, A. Minuto, F. Tinivella, and E. Schettini. Sustainable greenhouse systems. In A. Salazar and I. Rios, editors, *Sustainable Agriculture: Technology, Planning and Management*, pages 1–79. Nova Science Publishers, 2010.

H. Wainwright, C. Jordan, and H. Day. Environmental impact of production horticulture. In *Horticulture: Plants for People and Places, Volume 1*, pages 503–522. Springer, 2014.

E. F. Wallihan and M. J. Garber. Efficiency of glasshouse pot experiments rotating versus stationary benches. *Plant Physiology*, 48(6):789–791, 1971.

F. W. Went. Plant growth under controlled conditions. I. the air-conditioned greenhouses at the California Institute of Technology. *American Journal of Botany*, 30(2):157–163, 1943.

F. W. Went. Plant growth under controlled conditions. II. thermoperiodicity in growth and fruiting of the tomato. *American Journal of Botany*, 31(3):135–150, 1944a.

F. W. Went. Plant growth under controlled conditions. III. correlation between various physiological processes and growth in the tomato plant. *American Journal of Botany*, 31(10):597–618, 1944b.

F. W. Went. Plant growth under controlled conditions. V. the relation between age, light, variety and thermoperiodicity of tomatoes. *American Journal of Botany*, 32 (8):469–479, 1945.

F. W. Went. Recent work at the earhart plant research laboratory. *Engineering and Science*, 15(6):14–18, 1952.

F. W. Went and L. Cosper. Plant growth under controlled conditions. VI. comparison between field and air- conditioned greenhouse culture of tomatoes. *American Journal of Botany*, 32(10):643–654, 1945.

R. M. Wheeler. A historical background of plant lighting: an introduction to the workshop. *Horticultural Science*, 43(7):1942–1943, 2008.

L. F. Wockner, E. P. Noble, B. R. Lawford, R. McD. Young, C. P. Morris, V. L. J. Whitehall, and J. Voisey. Genome-wide dna methylation analysis of human brain tissue from schizophrenia patients. *Translational psychiatry*, 4(1):e339, 2014.

Z. Wu, J. Stoustrup, and P. Heiselberg. Parameter estimation of dynamic multi-zone models for livestock indoor climate control. In *29th AIVC Conference on advanced building ventilation and environmental technology for addressing climate change issues*, pages 149–154, Kyoto, Japan, October 2008.

Y. Yang, Y. Zheng, W. Cao, A. Titov, J. Hyvonen, J. R. Manders, J. Xue, P. H. Holloway, and L. Qian. High-efficiency light-emitting devices based on quantum dots with tailored nanostructures. *Nature Photonics*, 2015.

P. C. Young. *Recursive Estimation and Time Series Analysis: An Introduction for the Student and Practitioner*. Springer, 2011.

P. C. Young. Hypothetico-inductive data-based mechanistic modeling of hydrological systems. *Water Resour Res*, 49:915–935, 2013.

P. C. Young, L. Price, D. Berckmans, and K. Janssens. Recent developments in the modelling of imperfectly mixed airspaces. *Computers and Electronics in Agriculture*, 26:239–254, 2000.

A. Youssef, H. H. Yen, E. Ozcan, and D. Berckmans. Data-based mechanistic modelling of indoor temperature distributions based on energy input. *Energy and Buildings*, 43:2965–2972, 2011.

J. Yun and K.-H. Won. Building environment analysis based on temperature and humidity for smart energy systems. *Sensors*, 12(10):13458–13470, 2012.

F. Zhou, F. De la Torre, and J. K. Hodgins. Hierarchical aligned cluster analysis for temporal clustering of human motion. *IEEE Transactions on Pattern Analysis and Machine Intelligence*, 35(3):582–596, 2013.

Appendix A

Conveyor System Programming

A.1 Hardware

The features and operation of the control system were decided upon discussions with the industrial partner of the Grow Cell project, and the academic supervisors. The maximum budget available was set at £ 2,000. The programming, panel construction and hard-wiring tasks were undertaken by the author of this thesis. The primary consideration was the selection of a programmable logic controller (PLC) suitable for the needs of the application. Three modules were considered, namely the LOGO smart relay by Siemens, the alpha-2 by Mitsubishi, and the Zelio-SR3 series by Schneider Electric. The programming, input-output capacity and purchasing cost were similar for all three options. The latter module was selected due to its user-friendly software platform.

The selected Zelio module (SR3B261BD) is powered by a 24 VDC power supply. It is equipped with 10 digital and 6 analog inputs, and it has ten relay outputs that are compatible with either direct or alternating current. When switching alternating current, eight of these outputs can carry up to 8 A while the maximum capacity of the other two is 5 A. The module's digital inputs are "sinking", meaning that when voltage is applied, the current sinks to its ground point; hence, it can be only interfaced with three-wire PNP sensors (also known as sourcing type), and the common two-wire mechanical switches. The following sensors and switches were utilised for the conveyor to operate as described in Chapter 3:

- Photoelectric sensor 1 (PE1): It detects the presence or absence of a tray

hanger.

- Photoelectric sensor 2 (PE2): Mounted across PE1 and serves the same purpose.

- Reflective sensor (REF1): It controls the start-end position of the horizontal motion.

- Proximity sensor 1 (PRX1): It controls the start-end position of sweep motor 1

- Proximity sensor 2 (PRX2): It controls the start-end position sweep motor 2.

- Auto-Manual Switch: A single pole-double throw (SPDT) switch. When switched upwards, the automatic mode is active. When switched downwards, the manual mode is active. At the middle position, the system is in stand-by mode.

- Start push button: A switch that has momentary mechanical action. It initialises the conveyor system's operation in automatic mode.

- Jog button: It serves the same purpose as the start button but it is used when manual mode is active. The difference in this case is that only one circulation is carried out after it is pressed.

- Interlock: Safety (contact) switch. It detects whether the mechanical curtain that separates the growing area is in place.

Furthermore, the following outputs control the actuators and inform the user on the status of the system's operation.

- Sweep motors 1-2: To transfer the tray carriers across at each end.

- Main motor: To transfer the tray carriers horizontally.

- Auto ON: Green colour LED light that is ON when automatic mode is active.

- Stand-By ON: Blue colour LED light that is ON when stand-By mode is active.

- Manual Mode ON: Amber colour LED light that is ON when manual mode is active.

- Alarm ON: Red colour LED light that is ON when a fault has occurred

- Human Machine Interface (HMI): A minimal LCD panel that informs the operator about the source of a fault, should that occur

A.2   Software and programming

The logic developed for the operation of the conveyor system, as described in Chapter 3, is covered here in two parts; one for the sweep and another one for the horizontal transfer. Fault detection logic and auxiliary features are also presented. At start-up, the system will either undertake the sweep or horizontal transfer, depending on the position of the tray hangers. In both cases, a valid combination of sensors signals must be present in the smart relay; a working mode must be selected, and the interlock switch must indicate that the curtain is in place. The operator may then initialise the operation by pressing the start or jog button.

A.2.1   Sweep transfer

The sweep transfer will only occur when PE1=1, PE2=0, REF1=1 PRX1=1 and PRX2=1. This means that PE1 must detect a tray carrier, PE2 must not detect a carrier, and REF1, PRX1, PRX2 must indicate that the motors are in their starting positions. A configurable Boolean function block is utilised to yield a logic 1 when the latter combination of signals is present. The signal is then passed to a SR (Set-Reset) Flip-Flop. This is a very important and particularly useful digital circuit as it retains a signal that occurs momentarily. In this case for example, when the sweep transfer begins, the combination of signals will change causing the output of the Boolean function block to drop back to logic zero. Using the SR flip-flop in this manner, the system is not stalled. The SR circuit has two inputs, namely Set and Reset, and one output, Q. When the Set input is activated by one signal, it subsequently energizes the output Q. This output then remains in an active state even when the Set input is no longer active. The Reset input can be used to deactivate the output Q when it is appropriate to do so. Moreover, one may select whether priority is given to Set or Reset when both inputs are active.

As described earlier, even if the sensors indicate that a sweep transfer is ready to occur, this will not happen unless a mode is selected and the user triggers the

operation. Therefore, an AND gate merges these three signals before the actuator is activated. The first input is the retained signal from the Boolean function. The second is the retained signal from the start (or jog) momentary button. The third input is the retained signal of the Automatic (or manual) mode switch. Note here that even though the automatic/manual mode switch does not have momentary mechanical action, its signal is retained because if one switches to stand-by or manual mode during an on-going task, priority must be given to the completion of the current task before the system is stalled for new instructions. When all three signals are applied to the AND gate, its output will yield a logic 1. This output is then passed initially to a three second timer and on to an OR logic gate. The OR gate yields a logic high when at least one input is active. Its functionality in this application is that it either accepts the command to operate the sweep motors through the automatic mode or through the manual mode (these are slightly different code snippets).

Lastly, the output of the OR gate goes into another AND gate, which is combined with the status of the interlock safety switch. This is deliberately placed just before the the motor because it is a health and safety requirement to immediately freeze the motors in the case that the system is operating and someone tries to access growing area. After the tray carriers are swept across at each end, the sweep motors stop at their starting positions.

A.2.2 Horizontal transfer

Upon completion of the sweep transfer, the signal sequence should be now: PE1=0, PE2=1, REF1=1, PRX1=1, PRX2=1. This condition activates the horizontal transfer. As before, the signal goes to a SR flip-flop, and onto an AND gate. From there it goes to a timer, which is configurable via the HMI. The reason for this is that, when in automatic mode, the user might want to perform a single circulation every x seconds. If, during the timing period, the user switches to stand-by or manual mode, the timer gets reset. Otherwise, the signal passes as before to an OR gate, and onto an AND gate, which checks whether the interlock switch is ON. Under normal conditions, the signal will reach the actuator and the transfer will begin. When the photoelectric sensor 1 detects the new tray carrier, then the main motor returns to its starting position before it stops.

A.2.3   Fault detection circuitry

In this application there are five sensors, the combination of which results in activating or disabling three motors in a specific sequence. Given the number of sensors, there are twenty five different combinations that can occur, either when the system is at start-up or during operation. Some of those are expected to occur during normal operation. Other combinations will never occur unless a fault has emerged in the system, either of mechanical or electrical nature. For this reason dedicated timers monitor intermediate and undesired combinations of signals. For the former, some time is given before it is considered as a fault, whereas for the latter the system stops immediately to prevent any damage that may occur.

### A.2.4   Communication with the HMI

The HMI is incorporated in order to allow the user pre-set the time interval between circulations in automatic mode, and to be informed about the states of the sensors and the type of alarm, should that occurs. The HMI used for communicating with the module is the Schneider Electric XBTN-401. Exporting information to the HMI is available through dedicated blocks.

A.2.5   Control panel, hardware schematics, and code

Figures A.1, A.2, A.3, A.4 and A.5 illustrate the control panel, hardware schematics, and programming for the conveyor system.

Figure A.1: Control panel initial version, designed and hard-wired by the author.
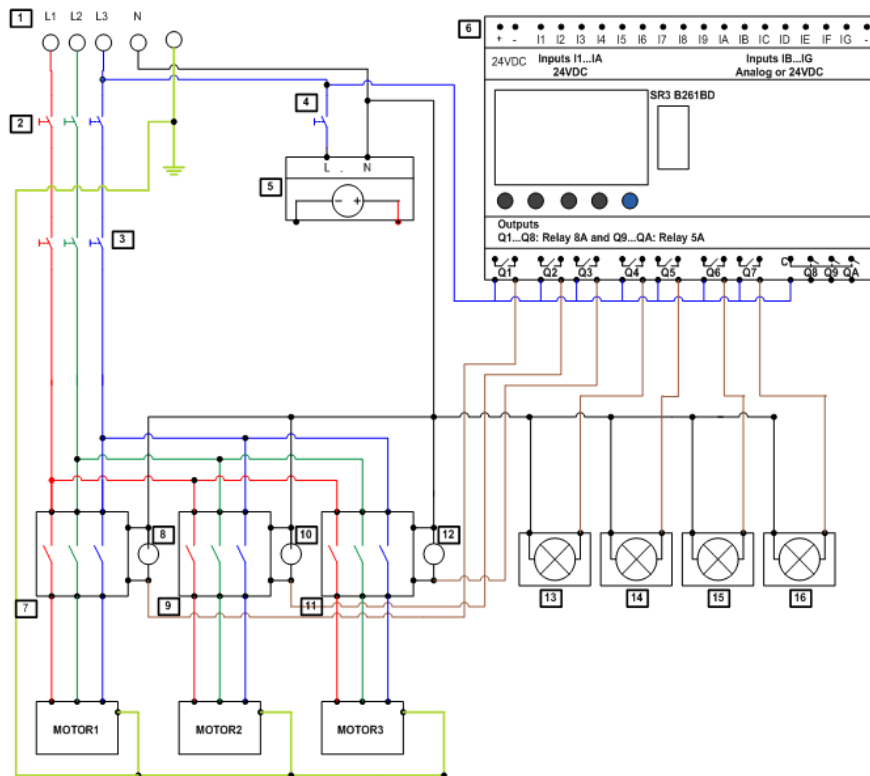
1	3phase power supply
2	Circuit breaker, 32A, 3 Pole, Type C
3	Motor protection breaker, 3pole, 8.5A FLC
4	Circuit breaker, 6A 1 pole, Type C
5	Step-Down transformer 220AC/24VDC, 2.5A
6	Smart relay
7,9,11	3 pole contactor, 5.5kW,12A,230Vac,1NO
8,10,12	Contactor coil (220AC)
13,14,15,16	220VAC light indicators

Figure A.2: Output hardware schematic as designed by the author.
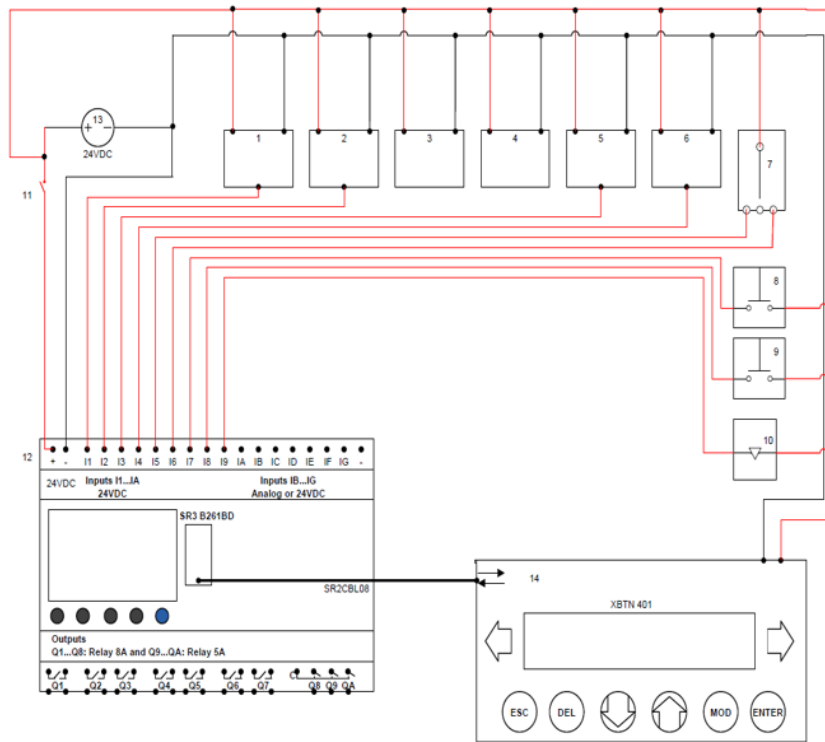
1	Photoelectric sensor 1 receiver
2	Photoelectric sensor 2 receiver
3	Photoelectric sensor 1 emitter
4	Photoelectric sensor 2 emitter
5	Proximity sensor 1
6	Proximity sensor 2
7	Single pole double throw (ON-OFF-ON) switch
8	Momentary pushbutton
9	Momentary pushbutton
10	Interlock switch
11	Circuit breaker, 1 pole, 1A DC
12	Zelio Smart relay
13	24VDC step down transformer output
14	XBTN-401 Human Machine Interface

Figure A.3: Input hardware schematic as designed by the author. Note that in this version, the reflective sensor that controls the starting position is not included as it was added later on.

Figure A.4: Main movement functions.
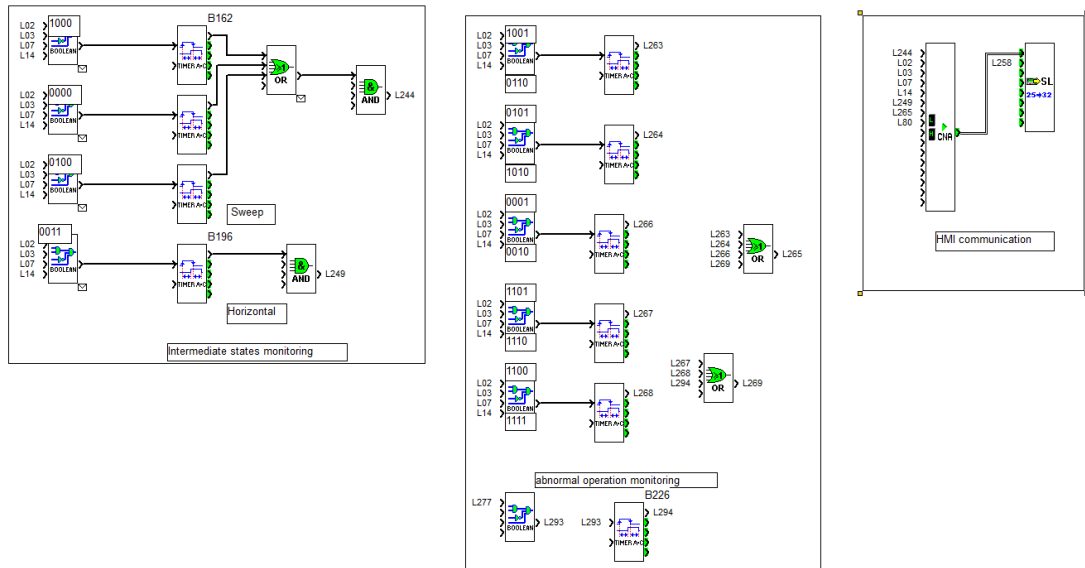
Figure A.5: Alarm monitors and HMI communication.

Appendix B

LED lights selection

In order to source appropriate lights for the grow-cell, five different products were assessed in terms of spectral output, PPFD output, and overall cost to cover the growing area. The review of units included products from the U.S., Chinese, Taiwanese and European markets, with cost ranging from £ 20 to £ 313. The following information relates to the basic features of the evaluated units.

- Illumitex Eclipse: 65 W, Red-blue light output, 121 cm × 5.5 cm, £ 160 per unit

- Valoya AP673: 100 W, Warm white light output, 120 cm × 7.3 cm, £ 313 per unit

- Solidlite: 42 W, Cool white light output, 50 cm × 30 cm, £ 42per unit

- Shenzen Ghel: 42 W, Red-blue light output, 60 cm × 5 cm, £ 29 per unit

- Szjiang Jing: 30 W, Red-blue light output, 64 cm × 4 cm, £ 20 per unit

Note that the cost does not include the power supply for each unit. Fig. B.1 shows the spectral output of all five units in relation to the photosynthetic efficiency curve. The two broad light output sources, i.e. Solidlite and Valoya are the best in this regard, as they include energy from more wavelengths that are also useful for a plant to grow. The two peaks of the Valoya light especially match very closely to the efficiency curve peaks, whereas the Solidlite yields more blue light than utilized by the plants.
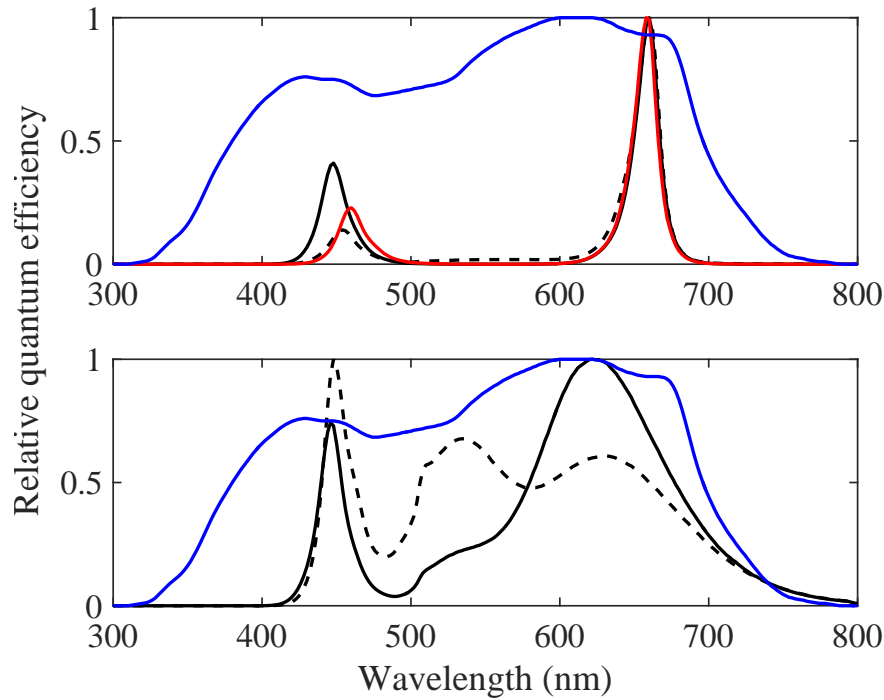
Figure B.1: Spectral output of each unit. Upper plot: Ghel, Illumitex (dashed trace), Jing (red trace). Lower plot: Valoya, Solidlite (dashed trace). In both plots the relative quantum efficiency curve of plants is depicted in blue colour.

Similarly, Fig. B.2 and Fig. B.3 show the PPFD distribution of each light at 20 cm above a 90 cm $\times$ 50 cm measuring board. Here, the best PPFD outputs are observed for the Illumitex and for the Valoya units. However, the former was discarded as the requirements shifted towards using a broad light unit. Between the two options (Solidlite and Valoya), clearly the latter outperformed the former. However, it would cost four times more to fill in the growing area with Valoya lights (£ 31,300, excluding the dimmable drivers); which exceeded the partner company's budget allocation. On the other hand, a relatively satisfactory performance could be achieved with a cost of £ 10,000, including the dimmable drivers (see Fig. 3.10). The compromise for selecting the Solidlite units relates to limiting the range of plants one could grow in the grow-cell. Nevertheless, as was seen from growth trials (Chapter 4), healthy plants developed quickly.
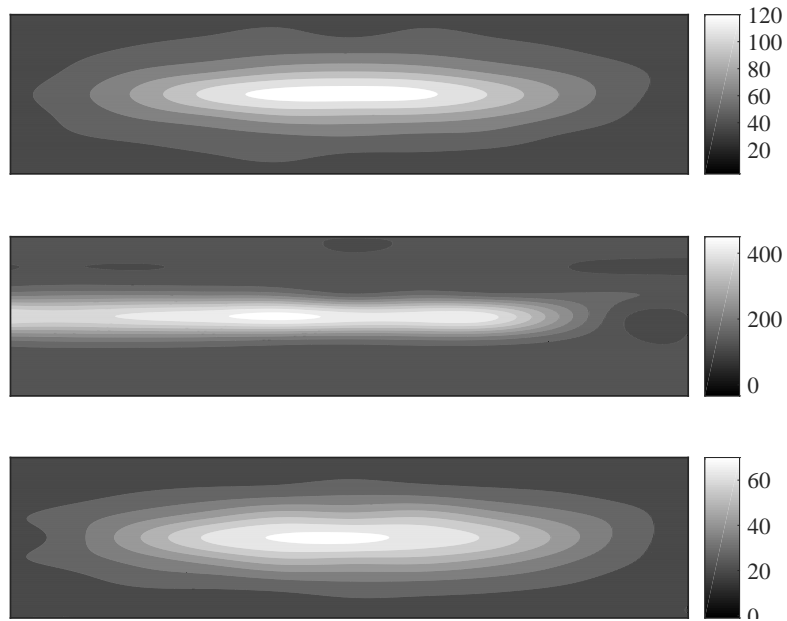
Figure B.2: PPFD distribution at 20 cm above a 90 cm × 50 cm measuring board. Top plot: Ghel. Middle plot: Illumitex. Bottom plot: Jing.
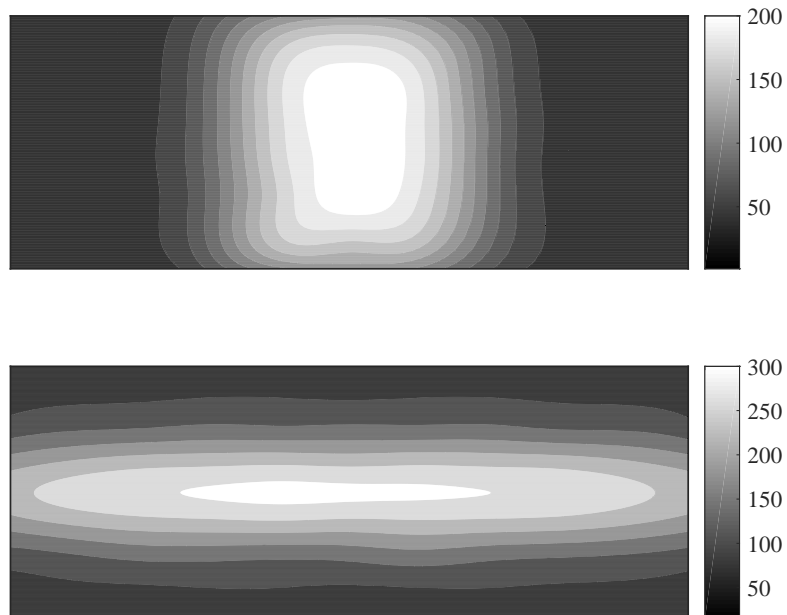

Figure B.3: PPFD distribution at 20 cm above a 90 cm × 50 cm measuring board. Top plot: Solidlite. Bottom plot: Valoya

Appendix C

Grow-Cell Subsystem Design Guidelines

Figures C.1, C.2, C.3 and C.4 show suggested subsystem design guidelines based on the experience gained in developing the grow-cell prototype.
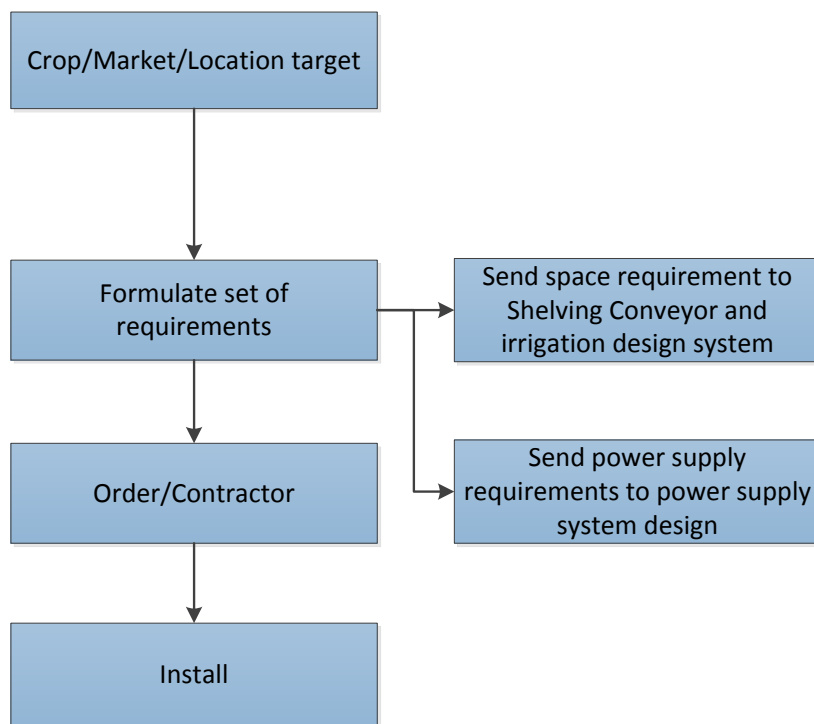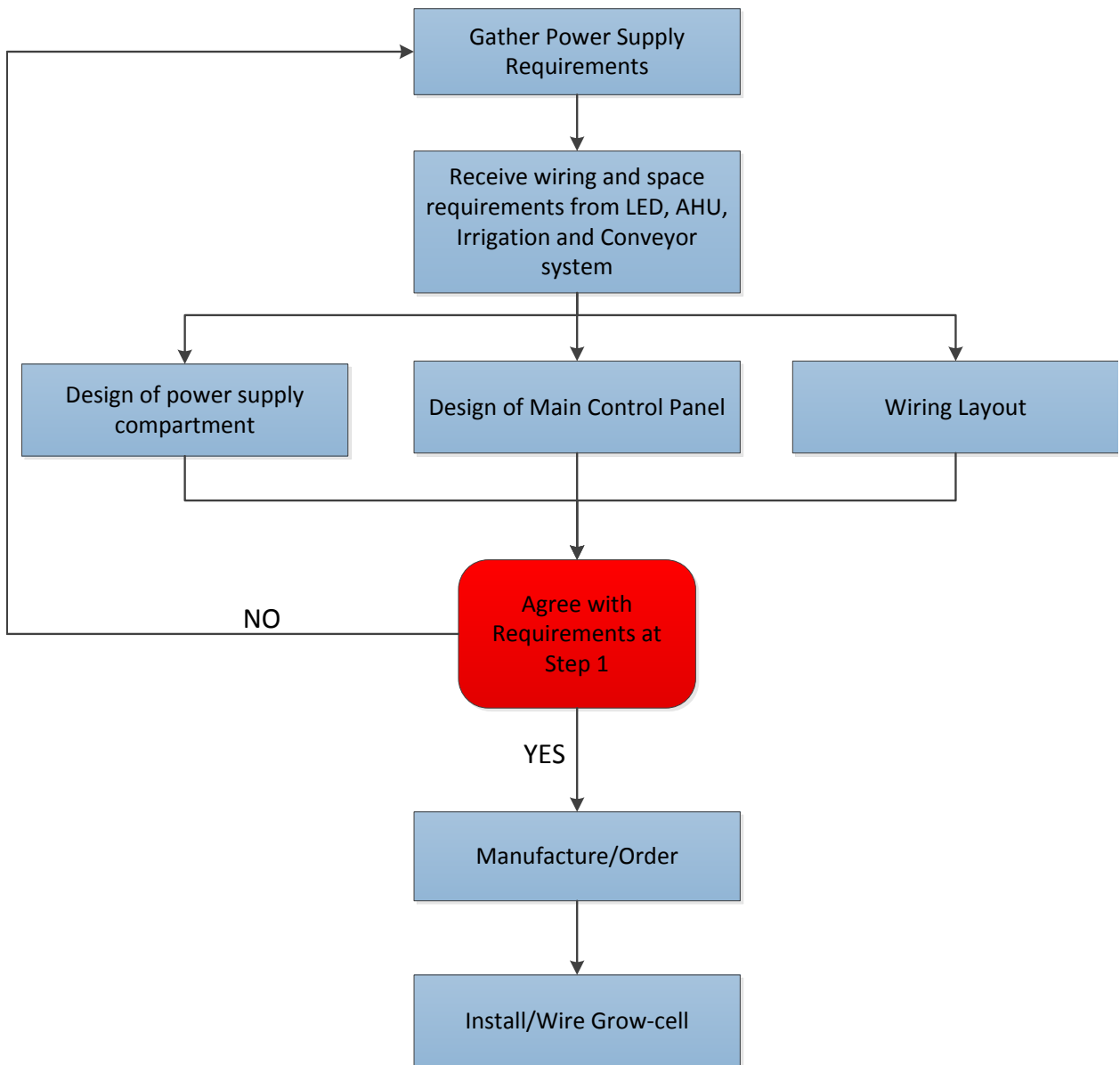
Figure C.1: *HVAC System Design.*
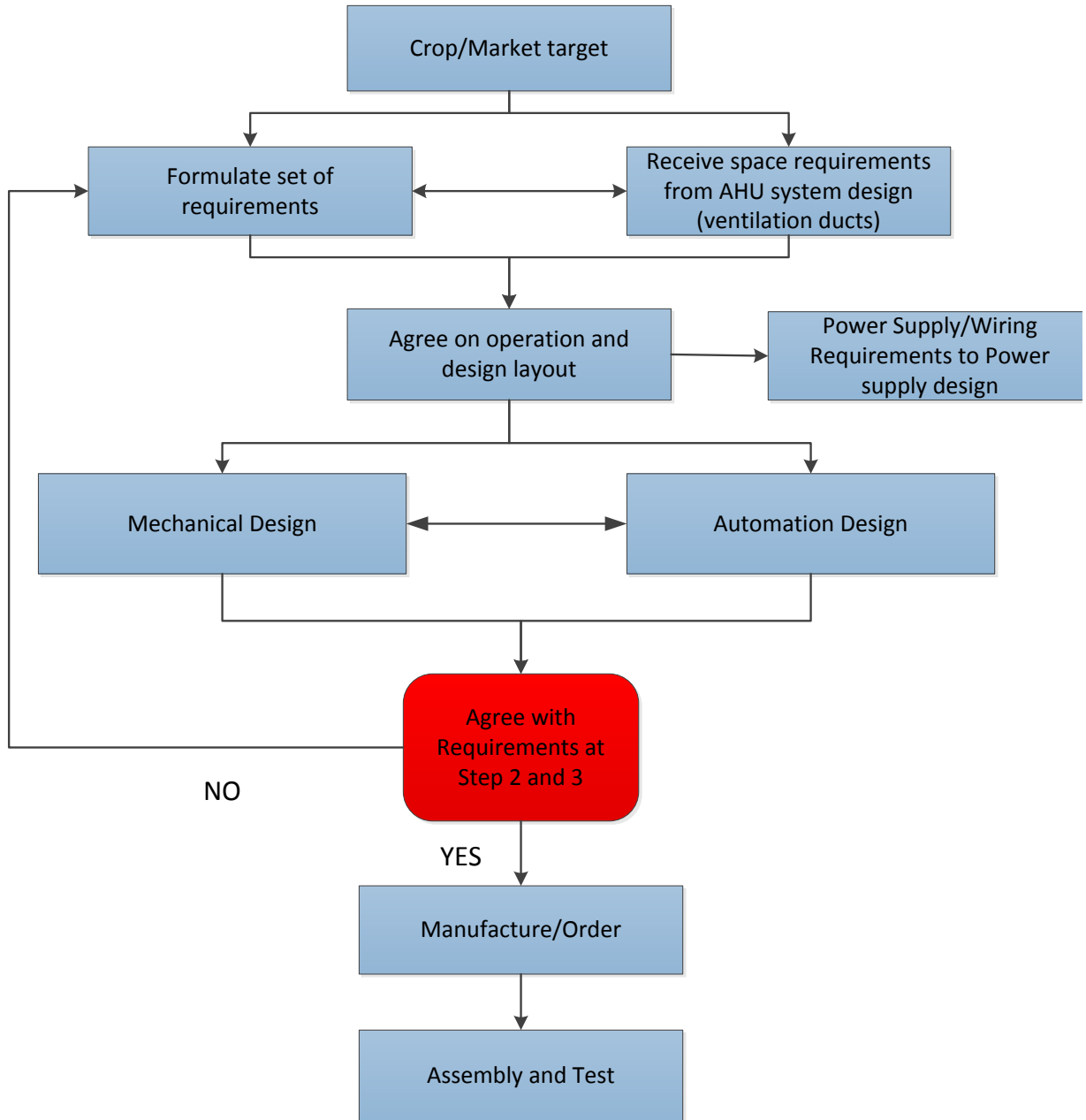
Figure C.2: *Power Supply System Design.*

Figure C.3: *Shelving, Conveyor and Irrigation System Design.*
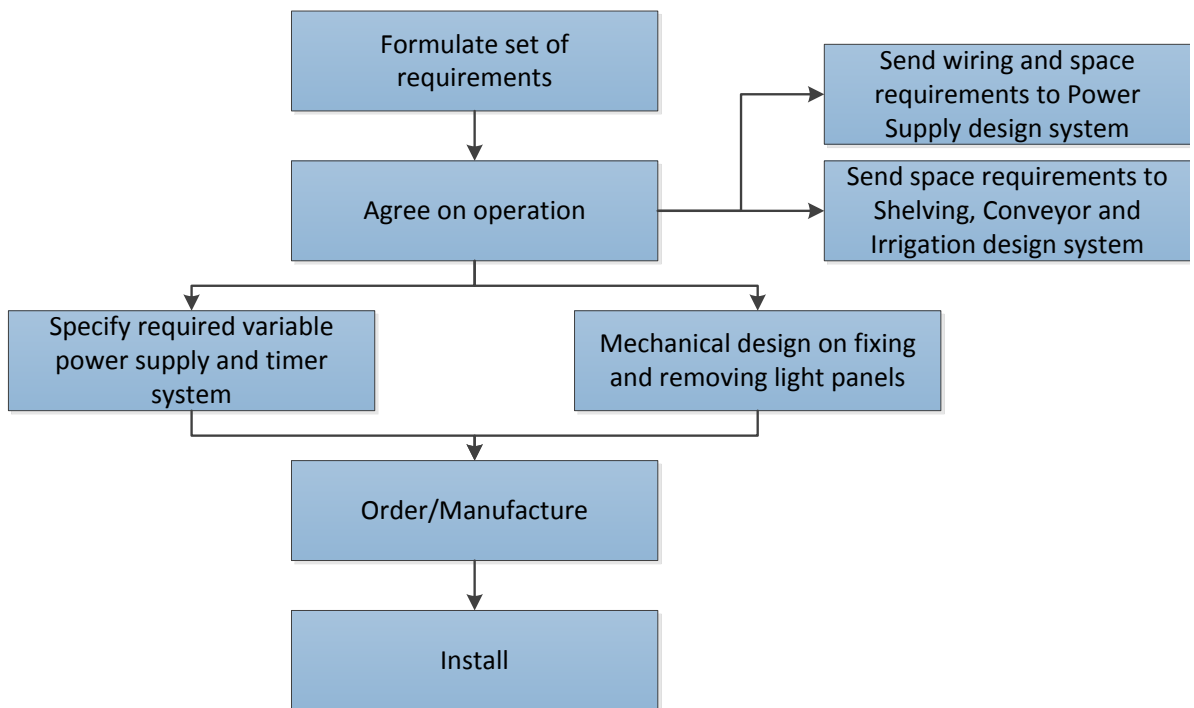
Figure C.4: *LED Lights System Design.*

Appendix D

Pictures of grow-cell apparatus

The following pictures are presented here as complementary to the work presented in Chapter 3, which relates to the development of the test grow-cell.

Figure D.1: Procured container

Figure D.2: The author hardwiring LED lights and connecting the conveyor's motors to the power supply. The chassis of the tray carriers can also be seen.

Figure D.3: On the top, one may see the pegs of the slotted lever mechanism that pushes the tray carriers. These are mounted on the horizontal movement rods.

Figure D.4: The variable power supplies that were utilised the change vary the light output of the LED lights.

Figure D.5: Inside the grow-cell before the growth trials. The curtain separates the growing area from the inspection area, which is also the trajectory that fresh air travels before it enters the growing area.
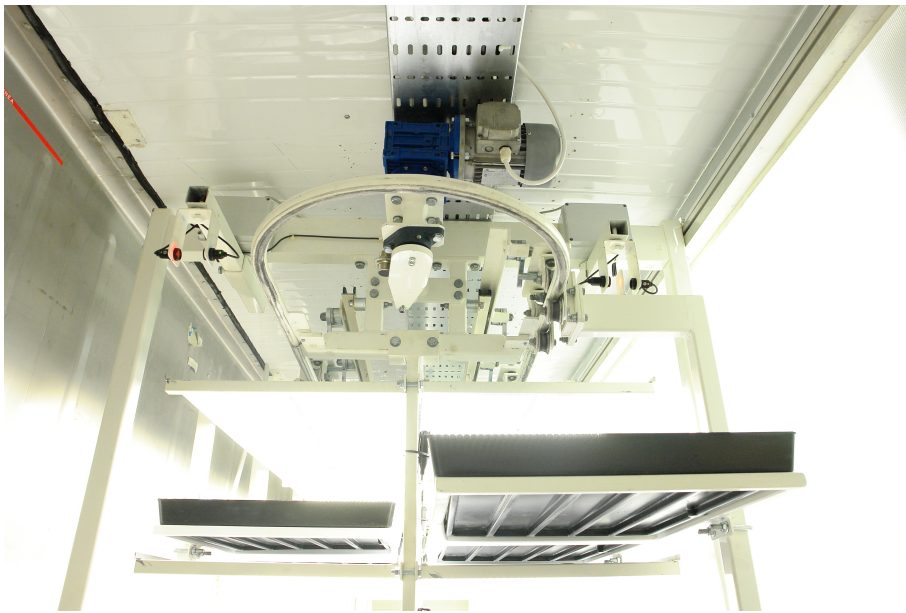
Figure D.6: At the top, one may see the sweep motor and its pushing arm sitting below its proximity sensor, which is also its initial position. Furthermore, on the top left and right one may see the photoelectric sensors that were utilised in the conveyor control logic.

Figure D.7: The control and power supply room before one enters the growing area. In this picture one may see the control panel that the author made for the conveyor system. Above it there is the main power supply panel. At the bottom and at the right lies the irrigation system that was installed by the partner company, before the author modified it for the purposes of the growth trials.